2008

An Observational Study of the Kuroshio in the East China Sea: Local, Regional and Basin-Wide Perspectives on a Western Boundary Current

Magdalena Andres
University of Rhode Island

AN OBSERVATIONAL STUDY OF THE KUROSHIO IN THE EAST CHINA SEA: LOCAL, REGIONAL, AND BASIN-WIDE PERSPECTIVES ON A WESTERN BOUNDARY CURRENT

BY

MAGDALENA ANDRES

A DISSERTATION SUBMITTED IN PARTIAL FULFILLMENT OF THE REQUIREMENTS FOR THE DEGREE OF

DOCTOR OF PHILOSOPHY

IN

OCEANOGRAPHY

UNIVERSITY OF RHODE ISLAND

2008

DOCTOR OF PHILOSOPHY DISSERTATION

OF

MAGDALENA ANDRES

APPROVED:

Dissertation Committee:

Major Professor Mark Wimbush

D. Randolph Watts

[illegible signature]

Harold D. Bibb

DEAN OF THE GRADUATE SCHOOL

UNIVERSITY OF RHODE ISLAND

2008

Abstract

The Kuroshio is the western boundary current of the North Pacific mid-latitude gyre. An observational study of the Kuroshio was conducted using data collected in the East China Sea (ECS) north of Okinawa from December 2002 through November 2004 with an array of inverted echo sounders and acoustic Doppler current profilers. Using these data, Kuroshio velocity structure and transport time series were obtained. Net absolute transport ranges between 4 and 29 Sv and has spectral peaks at periods of 60, 15 and 11 days. The mean net absolute transport is 18.5 ± 0.8 Sv. In conjunction with these *in situ* measurements, satellite altimeter data were used to extend the Kuroshio transport time series back to 1993. Comparison with net Ryukyu Current transport southeast of Okinawa shows that their mean sum (24 Sv), is less than the mean predicted Sverdrup transport. Additionally, Kuroshio and Ryukyu Current transports are positively correlated, with 60 day lag, due to the effect of mesoscale eddies impinging on the Kerama Gap. Finally, annually-averaged Kuroshio and Ryukyu Current transports correlate positively with the Pacific Decadal Oscillation (PDO) index. The correlations, r, which are highest at zero lag, are 0.76 for the Kuroshio and 0.49 for the Ryukyu Current. The combined transport variation correlated with PDO index variation is about 4 Sv. PDO index is strongly negatively correlated with NCEP wind stress curl over the central North Pacific at 20°–30°N.

Acknowledgements

My research was funded by the Office of Naval Research (ONR Grant number N000140210271). I appreciate their support and flexibility during this project.

I have had the good fortune to work with many collaborators and coauthors during this project. I appreciate their cooperation.

I would like to acknowledge the support and assistance, in deployment and recovery of instruments, of the following captains together with their crews, scientists, supporting staff and technicians: Capt. Sadao Ishida aboard the R/V Yokosuka of JAMSTEC, Capt. Bong-Won Lee aboard the R/V Onnuri of KORDI, Capt. Sunao Masumitsu aboard the T/V Kagoshima-maru of Kagoshima University, and Capt. Jeoung Chang Kim aboard the R/V Tamyang of Pukyong National University. Michael Mulroney, Gerry Chaplin and Karen Tracey provided invaluable assistance with IES preparation, deployment, recovery and data processing. The CTD data used in the GEM calculations were kindly provided by the Nagasaki Marine Observatory, Japan Meteorological Agency. I thank K.-I. Chang and B.-H. Lim for collecting and processing the C-line ADCP data.

I thank W.E. Johns for providing transport data from the PCM-1 array, T. Yamashiro for providing Naze and Nishinoomote tide gage data, and H. Nakamura for providing Kuroshio volume transport data through the Tokara Strait compiled from Oceanographic Prompt Reports (Nos. 188-196) of the Nagasaki Marine Observatory, Japan Meteorological Agency. I also thank H.-X. Zhu for providing Ryukyu Current transport data, S. Imawaki for providing ASUKA-line through-

flow and recirculation transports, and K. Kim for providing Tsushima Current transport data.

Helpful suggestions from anonymous reviewers greatly improved the manuscripts which comprise chapters 1 and 2.

I am grateful to my thesis advisor, Mark Wimbush, for his insight, encouragement and patience. I am fortunate to have such a dedicated mentor. I am also very grateful for the guidance of Jae-Hun Park, who never lacked enthusiasm for this project. I appreciate the dedication of my other thesis committee members: Randy Watts, Stephan Grilli, and Jim Miller.

I appreciate the camaraderie shared with my officemates, Andy-1, Andy-2 and Li, a very smart and funny bunch. I am grateful to my parents for their continued support. I also would not have gotten to this point without Jean-Guy Schilling, Meredith Clark and Eva Gallant.

Preface

This thesis is written in manuscript format. It discusses the Kuroshio from three different perspectives organized into separate chapters. Chapters 1 and 2 have been published as journal articles, except for Section 7 at the end of Chapter 1.

Observations of the world's oceans have identified a common feature: intense, narrow jets exist along the basins' western boundaries. Quantifying heat, mass, and momentum transport carried in these western boundary currents is critical for understanding local processes as well as the oceans' role in global budgets. As with many ocean phenomena, measuring the flow in western boundary currents is a technological challenge due, in part, to the spatial and temporal scales involved.

The mid-latitude North Pacific western boundary current is the Kuroshio. This current transports warm water northward along the basin-edge past Taiwan and China, and northeastward past Japan before separating from the continental shelf and flowing into the North Pacific as a free jet. Recent measurements of this current as it passes through the East China Sea, where it is called the ECS-Kuroshio, provide the first long-duration, high-resolution dataset from which an absolute transport time series can be deduced. These measurements, made with inverted echo sounders and acoustic Doppler current profilers, were an observational success and the results of the data analysis are reported in this thesis.

Chapter 1 discusses the ECS-Kuroshio from a local perspective. This chapter describes the instruments used in the East China Sea experiment, discusses

techniques used to convert acoustic-travel-time measurements to transport, and quantifies the behavior of the current during the 23-month observation period. Mean- and time varying- transport and velocity structure are reported as is the annual transport signal. A supplement at the end of Chapter 1 discusses periodic variations in the ECS-Kuroshio using spectral analysis, and complex empirical orthogonal function analysis.

Chapter 2 presents a regional perspective of the Kuroshio and other transports in the western North Pacific. Satellite altimetry data are used to extrapolate ECS-Kuroshio transport in time, resulting in a 14-year ECS-Kuroshio absolute transport time series. This is analyzed together with a similarly determined Ryukyu Current transport time series. The role of eddies in causing transport variations is investigated. Finally, the data are used with previously published results to deduce a regional mean-transport picture.

In the final chapter, Chapter 3, the mid-latitude North Pacific western boundary current system is examined from a basin-wide perspective. A significant correlation is found between the western boundary current transport and the Pacific Decadal Oscillation index. The role of wind stress curl over the North Pacific in causing this correlation is investigated. Additionally, correlations between PDO index and other regional signals are discussed.

Table of Contents

List of Tables

List of Figures

Chapter 1

Observations of Kuroshio Flow Variations in the East China Sea

1. Abstract

Kuroshio velocity structure and transport in the East China Sea (ECS) were investigated as part of a 23-month study using inverted echo sounders and acoustic Doppler current profilers (ADCPs) along the regularly sampled PN-line. Flow towards the northeast is concentrated near the continental shelf with the mean surface velocity maximum located 30 km offshore from the shelf break (taken as the 170 m isobath). There are two regions of southwestward flow: a deep countercurrent over the continental slope beneath the Kuroshio axis and a recirculation offshore which extends throughout the whole water column. There is a bimodal distribution to the depth of maximum velocity with occurrence peaks at the surface and 210 dbar. When the maximum velocity is located within the top 80 m of the water column, it ranges between 0.36 m/s and 2.02 m/s; when the maximum velocity is deeper than 80 m, it ranges between 0.31 m/s and 1.11 m/s. The 13-month mean net absolute transport of the Kuroshio in the ECS is 18.5 ± 0.8 Sv (standard deviation, σ = 4.0 Sv). The mean positive and negative portions of this net flow are 24.0 ± 0.9 Sv and −5.4 ± 0.3 Sv, respectively.

2. Introduction

The Kuroshio is a western boundary current, serving as the return flow for the wind-driven circulation of the North Pacific Subtropical Gyre. Its source is the

North Equatorial Current which bifurcates off the Philippines (Nitani, 1972). The northward flowing branch of this bifurcation, the Kuroshio, sometimes loops into the South China Sea before passing east of Taiwan. There, part diverts to the east forming the Ryukyu Current (Yuan et al., 1998; Ichikawa et al., 2004; Zhu et al., 2003), which flows along the eastern side of the Ryukyu Island chain, while the remainder enters the East China Sea (ECS) over the Ilan Ridge (sill depth ~775 m (Choi et al., 2002)) forming the ECS Kuroshio. The Ryukyu Island chain separates the ECS from the Philippine Basin (Figure 1). There is one deep channel in this chain, the Kerama Gap south of Okinawa, with a sill depth of about 1000 m (Sibuet et al., 1995). In the ECS, the Kuroshio flows mainly just seaward of the shelf break before leaving through the Tokara Strait, which is divided into two sections by a seamount (summit ~320 m depth); the northern section reaches ~460 m depth while the southern section reaches ~1400 m (Oka and Kawabe, 2003). East of the Tokara Strait, the Ryukyu Current and the Kuroshio rejoin and flow northeastward south of Japan until they leave the coast as a free jet known as the Kuroshio Extension. A schematic of the Kuroshio path inside and near the ECS is shown in Figure 1.

Previous studies of Kuroshio velocity structure in the ECS have reported northeastward Kuroshio surface currents reaching speeds of 3.5 knots (Su et al., 1990). A subsurface velocity maximum at about 200 m depth has been detected in some velocity sections northwest of Okinawa (e.g., Ito et al., 1995; Ichikawa and Beardsley, 1993; Su et al., 1990 and references therein). However, a subsurface maximum is absent in the mean absolute velocity section of Oka and Kawabe

(2003) and it is unclear whether this is related to instrument spacing or to the transience of the subsurface maximum. The Kuroshio lies over the slope and its position has a standard deviation of about 10 km (e.g., Yamashiro and Kawabe (2002)) due to Kuroshio meanders inside the ECS. The amplitudes of these meanders are much smaller than the meander amplitudes south of Japan and in the Kuroshio Extension.

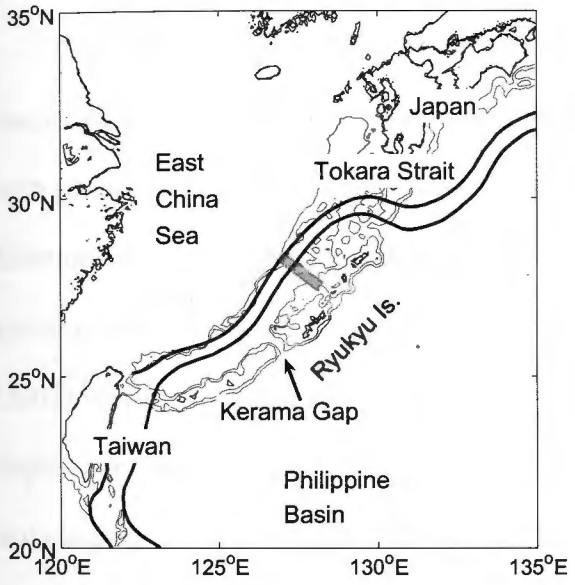

Figure 1. Regional ECS map.
Kuroshio path, shown with heavy black lines, is estimated from 2002-2004 Mean Absolute Dynamic Topography produced by Ssalto/Duacs and distributed by AVISO with support from Cnes. Array location shown as gray rectangle. Depth contours in light grey at 500 m and 1000 m.

A southwestward flowing countercurrent beneath the Kuroshio has been reported (e.g., Ito et al., 1995; James et al., 1999). Moored current-meter data collected during 2004-2006 along the slope in water about 700 m deep show southwestward flow in the mean, about 100 m above the seafloor (H. Nakamura et al., Deep countercurrent beneath the Kuroshio in the Okinawa Trough of the East

China Sea, submitted to Journal of Geophysical Research, 2008). The countercurrent transport and structure, however, are not well resolved, since these are a few discrete point measurements.

Southwestward flow has also been reported between the Kuroshio and the Ryukyu Islands forming a recirculation (e.g., Oka and Kawabe, 2003; James et al., 1999). This flow is typically strongest at the surface where southwestward surface currents can reach 2 knots (Su et al., 1990).

Previous studies of Kuroshio transport in the ECS include calculations for the period between 1986 and 1988 made from 39 hydrographic sections referenced with surface current data measured by ADCP and Geomagnetic Electrokinetograph (GEK) (Ichikawa and Beardsley, 1993). The mean northeastward absolute transport for these sections was 23.7 Sv. Johns et al. (2001) measured the transport just upstream of the ECS east of Taiwan between September 1994 and May 1996 along a WOCE line, using moored current meters and acoustic Doppler current profilers (ADCPs) and determined that the 20-month mean absolute net transport was 21.5 Sv. James et al. (1999) deployed inverted echo sounders (IESs) north of Okinawa to measure acoustic travel time and bottom pressure from August 1991 until October 1992. Their study, however, focused on the characteristics of ECS Kuroshio meanders instead of transport, because current measurements were unavailable for referencing.

The previous studies of Kuroshio position and velocity structure inside the ECS are limited spatially or temporally. There has been no long-term continuous measurement of absolute transport within the ECS; reports of mean transports in

the ECS have relied on averaging snapshots taken over many years. Here we present a 23-month time series of Kuroshio net absolute transport in the ECS. We also report on the time-and-space varying velocity structure of the Kuroshio over the last 13 of these months (when measurements were more complete) and calculate the corresponding positive and negative transport time series. In addition to quantifying the Kuroshio volume transports, we investigate their time variabilities as well as those of Kuroshio position and width.

3. Data

The primary data sources for this investigation are 11 IESs which were deployed in the Okinawa Trough region of the ECS for nearly two years and 2 ADCPs deployed nearby on the outer shelf for 7-13 months (Figure 2, Table 1).

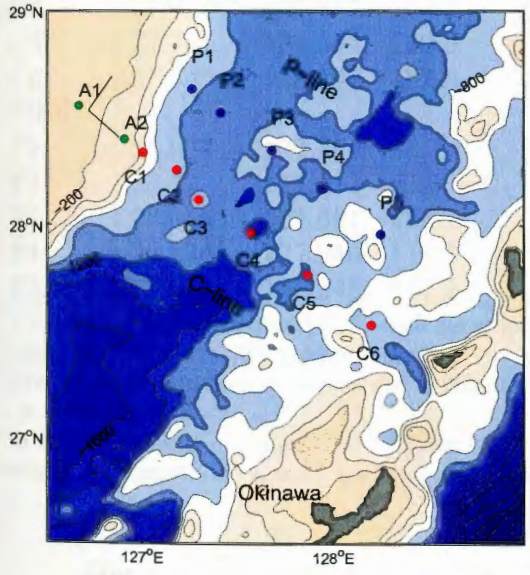

Figure 2. Array map.
Green dot = ADCP; red = CPIES; blue = PIES. Contour interval is 200 m. Black lines show origin as well as cross-stream (x, 128°) and downstream (y, 38°) directions.

3.1. IES

Eleven IESs were deployed on the seafloor across the Kuroshio in two parallel lines separated by 40 km (C-line and P-line with 6 and 5 instruments, respectively) from December 2002 until November 2004. The C-line nearly coincided with the PN-line along which hydrographic data are regularly collected four times per year by the Nagasaki Marine Observatory of the Japan Meteorological Agency.

Table 1. Locations, mean pressures, and measured near-bottom currents of array instruments.

	Lat. (°N)	Long. (°E)	x position [a] (km)	Pressure [b] (dbar)	υ (cm/s) [c] Mean	Std
ADCP						
A1	28.558	126.670	–5.6	152	1.5	11.0
A2	28.405	126.910	23.3	286	-0.3	15.3
CPIES						
C1	28.343	127.006	35.0	554	-1.3	7.5
C2	28.262	127.182	54.1	1006	-2.8	5.6
C3	28.123	127.297	72.5	1131	10.7	6.6
C4	27.971	127.571	104.2	1339	-0.3	2.9
C5	27.771	127.864	140.6	1115		
C6	27.540	128.197	182.6	891	-3.7	2.7
PIES						
P1	28.637	127.264	34.7	1033		
P2	28.527	127.412	53.6	1121		
P3	28.353	127.681	86.3	856		
P4	28.174	127.946	119.1	1080		
P5	27.961	128.248	157.2	750		

[a] x is seaward distance (toward 128°) with the origin taken as the shelf break (170 m isobath) on the C-line: 28.536°N, 126.723°E (see Figure 2).

[b] Pressures are mean pressures recorded at instrument locations: A1 0.5 m, A2 5 m, and C1-6/P1-5 1 m above the seafloor.

[c] υ is the downstream (rotated 38° clockwise from 0° True) velocity component measured near-bottom: A1 6 m, A2 15 m, and C1-6 51m, above the seafloor.

Horizontal spacing of the instruments varied from about 20 km beneath the main Kuroshio axis at the northwestern end of the line to 40 km at the southeastern end. Each P-line instrument (PIES) was equipped with a Digiquartz pressure

sensor, and each C-line instrument (CPIES) was equipped not only with the pressure sensor but also an RCM11 Aanderaa current sensor moored 51 m above the bottom. These instruments measured round-trip, bottom-to-surface acoustic-travel-time (τ), bottom pressure and bottom temperature every hour. In addition, the upstream instruments (C-line) made hourly measurements of current velocity and temperature 51 m above the bottom. The data set is complete except for the current record and about 1/3 of the pressure record at site C5. The velocity cross section and transport results discussed here focus on the C-line, however the τ measurements from the P-line are used in the optimal interpolation mapping procedure described in Section 3.1.2.

3.2. ADCP

The portion of the Kuroshio which flowed in waters shallower than 550 m, near or over the shelf, was outside the region sampled by the IESs. For part of the 2-year IES deployment, this portion of the flow was measured with two bottom-mounted ADCPs on the shoreward extension of the C-line. Details of the velocity structure measured by the ADCPs are reported elsewhere (Lim, 2008). Here the ADCP data are mainly used to calculate the transport of the Kuroshio on the upper slope and shelf.

The ADCP data set is incomplete spatially and temporally. Section 4.2 presents results of various methods used to extrapolate these data in space and time with the details given in the Appendix. The shallower ADCP (A1) was operational for 7 months from May 2004 until November 2004. This instrument measured velocity from 152 m depth (0.5 m above the seafloor) to 30 m below the

surface with 4 m bin sizes. The deeper instrument (A2) was operational for 13 months from October 2003 until November 2004 and measured velocities from 285 m depth (5 m above the seafloor) to 179 m below the surface with 8 m bin sizes.

3.3. Processing

Acoustic-travel-time data, τ, measured at the seafloor by each instrument, were converted to travel time referenced to a common pressure level, τ_{ref}, by the following method. First the instrument's pressure level was determined from the mean of its pressure record. Then from historic hydrographic profiles collected in the ECS over the last 80 years (data from North Pacific Hydrobase, (Macdonald et al., 2001) and the Nagasaki Marine Observatory of the Japan Meteorological Society) we selected 1833 which reached at least 700 dbar. From these profiles two synthetic travel times were calculated: (1) that between 700 dbar and the surface (τ_{ref}), and (2) that between the instrument pressure level and the surface (τ_p). The linear relationship between τ_{ref} and τ_p was determined by least squares fitting. This relationship was then used to convert the instrument's measured τ time series to a corresponding τ_{ref} time series. The whole procedure was repeated for each IES instrument.

All τ_{ref}, pressure, and current (from CPIES or ADCP) data were lowpass filtered using a second-order Butterworth filter with 48-hour cutoff period run forward and backward. The records were then subsampled at 12-hour intervals. Details about the data processing, including removal of occasional "jumps"

(probably due to bottom-fishing boats dragging the IESs), detiding pressure records and correction of pressure-sensor drift, are described in detail in a data report (Andres et al., 2005).

Current data were corrected for the local magnetic declination (roughly 5°W) and rotated 38° clockwise so that U is the offshore cross-stream (x) velocity component and V is the downstream (y) velocity component. This rotation is consistent with the orientation of the PN-line (Figure 2).

4. Obtaining velocity fields and transports

4.1. Off-shelf – interpreting the IES data

4.1.1. GEM fields

For sea water, sound speed and specific volume anomaly (δ) both depend only on temperature, salinity and pressure. As a result, in many regions τ_{ref} can be used as a proxy for a water column's δ profile (He et al., 1998). This relationship of δ to τ_{ref} and pressure is called the Gravest Empirical Mode (GEM) (Sun and Watts, 2001), and the GEM empirical lookup table typically resembles first-mode baroclinic variations in the water-column density distribution. In strong baroclinic current regions the GEM usually represents the pycnocline sloping across the current system and accounts for most of the observed variability in δ (Willeford, 2001; Meinen, 2001; Sun and Watts, 2001; Book et al., 2002; Rodrigues, 2004; Park et al., 2005). Other sources of variability, such as internal waves or bottom-intensified topographic waves, can exist without being represented by the GEM.

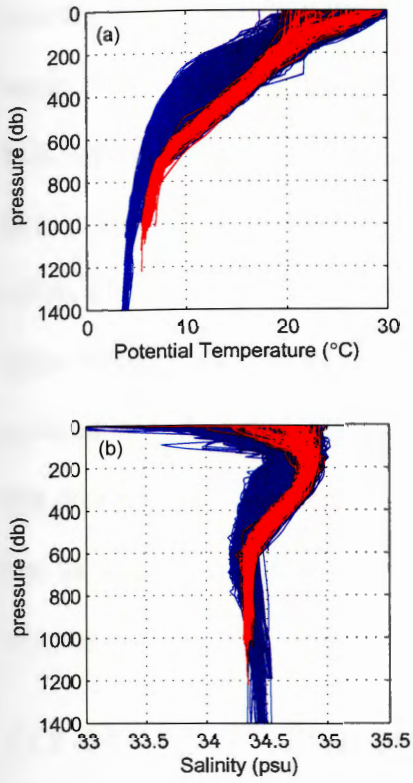

Figure 3. ECS hydrocast profiles.
Panel (a) shows temperature and (b) shows salinity (b). Red are 113 profiles from Okinoerabushima Basin used to construct the localized GEM for C6. Blue are 1720 profiles from the rest of the ECS used to construct the main ECS GEM.

In many applications, a single GEM field is used as a δ-lookup table for a given region, but in the ECS, we constructed two separate fields: a localized GEM for a small region around C6 and a main GEM for the rest of the IES sites. Detailed bathymetry data with 1-minute resolution (Choi et al., 2002) reveal that deep water near site C6 (883 m depth) is isolated from similar-depth water in the rest of the ECS, because it is situated within a small Y-shaped basin with a sill depth of ~800 m and a maximum bottom depth of ~1200 m (Figure 2). This basin lies just off the west coast of the island of Okinoerabushima in the Ryukyu Island chain, and thus we call it the Okinoerabushima Basin. A comparison of

temperature profiles from the 1833 historic ECS hydrographic profiles shows that water within this basin is warmer than water at the same depths elsewhere in the ECS, typically about 1.5°C warmer at 850 dbar (Figure 3). Hence, only the 1720 ECS profiles from outside the basin region are used to compute the main ECS GEM, while the localized GEM is calculated exclusively from the 113 hydrocasts taken within the basin region. Details of generating the GEM lookup tables are reported in Andres et al. (2005). Errors in the GEM lookup table between 100 and 200 dbar caused by second-mode internal tides are reported in Park et al. (2006), but, as they point out, such errors are effectively removed by 48-hour lowpass filtering of the data.

4.1.2. Off-shelf – calculating the transport

The lowpass filtered τ_{ref} data from the CPIESs and PIESs were gridded at 10 km spacing in x and y using optimal interpolation (OI) (Bretherton et al., 1976; Watts et al., 1989) with an empirically determined correlation length scale for τ_{ref} of 55 km and the assumption of horizontally non divergent flow. For flow over sloping topography, this assumption results in isopycnals which are cut off rather than compressed by the topography. Using the GEM relationship, a time series of C-line δ cross sections was generated from the mapped τ_{ref}. These cross sections were used with the thermal-wind equation,

$$\frac{\partial v}{\partial z} = -\frac{g}{\rho f}\frac{\partial \rho}{\partial x}, \qquad (1)$$

to calculate time series of the Kuroshio's downstream baroclinic velocity, v, and transport both referenced to 700 dbar (Figure 4, upper line). Here z is in the upward vertical direction, g is gravity, ρ density, and f the Coriolis parameter.

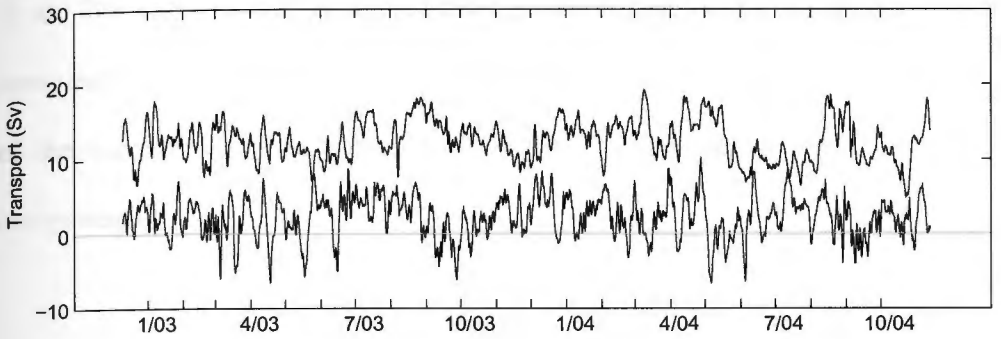

Figure 4. Off-shelf transport.
Calculated as described in the text from CPIESs between x = 35 km and x = 195 km where x = 0 at the shelf break (170 m isobath). In order to capture the transport flowing between the Ryukyu Islands and the most offshore instrument (C6 at x = 182.6 km), τ_{ref} was OI mapped slightly beyond the instrument array. This 12.4 km extrapolation is over a short distance relative to the τ_{ref} correlation length scale of 55 km. Upper line is the baroclinic transport referenced to 700 dbar. Lower line is the barotropic transport. Tick marks denote the beginning of each month.

In order to calculate the barotropic reference velocity (i.e., the absolute velocity at 700 dbar) and its corresponding transport across the C-line, one needs to know the horizontal pressure gradient on an appropriate geopotential (level) surface. Since the depth of each instrument was not known with sufficient accuracy (because pressure sensors cannot deliver 1-to-10 ppm absolute accuracy), time-averaged current data from the CPIES current sensors were used to reference or "level" the pressure data.

Because of significant deep geostrophic shear in the ECS, the following method was used to "level" the C-line instruments. For each instrument site, i, the mean downstream velocity, $\overline{V}_i$, at any level, is related to the mean pressure, $\overline{P}_i$, at that level by geostrophy,

$$\overline{V}_i = \frac{1}{\rho f}\frac{\partial \overline{P}_i}{\partial x}, \qquad (2)$$

where the derivative is taken along the geopotential (level) surface. The velocity at the 700 m level for each instrument location can be written as the velocity measured by the current sensor plus the velocity difference between the depth, d_i, of the current sensor and the 700 m surface. Thus in the mean, for the *y*-component,

$$\overline{V}_i = \frac{1}{T}\sum_{t=0}^{T}\left[\upsilon_i(t) + \int_{-d_i}^{-700m}\frac{\partial v_i(z,t)}{\partial z}dz\right], \qquad (3)$$

where t is time, T the duration of the measurements, υ_i the y-component of velocity measured by the current sensor, and the velocity shear in the last term is determined from the travel-time measurements using the GEM and Equation (1). So using Equations (2) and (3) and OI with an empirically determined correlation length scale for pressure of 35 km, the mean (relative) pressure on the chosen geopotential surface at each site, $\overline{P}_i$, was calculated from the measured current velocity, $\upsilon_i(t)$, and acoustic-travel-time, $\tau_i(t)$. By comparison of this calculated mean pressure with the mean of the measured pressure record, $\overline{p}_i$, a leveling constant, LC, was determined for each instrument and added to the respective pressure record:

$$LC_i = \overline{P}_i - \overline{p}_i. \qquad (4)$$

With a second OI step, this time using the current sensor measurements and the "leveled" pressure measurements, $P_i = p_i + LC_i$, the barotropic velocity and transport were calculated (Figure 4, lower line). The approximation made here is that the barotropic velocity, which is defined in this work as the velocity at 700 dbar, is equivalent to the velocity at 700 m. The difference in velocity between 700 m and 700 dbar is very small, because both Δz and $\partial v/\partial z$ are small.

4.2. Shelf and upper slope – interpreting the ADCP data

The ADCPs were deployed for only the last 13 months of the 23-month period during which CPIES data were collected. Even when the ADCPs were operational, current velocities were not measured in the topmost 30 m and 179 m at sites A1 and A2, respectively. In an attempt to establish reasonable estimates of the Kuroshio transport over the upper slope and shelf (i.e., shallower than 550 m) for the entire 23-month period, several extrapolation methods were attempted. Two of these are spatial extrapolations (filling in the tops of the velocity profiles) and one is temporal (extending into the first 10 months of IES deployment for which no contemporaneous ADCP data are available). In all cases, once the velocity profiles were determined, they were mapped onto a regular grid with 10 km horizontal spacing by linear interpolation. Zero velocity was assumed 15 km shoreward of the shelf break. The gridded velocities were then integrated to calculate the transport over the outer shelf and upper slope between x = –15 km (130 m depth) and x = 35 km (550 m depth), the position of C1. Because of low velocities at site A1 and shallow water shoreward of this, the transport calculations

are insensitive to the location of the zero velocity point. Specifically, moving this point 10 km further shoreward increases the mean transport by only 0.1 Sv.

4.2.1. Spatial extrapolation

The spatial extrapolation methods were 1) vertical extension with a GEM and 2) a horizontal smoothing method. These spatial extrapolation methods are described in the Appendix. Resulting time series of transport over the upper slope and shelf are plotted in Figure 5. It is encouraging that the vertical-extension and horizontal-smoothing methods generally resulted in similar transport time series even though the procedures are entirely different. The rms difference between the transports calculated by these two methods is 1.0 Sv. Occasionally, however, the vertical extension method gave higher shelf transports (e.g., around the beginning of July 2004 in Figure 5). During these times vertical profiles of velocity (figure not shown) generated by the horizontal smoothing method appear unrealistic, with velocities changing abruptly with depth. Also, during these times, the vertical extension method suggests there is a velocity maximum near A2. The horizontal smoothing method simply cannot reproduce situations where there is such a maximum between A1 and C1. Consequently, we choose the vertical extension method as the more realistic method of spatial extrapolation.

Velocities measured at A1 were typically small (usually of order 0.2 m/s or less) and thus the transport calculations are insensitive to A1 measurements. The vertical extension method was attempted both with and without the A1 velocity measurements as inputs to the OI calculations, and the resulting transports are nearly the same (Figure 5, blue and red lines, rms difference 0.6 Sv). By using

only the A2 measurements we obtain a transport time series for 13 months instead of just the 7 months of A1 operation.

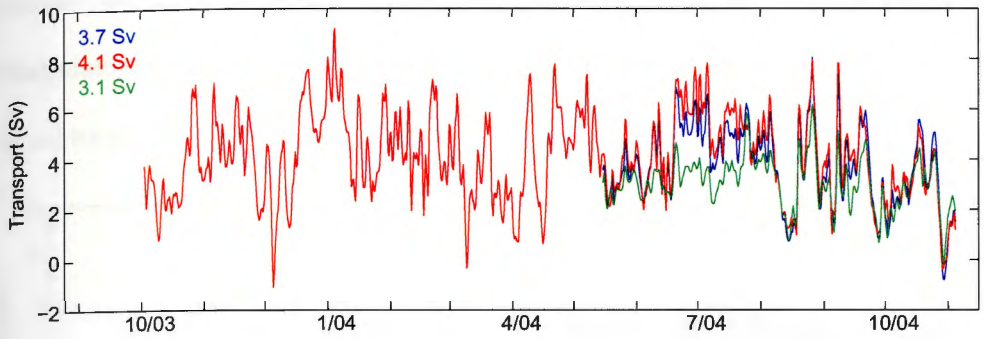

Figure 5. Net transport from the vertical extension method.
Net transport on the upper slope and shelf (i.e., x < 35 km) determined from ADCPs, from vertical extension method using data from A1 and A2 (blue), A2 only (red) and from horizontal smoothing method (green). Tick marks denote the beginning of each month. In upper left corner, mean values are listed in their respective colors.

4.2.2. Temporal extrapolation

The majority (77%) of the Kuroshio mean net transport was measured by the CPIESs with the remainder (that on the upper slope and shelf) measured by the ADCP(s). In order to obtain an estimate of this flow for the first 10 months of CPIES deployment, during which the ADCPs were not operational, the position and strength of the Kuroshio were established using off-shelf velocities from the CPIESs. Then an empirically determined analytical shape formula was used to extrapolate the net transport over the upper slope and shelf. The method is described in the Appendix. Figure 6 shows that during the 13 months when ADCP data were available, the transport values calculated by this extrapolation agree reasonably well with 20-day low-pass filtered net transports determined from the ADCP data (rms difference = 1.4 Sv). This extrapolation of net transport enables

the analysis of seasonal variability by extending the time series to nearly 2 years. However, since the method oversimplifies the complex time-varying velocity structure of the Kuroshio, we use it to infer net transport only, and not to extrapolate the velocity structure or to calculate the positive and negative pieces of the net transport.

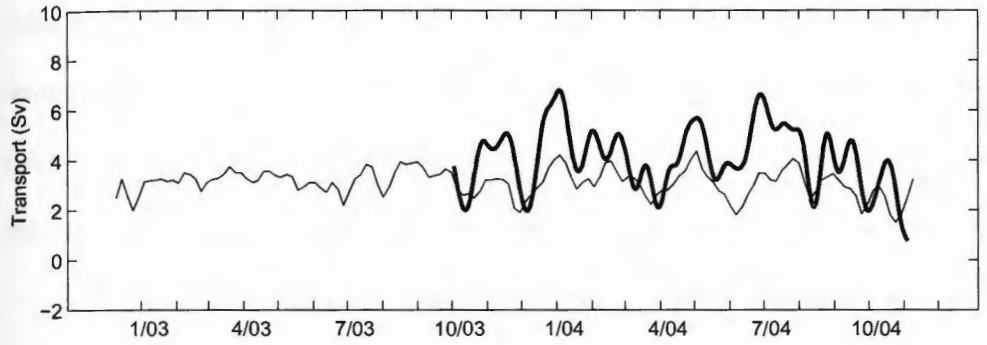

Figure 6. Net transport from the analytic-shape method.
Net transport on the upper slope and shelf (i.e., x < 35 km) determined from the analytic-shape method (thin line) and 20-day lowpass filtered transport from the vertical extension method applied to A2 ADCP data (thick line). Tick marks denote the beginning of each month. 13-month mean values are 3.0 Sv and 4.1 Sv for the analytic shape and 20-day lowpassed methods, respectively; the 23-month mean for the transport derived from the analytic-shape method is 3.1 Sv.

5. Results

In this section we report on the mean and variability of the observed velocity field and the transports.

5.1. Mean velocity structure

Using the CPIES and ADCP data as described in the previous section, C-line flow is determined over a 210 km span from a point 15 km shoreward of the shelf-break to a site near the Ryukyu Island chain. Figure 7 displays the mean velocity cross section (upper panel) and the standard deviation (lower panel) for

the 13-month CPIES + ADCP observation period. The mean cross section shows a region of positive (northeastward) flow containing two local velocity maxima: a surface maximum (0.65 m/s, σ = 0.41 m/s) 30 km offshore from the shelf break and a subsurface maximum (0.68 m/s, σ = 0.15 m/s) at 170 m depth, 70 km from the shelf break. Positive mean velocities extend to the seafloor below this subsurface velocity maximum. In the mean, the subsurface maximum is slightly stronger than the surface maximum. Nevertheless, the highest velocities in the record do occur near the surface which explains why the standard deviation around the surface maximum is three times larger than that around the deeper maximum.

Other authors have observed a subsurface velocity maximum within 150 km of the C-line in the ECS. Ito et al. (1995) found a subsurface maximum of ~0.7 m/s at 250 m depth using an ADCP on a towed "fish" about 140 km upstream of the PN-line, and Ichikawa and Beardsley (1993) found a subsurface velocity maximum of ~1 m/s at about 200 m depth using hydrocasts referenced with surface ADCP and GEK measurements near the PN-line. The subsurface-maximum structure, however, is not obvious in mean velocity sections from Oka and Kawabe's (2003) hydrographic and shipboard ADCP measurements, or from Guo et al.'s (2006) numerical models.

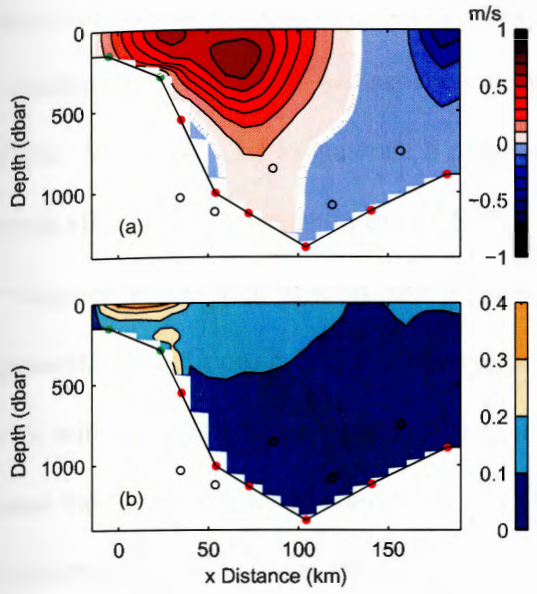

Figure 7. Velocity mean and standard deviation.
Velocity (y-component) mean (top) and standard deviation (bottom) cross sections on the C-line. Here x = 0 at the shelf break (depth = 170 m). Green and red dots indicate locations of ADCPs and CPIESs, respectively. Open circles indicate locations of PIESs 40 km downstream from the C-line. 0.1 m/s contour interval; zero contour white.

There are two regions of mean negative flow: a deep countercurrent over the continental slope and a recirculation further offshore which extends throughout the water column. These features have been reported by other authors (e.g., Bingham and Talley, 1991; Ichikawa and Beardsley, 1993; Ito et al., 1995; James et al., 1999; Oka and Kawabe, 2003). Figure 7 and the near-bottom velocities measured by the ADCPs and CPIES current sensors (Table 1) show that, in the mean, the countercurrent at C1 and C2 does not extend over the shelf to A1 and barely reaches A2 (mean at A2 is –0.3 cm/s 15 m above the seafloor and positive at higher elevations).

The mean velocity cross section along the PN-line reported by Oka and Kawabe (2003) (their Figure 3a) does not show vertical shear in the recirculation

as strong as that in Figure 7. We verified that our vertical shear is not an artifact resulting from the use of two separate GEMs (the main GEM and the C6 "warm" GEM, Section 3.1.1.) to generate δ profiles. Even when a single GEM generated from all of the hydrocasts in the ECS (but including only the upper 700 m of the "warm casts") is used to determine δ profiles, the shear in the recirculation is still present. In addition, calculations based only on the mean travel times at C5 and C6, without an OI mapping step, result in strong vertical shear although in this case the shear is located between C5 and C6 rather than at the eastern edge of the instrument array. These tests indicate that while the vertical shear is real, its horizontal structure is uncertain since the instrument spacing on this end of the line is 40 km. Note, however, that the C-line cross section shown in Figure 7 has the P-line instruments' x-positions (see Table 1) superimposed on it (open circles). Instruments from the P-line were used in OI mapping τ (described in Section 3.1.2). Since this line, which is 40 km downstream of the C-line, falls within the empirically determined τ correlation length scale (55 km), the P-line data help constrain the location of this vertical shear.

5.2. Velocity variations

While the mean velocity cross section in Figure 7 shows surface and deep velocity maxima of comparable strength coexisting, the velocity cross section time series generated from the 2-day lowpass filtered data shows variability in the Kuroshio velocity structure. Examples of velocity cross section snapshots are shown in Figure 8, including the days with the highest and lowest recorded net transports (panels b and c, respectively). Snapshots from 8 March 2004 (panel a)

and 9 September 2004 (panel d) have no localized subsurface maximum; the strongest jet is confined to the surface. In contrast, snapshots from 28 April 2004 (panel b) and 5 June 2004 (panel c) do have localized subsurface maxima. On 28 April the subsurface maximum is stronger than the surface maximum (1.1 m/s compared to 0.7 m/s) while on 5 June the maxima are comparable (0.4 m/s surface maximum and 0.3 m/s subsurface maximum) . EOF analyses of the time-varying velocity structure are reported elsewhere (Lim, 2008).

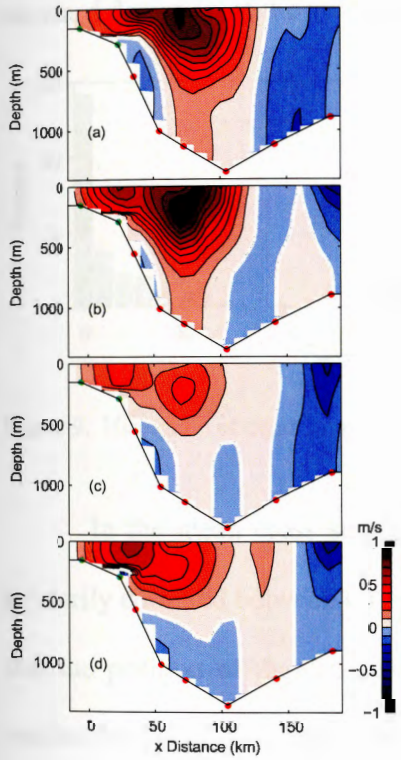

Figure 8. Velocity snapshots.
Velocity (y-component) snapshots plotted with $x = 0$ at the shelf break (depth = 170 m). Green and red dots indicate locations of ADCPs and CPIESs, respectively. Contour interval is 0.1 m/s; zero contour white. (a-d) 8 March, 28 April, 5 June, and 9 September 2004, respectively.

The depth of the overall maximum velocity is bimodally distributed with occurrence peaks at the surface and 210 dbar (Figure 9). The overall velocity

maximum is deeper than 80 dbar 47% of the time. It is interesting to note that while the deep frequency peak is at 210 dbar, the location of the subsurface maximum in the mean cross section (Figure 7) is shallower at 170 dbar

When the highest velocities are in the layer between the surface and 80 dbar, the maxima range between 0.36 m/s and 2.02 m/s and the standard deviation of the velocity maximum's x-position is 17 km. When the highest velocities are deeper than 80 dbar, the maxima range between 0.31 m/s and 1.11 m/s and the standard deviation of the velocity maximum's x-position is 14 km.

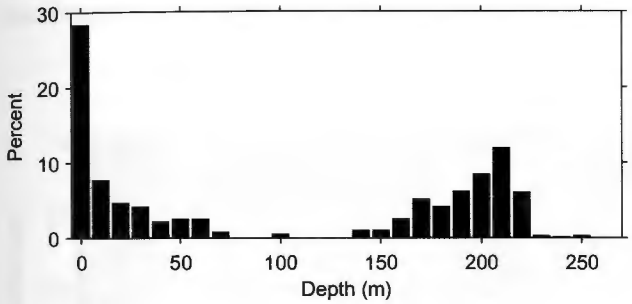

Figure 9. Histogram of depth of overall maximum velocity.

In the mean cross section shown in Figure 7, the slope countercurrent is primarily confined between C1 and C2. The snapshots in Figure 8, however, show that the position of the countercurrent moves on- and offshore and occasionally reaches beyond C3, although the near-bottom velocity measured by the C3 current sensor is negative for only 6% of the 23-month record. Since the countercurrent width is comparable to the instrument spacing over the slope, our data do not adequately resolve this countercurrent.

Nitani (1972) suggested using the location of the 18°C isotherm at 200 dbar as an indicator of ECS Kuroshio position (i.e., location of maximum surface

velocity). Our data show what previous authors (e.g., Su et al., 1990) have pointed out, namely, that the maximum surface velocity often falls shoreward of the 200 dbar isobath, and thus the location of an isotherm at 200 dbar is not always a useful proxy for Kuroshio position. Guan (1980) defined the "core" of the Kuroshio as the region between the surface 0.4 m/s isotachs. We have adopted this definition of the "core" and take its midpoint to be the "position" of the Kuroshio. (Using the maximum surface velocity location results in a "jumpy" time series of position due to the difficulty in resolving the exact location of a maximum with instruments spaced ~20 km apart.)

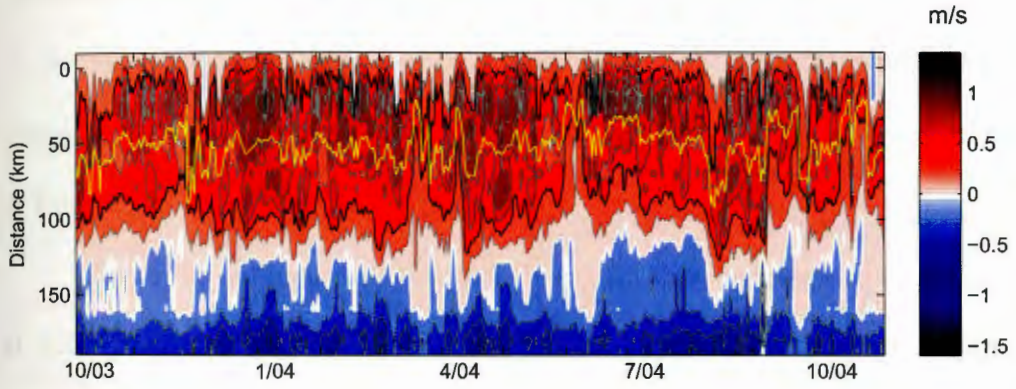

Figure 10. Surface velocity.
Surface velocity (y-component) across the C-line shown on a t-x plot.
Zero contour is white. Contour interval is 0.2 m/s. Black lines are edges of the Kuroshio "core" according to the definition of Guan (1980) and yellow line, mid-way between the black lines, is our "Kuroshio position." Distances are given relative to the shelf-break (170 m depth). Tick marks indicate beginnings of months.

Figure 10 shows the time series of surface velocity across the C-line with the 0.4 m/s isotachs drawn in black and position in yellow. With this definition, the mean core width over 13 months is 75 km, comparable to the widths of 70-110 km observed by Guan (1980) with GEK measurements. Occasionally, the core (thus defined) disappears altogether, such as early June 2004 (Figure 10). During

these periods (0.88% of the total) we interpolate the position time series. The maximum Kuroshio width was 121 km on 1 March 2004. The position of the Kuroshio core varies between x = 21 km on 27 October 2004 and x = 93 km on 13 August 2004. Based on the 13 month measurements, the mean position is x = 52 ± 2 km (σ = 13 km). The maximum surface velocity varies between 0.31 m/s on 4 June 2004 and 2.02 m/s on 5 January 2004, with an average of 0.78 m/s.

5.3. Mean transport

From the full 23 months of measurements, the mean net absolute transport across the C-line is estimated to be 18.7 ± 0.5 Sv (σ = 4.0 Sv). This is very similar to the mean estimated from the 13 months for which the most reliable shelf transport values are available, 18.5 ± 0.8 Sv (σ = 4.0 Sv). Means are summarized in Table 2.

The mean net transport is about 3 Sv smaller than that reported by Johns et al. (2001) for flow into the ECS east of Taiwan. Their 20-month mean absolute transport from September 1994 to May 1996 is 21.5 Sv. Also their maximum transport (33 Sv) and minimum (12 Sv) are both larger than the extrema observed in this study (Section 4.4). While this discrepancy in the means may reflect interannual variability in Kuroshio strength, it also may indicate that the system is not closed between the Ilan Ridge and the C-line with flow onshelf and/or leakage through the Ryukyu Island chain.

Table 2. Mean transports (Sv) for the two periods December 2002-November 2004 and November 2003-November 2004.

	Averaging period					
	23-month			13-month		
Net absolute transport	18.7	0.5[a]	4.0[a]	18.5	0.8	4.0
Positive absolute transport	[b]			24.0	0.9	4.4
Negative absolute transport in countercurrent	[b]			–0.5	0.1	0.4
Negative absolute transport in recirculation	–5.3	0.3	2.1	–4.9	0.3	1.8
Baroclinic transport[c]	12.8	0.4	2.8	12.6	0.6	2.9
Barotropic transport[c]	1.6	0.2	2.4	1.6	0.3	2.3

[a] Beside each mean, the mean standard error (left) and standard deviation (right) are listed.

[b] Because of the lack of ADCP data during the first 10 months, 23-month values are unavailable.

[c] Baroclinic and barotropic transports (referenced to 700 dbar) are reported only for transport across the 160 km measured by C1 through C6. Using the definitions of Ichikawa and Beardsley (1993), the 13 month mean "baroclinic" and "barotropic" (positive) transports across the entire Cline are 9.9 Sv and 14.1 Sv, respectively; across the 160 km measured by C1 and C6 they are 9.0 Sv and 10.9 Sv, respectively.

In a fine-resolution numerical model Guo et al. (2006) estimated the time-averaged Kuroshio transport onto the shelf, across the 200 m isobath in the ECS between the region east of Taiwan and west of Kyushu to be about 1.46 Sv with maximum (~3 Sv) in fall and minimum (<0.5 Sv) in summer. The model-derived fall onshelf transport is consistent with that inferred from observation (Teague et al., 2003). South of the PN-line, the model's onshelf transport is about 1.6 Sv (Guo et al., 2006). Observations indicate that flow is driven onshelf by a permanent cyclonic eddy north of Taiwan (Su et al., 1990; Wong et al., 2000) and by warm rings and filaments shed by Kuroshio meanders with wavelengths of 100–150 km and periods of 14–20 days propagating over the shelf-slope, observed in satellite infrared images (Qiu et al., 1990) . Further evidence of upwelling onto the shelf related to the propagating meanders comes from towed ADCP measurements

taken just southwest of the PN-line where horizontal confluence over the slope results in upward vertical velocities reaching 2.8 cm/s (Ito et al., 1995).

In addition to the onshelf flow, there may be flow from the ECS into the Philippine Basin through the Ryukyu Islands south of the C-line, perhaps through the Kerama Gap, but the strength, and even the direction, of that flow have not been measured. Model results exhibit a southward leakage of about 0.7 Sv through the Ryukyu Island chain (Guo et al., 2006) south of the PN-line (our C-line). Considering this leakage and onslope transport of the Kuroshio south of the C-line, the difference in mean transports into (from Johns et al. (2001)) and within the ECS (from this study) is reduced to about 0.5 Sv. This difference could be due to interannual variation or errors in estimating the transport over the shelf and slope.

For the period when ADCP data are available on the shoreward edge of the Kuroshio, net absolute transport can be divided into the positive (northeastward) and negative portions of flow (Figure 7). (The negative transport in the recirculation can be determined for the entire 23 months, since it is always within the area measured by the IESs.) The 13-month combined mean negative transport is -5.4 ± 0.3 Sv of which the major part (~91 %) is the recirculation in the eastern side of the channel. The mean positive transport is 24.0 ± 0.9 Sv and shows greater variability ($\sigma = 4.4$ Sv) than the combined negative transport ($\sigma = 1.8$ Sv). Relative to their respective means, however, the negative transport variability is stronger by a factor of 2. Our mean positive transport is similar to that reported by

Ichikawa and Beardsley (1993), 23.7 ± 2.0 Sv (their 'KVT' which is the integral of all positive velocities along the section).

Net absolute transport measured by the CPIESs can also be split into baroclinic (referenced to 700 dbar) and barotropic components. The 23-month mean baroclinic transport measured by C1 through C6 (160 km of the C-line) is 12.8 Sv; the mean barotropic transport is 1.6 Sv. The barotropic component is only 11% of the total mean transport. A fine resolution numerical model (Guo et al., 2003) also predicts a barotropic component (consistent with the definition used here) which is 11% of the total transport. While this small barotropic component would seem to justify the assumption, made in previous ECS studies (e.g., Hinata, (1996)), that the baroclinic transport referenced to 700 dbar calculated from hydrography is a reasonable estimate of total transport, this is not necessarily the case at a particular time. As can be seen from the time series in Figure 4, the baroclinic and barotropic transports vary considerably in time. The two are nearly equal on 18 July, 2004.

In Ichikawa and Beardsley's (1993) study of the positive flow (KVT) of the Kuroshio in the ECS, they defined baroclinic transport (BCKVT) as the positive flow in excess of the depth-averaged flow and the barotropic transport (BTKVT) as the difference between the KVT and the BCKVT. They found that the ratio of barotropic to baroclinic mean flow in the positive transport is about 3:1 near our C-line. According to their definitions, this ratio is 3:2 in our study.

In the above discussions, all transports were calculated by integrating velocity from the surface to the seafloor where the depths were determined by

interpolating the bathymetry data of Choi et al. (2002) onto a straight line running at 38° through the shelf break (28.536°N, 126.723°E). Since the instrument locations deviate slightly from a straight line, this results in some discrepancies between the integration depth and the actual instrument depth. Alternatively, seafloor depths can be estimated by simply linearly interpolating the depth between instruments. This increases the net transport by 0.1 Sv. Amongst the components of the net transport (positive flow, countercurrent and recirculation) the largest effect is in the recirculation whose magnitude is increased by 0.5 Sv.

There is a small component of transport in the ECS which is not captured here, namely that flowing across the 25 km between the southeastern end of the C-line and the Ryukyu Island chain. If the velocity goes to zero linearly from the end of the C-line to the island chain, we are missing about −1.3 Sv of the recirculation transport. Some of this may be southward flowing water that has seeped through the island chain rather than recirculation of Kuroshio water in the ECS.

5.4. Transport variations

Time series of absolute transports across the C-line are shown in Figure 11. The overall maximum net transport was 29.5 Sv on 28 April 2004, followed 38 days later by the overall minimum of 4.0 Sv on 5 June 2004. This may be related to a Kuroshio path transition to the large meander state south of Honshu, Japan, which occurred in July 2004 (Qiu and Chen, 2005, Figure 7a).

Previous studies have reported that Kuroshio transport in the ECS is typically highest in summer and lowest in autumn (Fujiwara et al., 1987 and Hinata, 1996, both reporting transports referenced to 700 dbar; Ichikawa and

Beardsley, 1993, reporting absolute transport). These results were based on snapshots of the transport each season over many years. When the transports from the present study are averaged by season (Figure 12, crosses), the highest transport is indeed in summer (19.6 Sv) but the fall transport (18.3 Sv) is the second lowest; the lowest transport (17.6 Sv) is in spring.

Kawabe (1988) investigated the seasonality of the Kuroshio as it exits the ECS through the Tokara Strait by using sea-level difference from tide-gage data at Naze and Nishinoomote as a proxy for transport. For 19 years (1965-1983) averaged by month, the maximum sea level difference (and by inference the maximum transport) was in July and the minimum in October. However, the character of seasonal signal varied between years and was split into four types by Kawabe: small-amplitude, semiannual, and annual signals with two different phases. Monthly averaged transports for the present study are shown in Figure 12. When monthly mean net absolute transports are calculated as an average of all data values falling within a given month over the two-year period, the highest transport is in August (21.4 Sv) and the lowest is in October (15.9 Sv), which is close to the 19-year mean result reported by Kawabe. The seasonal signal in the data from the current study most closely (though not exactly) resembles Kawabe's semiannual type which has maxima occurring January to April and July to September and minima falling in April to June and October to November.

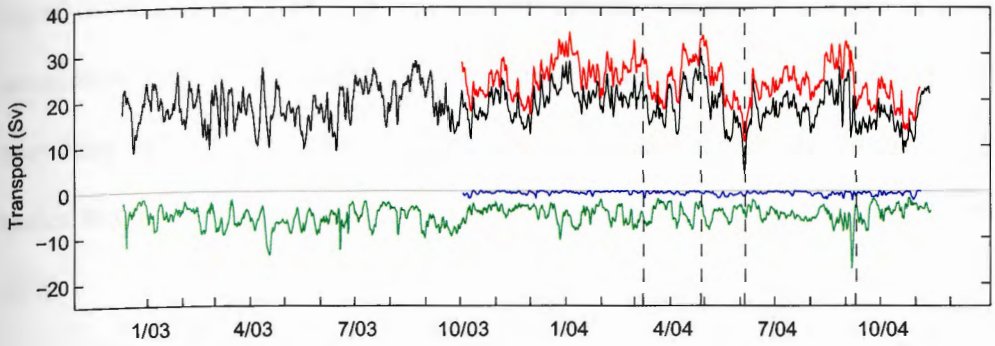

Figure 11. Absolute transports across the C-line.
Red = positive, blue = negative onslope (countercurrent), green= negative offslope (recirculation), black = net. Tick marks denote the beginning of each month. Dashed lines show times of velocity snapshots plotted in Figure 8.

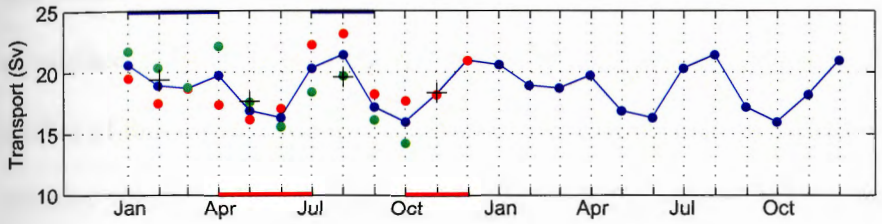

Figure 12. Monthly-mean net absolute transport.
Red dots represent monthly means for the first year; green dots represent monthly means for the second year; blue dots represent monthly means for the two years averaged together (these are plotted and joined over a two year period to show clearly the yearly cycle). + = seasonal (3-month) means for the two years averaged together. Complete data for November and December are only available for the first year. Red and blue bands show periods of Kawabe's (1988) semiannual-type minima and maxima, respectively (see text).

6. Conclusions

Near the PN-line north of Okinawa, we have obtained transport and velocity cross section time series lasting nearly two years. These show net absolute transport varying between about 4 Sv and 30 Sv with a 19 Sv mean value. While the maximum and mean transports are comparable to those reported previously, the minimum transport from this study is lower than any transport from previous studies (Johns et al., 2001 and references therein). The seasonal

signal of transport from this study most closely resembles Kawabe's (1988) semiannual-type with monthly mean transport minima in both years occurring in May/June and October. Surface velocities reach 2 m/s and the Kuroshio position varies through 70 km. These findings are consistent with previous work in the ECS.

The bimodal distribution of the depth of overall velocity maximum has not been reported previously. With occurrence peaks at the surface and 210 m depth, over 13 months, the maximum velocity is deeper than 80 m nearly half of the time and occurs between 80 m and 130 m less than 1% of the time. The existence of a subsurface velocity maximum, has been reported in some, but not all, previous studies of this region. It may be absent in some studies because (1) the subsurface velocity maximum is ephemeral and may not be present in an isolated cross section, (2) a local maximum may be missed if instrument spacing is not sufficiently dense as demonstrated by the analysis of Ichikawa and Beardsley (1993), or (3) the subsurface maximum has a significant barotropic component and may not be represented in the baroclinic field alone. This third possibility is demonstrated in Figure 13 which shows the mean velocity determined from the IES instruments split into the baroclinic shear (relative to 700 dbar) and the barotropic reference velocity.

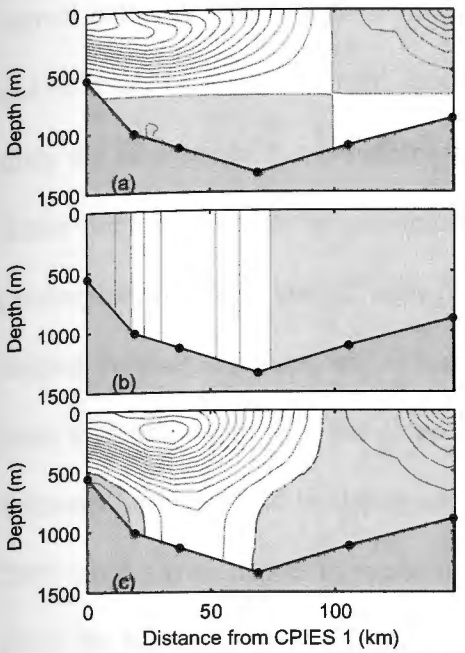

Figure 13. Shear and reference components of mean absolute velocity.
Mean absolute velocity (bottom panel) is split into the shear (top panel) and the reference velocity (middle panel). The bottom panel is the sum of the two upper panels. Negative velocities are shaded grey. Contour interval is 5 cm/s. Black dots = CPIES locations.

Modeling by Nakamura (2005) suggests that the shape of the velocity cross section (e.g., position of surface velocity maximum and rate of velocity decrease with depth), rather than the magnitude of the transport, determines whether most of the Kuroshio leaves the ECS through the northern or southern section of the Tokara Strait. This in turn is thought to influence the large meander state of the Kuroshio south of Japan (Oka and Kawabe, 2003). Nakamura's (2005) study was performed using a shape formula from Xue and Mellor (1993) having a single velocity maximum at the surface. It would be interesting to determine the effect of a subsurface maximum on the modeled path of the Kuroshio as it exits the ECS.

This study confirms the presence of a persistent countercurrent beneath the Kuroshio. Notably the near-bottom velocity at site C2 measured by the CPIES

current sensor is in the downstream direction for only 26% of the 23-month record and its mean value is −3 cm/s More densely spaced instruments are required to study the structure of this countercurrent since it is typically only 20-30 km wide. While there is certainly a countercurrent present, in order to capture (1) non-geostrophic dynamics and (2) dynamics associated with higher-mode or bottom-trapped vertical structure one would need to deploy current sensor moorings at more than one depth over the slope. This study helps determine where such an instrument array should be deployed. H. Nakamura et al., (submitted manuscript, 2008) used current meters to measure velocity in the countercurrent 100 and 200 m above the bottom at four ECS sites in water about 700 m deep. Their observations show velocities and directions were more variable than those recorded by us at site C2, suggesting that their measurements were somewhat shoreward of the persistent countercurrent.

7. Supplement – Periodic variability

Previous researchers have reported that Kuroshio position and transport fluctuate with variability concentrated in specific frequency bands. James et al. (1999) used inverted echo sounders to study Kuroshio meanders in the ECS. During their 14.5-month deployment, they found evidence of persistent meanders with 11-day period and intermittent meanders with 7- and 16-day periods. According to their instability model, the 11-day wave corresponds to the period of the fastest growing instability.

Variability of the inflow to the ECS east of Taiwan during a 20-month deployment of moored ADCPs is reported by Johns et al. (2001). The most energetic spectral peak is at 3-4 month period (~100 days) with secondary peaks at 35- and 15- day period. The 100-day peak is thought to be related to the arrival of mesoscale eddies from the ocean interior (Zhang et al., 2001, Yang et al., 1999). While causes of the 15-day variability are not discussed, Johns et al. (2001) noted that the transport below the main thermocline showed this peak more strongly than the transport above this level.

Periodic variability of the Kuroshio in the East China Sea during our instrument deployment is examined with (1) spectral analysis of transport and position and (2) complex empirical orthogonal function (CEOF) analysis of τ. Spectral analyses are performed for the 13-month time period during which data from the ADCP at site A2 are available (October 2003 – November 2004) since the transport calculations and position estimates are most reliable during this period. CEOF is analysis is performed using the the entire 23-month τ records. Results are compared with previous studies in the region and with ECS wind data.

7.1 Spectra

As described in Section 5, transport crossing the C-line in the ECS is composed of a region of positive flow (towards the northeast) close to the shelf break and a deep recirculation (towards the southwest) between the positive flow and the Ryukyu Islands. In addition, there is a persistent countercurrent on the slope beneath the Kuroshio. However, since the countercurrent is narrow relative

to the instrument spacing, its transport is small and not well-resolved, so it is not discussed further here.

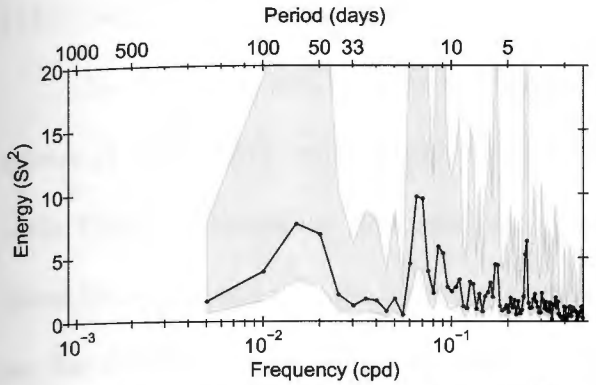

Figure 14. Variance preserving spectrum of net absolute transport.
Spectral analysis was performed using a Hanning window of length of 199 days with a 50% overlap. Shaded area shows the 95% confidence interval.

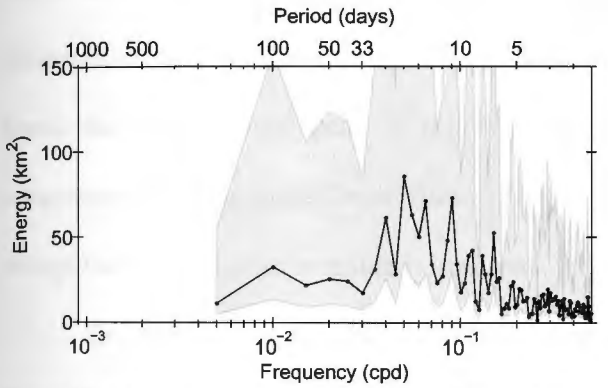

Figure 15. Variance preserving spectrum of Kuroshio position.
Analysis parameters as in Figure 14..

Figure 14 shows spectral peaks in net absolute transport at 60 days (49.8-66.3 days), 15 days (14.2-15.3 days), and 11 days (11.1-11.7 days). Figure 15 shows the variance preserving spectrum of position (defined as the center between the 0.4 m/s isotachs as in Section 5.2). Most of the energy is between 10- and 30-day periods. Kuroshio position and net transport are only weakly positively correlated ($r = 0.24$ which is statistically significant at the 95% confidence limit). Coherence calculations (not plotted), show that while position and net transport are

not coherent at the 60- or 15-day periods, they are coherent near 11 days (squared coherence reaches 0.91 at 10.5-day period with transport leading position by 115.1°, which corresponds to 3.4 days)

Net transport can be split into various components. Figure 16 shows spectra of the positive (panel a) and recirculation (panel b) components of flow, while Figure 17 shows the flow split into upper layer (panel a) and deep layer (panel b) components with the interface taken at 200 dbar. From these spectra we see that the 60-day peak is most pronounced in the positive flow and in the upper layer; it is barely present in the recirculation, and completely absent in the flow below 200 dbar. In contrast, the 15-day peak is the dominant peak in the recirculation and the deep flow. This is consistent with Johns et al. (2001) who found that their 15-day peak in inflow through the East Taiwan Channel was concentrated in the lower layer flow. The 11-day peak, is small in all spectra except the recirculation in which it is absent.

In order to isolate the variability occurring at these spectral peaks and determine if their amplitudes vary in time, transports are band-pass filtered (Figure 18). In each case, the band-passing is done on that component of the flow in which a given peak is most pronounced: net transport is band-passed to isolate the 11-day peak (panel a), lower layer transport is band-passed to isolate the 15-day peak (panel b), and positive transport is band-passed to isolate the 60-day peak (panel c).

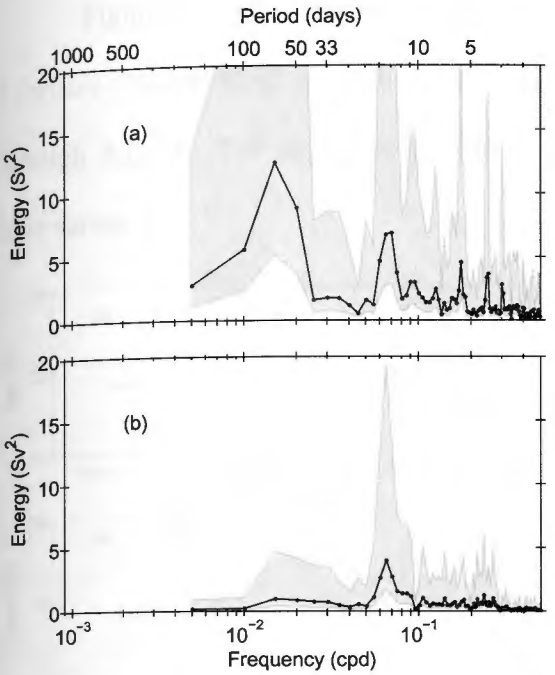

Figure 16. Variance preserving spectra of positive and recirculation transports.
Panel (a) is for positive transport and panel (b) is for the recirculation. Analysis parameters as in Figure 14.

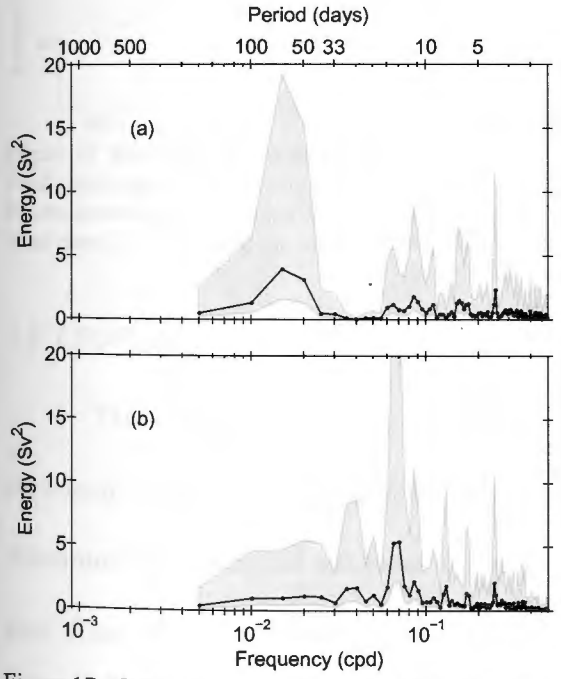

Figure 17. Variance preserving spectra of shallow and deep transports.
Panel (a) is for net absolute transport above 200 dbar and panel (b) is for net absolute transport below 200 dbar. Analysis parameters as in Figure 14.

Figure 18 shows that the 11-day signal is most pronounced during 2004 February through April, while the 15-day signal is most pronounced during March through August. The 60-day variability is pronounced throughout the 13-month time series.

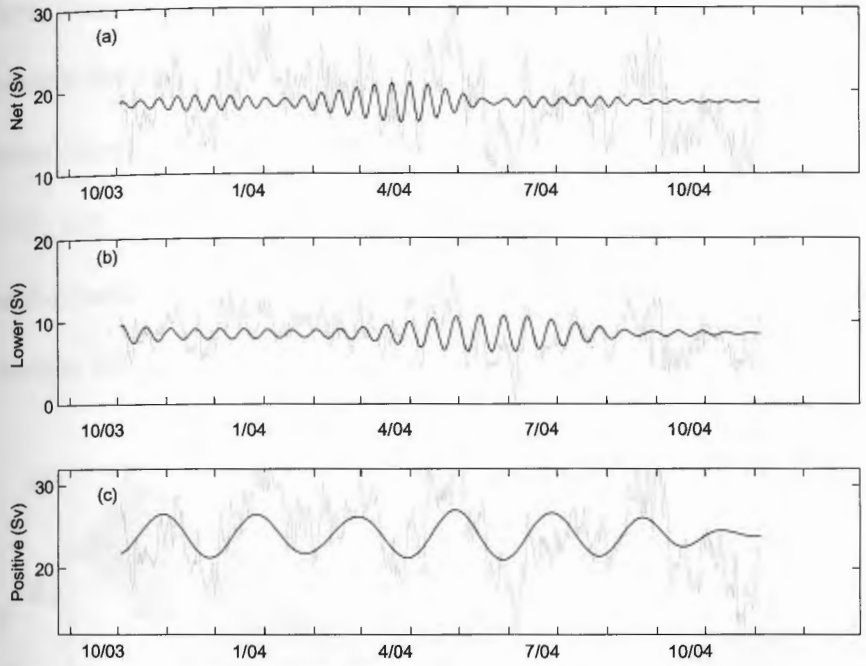

Figure 18. Band-passed transport time series.
In all panels gray line is 2-day low-pass filtered transport and black line is band-passed signal. Panels show (a) net transport with 11-day band-pass (10-12), (b) lower layer transport with 15-day band-pass (13.5-16), and (c) positive transport with 60-day band-pass (45-70).

7.2 CEOF analysis

The 11-day and 60-day spectral peaks are further investigated using τ measured by the P-line instruments in conjunction with the C-line instruments to determine the horizontal structure of these waves. For each wave, we first band-pass filter the 11 τ records. Then we use CEOF analysis of the band-passed records to diagnose the waves, allowing for the possibility that they are propagating rather than standing waves.

7.2.1 CEOF – 11-day wave

For 11-day band-passed τ, magnitude, phase, and amplitude time series of the first CEOF mode are plotted in Figure 19. For this band, 86.6% of the variance is described by the first mode. The magnitude is largest in the region of positive flow, near the shelf break. Phase propagation there is in the direction of flow, towards the northeast. In the recirculation region, amplitude is very low and hence phase estimates are unreliable. Maxima in the amplitude time series occur in April 2003, July 2003, and April 2004. The April 2004 maximum is consistent with the band-passed net transport time series which does not include times prior to October 2003 (Figure 18, panel a).

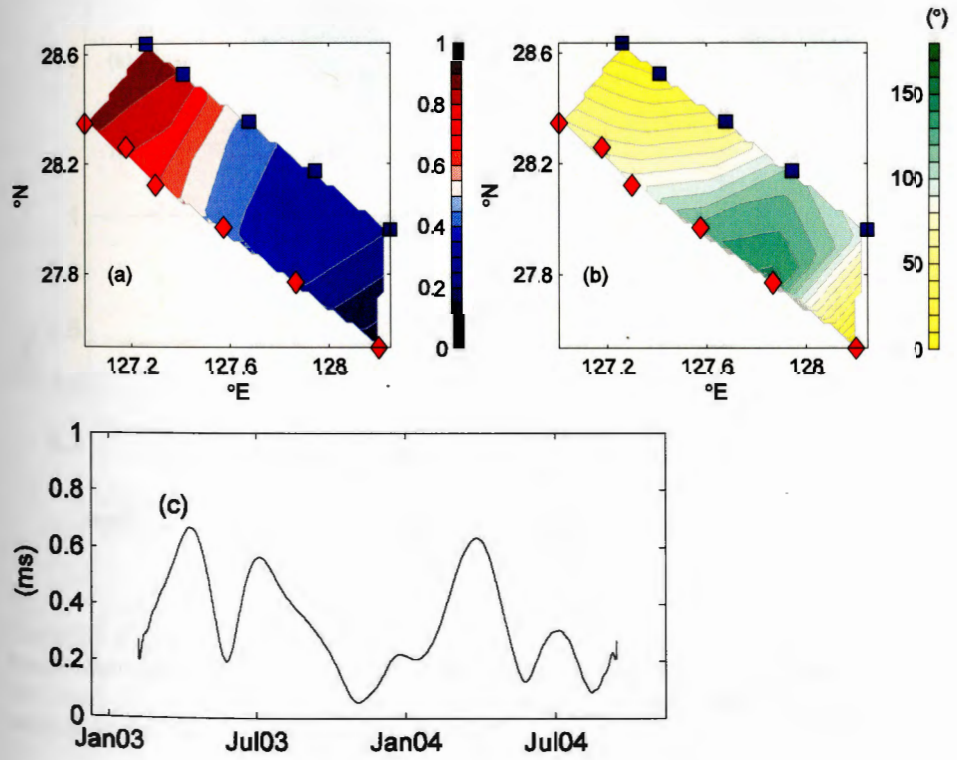

Figure 19. 1st mode CEOF of 11-day (10-12) τ.
Panels show (a) magnitude, (b) phase, with propagation from high to low values, and (c) amplitude time series. Locations of CPIESs (red diamonds) and PIESs (blue squares) are shown. Tick marks denote beginnings of designated months.

7.2.2 CEOF – 60-day wave

For 60-day band-passed τ, the first CEOF mode (Figure 20) describes 81.2% of the variance. The first-mode magnitude is largest along the shelf edge and the direction of phase propagation is mainly towards the shelf. The 60-day wave grows in amplitude as it propagates towards the shelf. The amplitude time series (panel c) is consistent with the band-pass filtered time series in Figure 18 panel (c). Both indicate that 60-day waves were energetic in 2004 May.

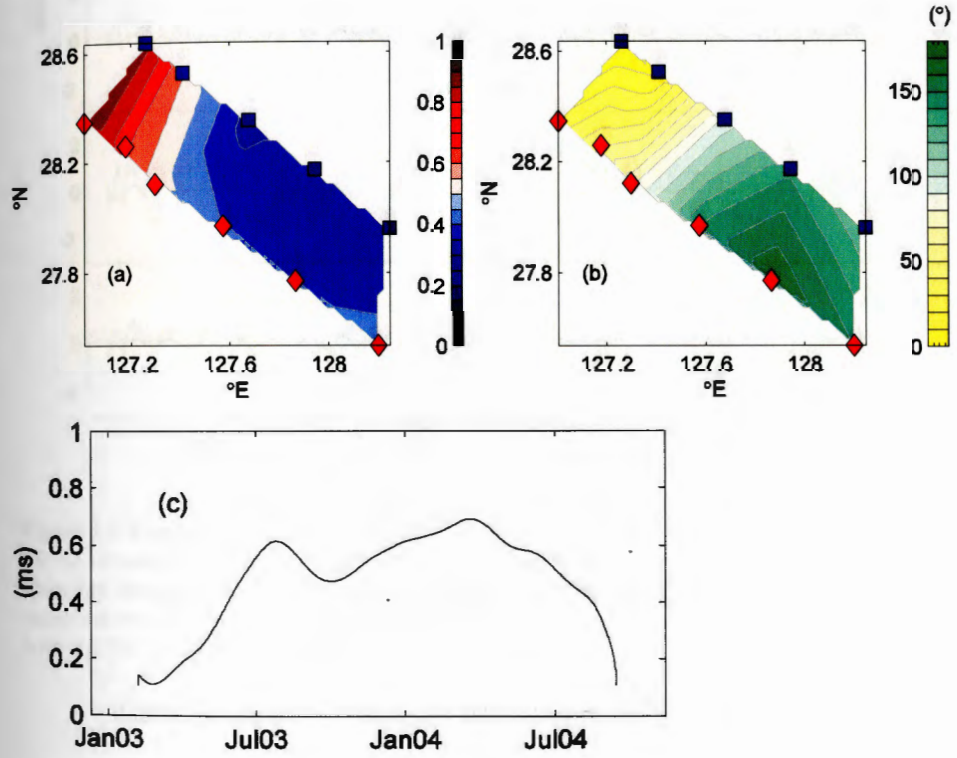

Figure 20. 1st mode CEOF of 60-day (45-70) τ.
Panels show (a) magnitude, (b) phase, with propagation from high to low values, and (c) amplitude time series. Locations of CPIESs (red diamonds) and PIESs (blue squares) are shown. Tick marks indicate beginnings of designated months.

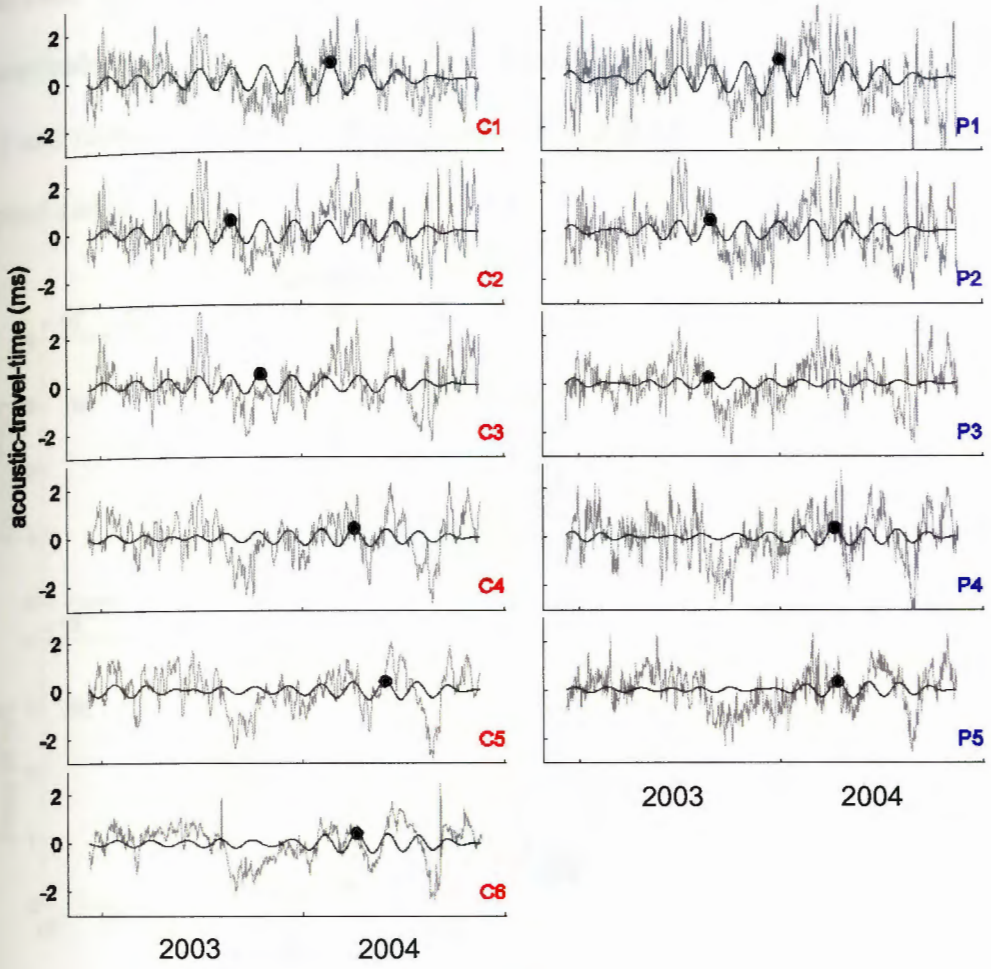

Figure 21. τ records.
CPIESs shown in left column and PIESs in right column.
Two-day low-pass filtered records are shown in gray with 60 day (45-70) band-passed signals superimposed in black. For each record, the maximum in the band-passed record is highlighted with a filled circle (see text).

While phase propagation of the 60-day wave is directed towards the shelf, energy propagation is different. Figure 21 shows τ records for the individual instruments. C-line instruments (CPIES) are plotted on the left and P-line instruments (PIES) are plotted on the right. Superimposed on the 2-day lowpass filtered records (gray) are 60-day band-passed records (black). Energy propagation (or group speed) of a wave is in the direction of propagation of wave

packets. The envelope of the wave packet is tracked by identifying the maximum amplitude of this envelope (black solid dots). The energy appears first at C2 and P2 and radiates outward from there. Between C2 and C4 (or P2 and P4) the group speed and phase speed oppose one another.

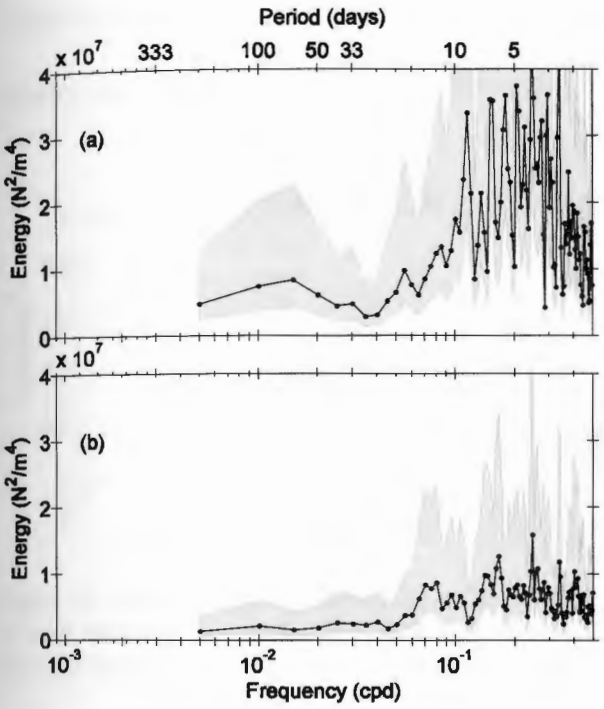

Figure 22. Variance preserving spectra of area-integrated wind stress.
Panel (a) shows y wind stress and (b) shows x wind stress. Area of integration is over the ECS shelf region 26°N - 33°N, 121°E - 125°E. Analysis parameters are as in Figure 14.

The cause of the 60-day variability in transport remains an enigma. No 60-day peak was identified in transport flowing into the ECS east of Taiwan by Johns et al. (2001) or in dynamic height variability inside the ECS near the PN-line by James et al. (2001) in different years. The 60-day variability may be related with ECS wind. Figure 22 shows variance preserving spectra of wind stress integrated over the ECS shelf in the y- (panel a) and x- (panel b) directions. While most of the variability is at short periods (< 10-day period), there is long period variability

in the area-integrated *y*-wind stress with a peak near 60-days, perhaps related to the Madden-Julian oscillation. Figure 23 shows the squared-coherence between the area-integrated wind stress curl and τ at instrument site C1. The squared-coherence at 60-day period is 0.66 which is significant at the 95% level. This coherence suggests that the winds may play a role in generating the 60-day wave locally, but the mechanism remains uncertain.

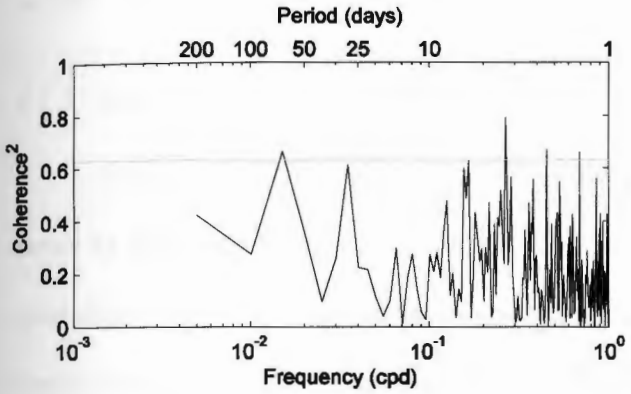

Figure 23. Coherence-squared between τ at C1 and the area integrated wind stress curl. Area of integration is over the ECS shelf region 26°N - 33°N, 121°E - 125°E. Gray horizontal line shows the 95% confidence level (0.63).

Finally, we note the spectrum of transport crossing the C-line does not exhibit a ~100-day peak. It is not known why the ~100-day peak in transport detected by Johns et al. (2001) in 1994-1996 at the Kuroshio's entrance to the ECS is not seen in our data. Either there was relatively little mesoscale eddy activity east of Taiwan during our instrument deployment, or the ~100 day signal is attenuated once the Kuroshio enters the ECS. The relationship between Kuroshio transport and eddies is investigated further in Chapter 2.

8. Appendix: Extrapolation methods

8.1. Spatial extrapolation by vertical extension

The first method for spatial extrapolation of the ADCP data uses a GEM lookup table (with 150 m streamfunction Ψ_{150}, rather than τ_{700}, as the lookup index) to obtain vertical extensions of the velocity profiles in the manner described below.

8.1.1. Input data

From the ADCP A1 and A2 time series, one can extract V_{150}, the time series of absolute velocity at 150 m depth. (At A1, measurements of V_{150} were used directly; at A2, V_{150} was determined by extrapolation from 179 m to 150 m depth using a spline fit to the measured velocity profile.) Likewise, time series of V_{150} at C1-C6 are known from OI mapping of τ_{ref} and bottom pressure data (leveled with near-bottom current measurements). At each CPIES site the time series of absolute streamfunction at 150 m, Ψ_{150}, can be calculated:

$$\Psi_{150} = \frac{\Phi_{700}^{150}}{f} + \frac{P}{\rho f}, \tag{5}$$

where $\Phi_{700}^{150} = -\int_{700}^{150} \delta \, dp$ is the geopotential anomaly of the 150 dbar surface relative to the 700 dbar surface. This is readily determined from τ_{ref} using the GEM lookup table. The second term on the right-hand side of Equation 5 represents change in mass of the water column above the 700 dbar level. This is determined directly from the leveled pressure-sensor data.

The absolute velocity normal to the line of instruments is given by the gradient of the absolute streamfunction:

$$\frac{\partial \Psi_{150}}{\partial x} = -V_{150}. \tag{6}$$

Using V_{150} at all sites and Ψ_{150} at the CPIES sites as input data, OI mapping is used to determine the time series of Ψ_{150} at sites A1 and A2 as described next.

8.1.2. Mapping the mean field and the residual

The OI mapping is done in two steps. Streamfunction and velocity are decomposed into the time-mean and a residual:

$$\Psi_{150}(x,t) = \overline{\Psi}_{150}(x) + \Psi'_{150}(x,t) \tag{7}$$

$$V_{150}(x,t) = \overline{V}_{150}(x) + V'_{150}(x,t), \tag{8}$$

where the overbar represents a time average over the duration, T, of the measurements.

The time-mean fields are mapped using a relatively large correlation length scale (85 km). The resulting mean fields are plotted in Figure 24. Note that the velocity plot is simply the first derivative of the streamfunction plot.

In the second OI step, the residual is mapped using a shorter correlation length scale of 35 km. This correlation length scale was determined from a plot (not shown) of correlation coefficient versus distance for pressure data with the common-mode signal removed. At each time, t, when $\Psi'_{150}(x,t)$ has been

determined, the mean field, $\overline{\Psi}_{150}(x)$, is added to produce, by the first of these two equations, the time series of absolute streamfunction, $\Psi_{150}(x,t)$.

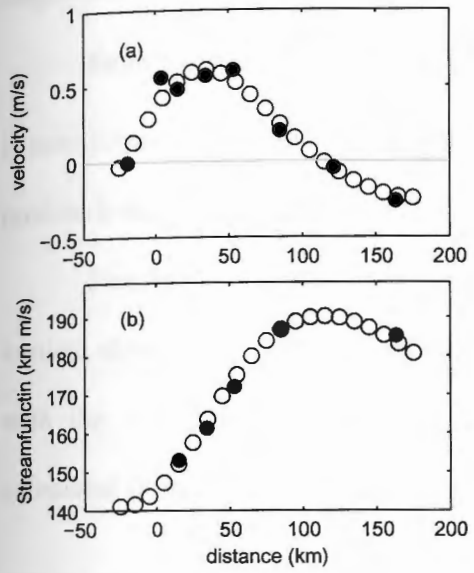

Figure 24. OI map of 150 m mean fields.
Panels show: (a) velocity, (b) streamfunction. Closed circles are input data, open circles are OI mapped data.

8.1.3. Lookup table

The next step in determining the velocity profiles at sites A1 and A2 is to relate the streamfunction to the specific volume anomaly, δ. The absolute streamfunction can be separated into baroclinic and barotropic components:

$$\Psi_{150} = \Psi_{bc} + \Psi_{bt}\,. \tag{9}$$

Assuming $\Psi_{150} \approx \Psi_{bc}$ gives

$$\Phi_{700}^{150} \approx f\,\Psi_{150}\,. \tag{10}$$

This assumption is a potential source of error, but its validity was verified by good agreement between the shapes of those portions of the velocity profiles measured by the ADCPs (from 30 to 152 dbar and 179 to 285 dbar for sites A1 and A2 respectively) with those calculated by the procedure described here.

From hydrographic data, a GEM lookup table relating δ profiles and Φ_{700}^{150}, is constructed. Using this lookup table, a time series of specific-volume-anomaly profiles is determined from the streamfunction time series.

Finally, the horizontal gradients in δ profiles were used to determine vertical shears of velocity at sites A1 and A2. These shears were then referenced with the V_{150} values, and the transport over the upper slope and shelf was calculated (Figure 5, blue line) by integrating the velocities.

8.2. Spatial extrapolation by horizontal smoothing

The second method for spatial extrapolation of the ADCP profiles assumes that velocity varies smoothly along horizontal surfaces between C1 and A1, separated by about 41 km. The velocity profile at C1 was estimated from the CPIES, as described in Section 3.1.2. At A1 a mixed layer in the upper 30 m of the water column was assumed and the shallowest velocity measurement was simply projected up to the surface. Velocity measurements at A1 together with velocity and pressure at the CPIES sites were used as input to an OI mapping of the absolute stream function, Ψ_i, at each level, i, in 10 m increments between 150 m depth and the surface. The OI procedure was done in two steps: first the mean fields and then the residuals (at 12-hour intervals) were mapped. Once Ψ_i was mapped over the upper slope and shelf, the horizontal Ψ_i gradient was used to

calculate an absolute velocity time series at A2 for that level. The A2 velocities calculated at each level between 150 m and the surface were then combined with the measured A2 velocities to obtain complete profiles. A2 velocities between 180 m (highest level measured by the ADCP) and 150 m (lowest level determined by horizontal smoothing) were linearly interpolated to avoid vertical discontinuity in the velocity profiles. The resulting transport time series is plotted in Figure 5 (green line).

8.3. Temporal extrapolation using an analytical shape formula

James et al. (1999) developed an analytical shape formula, based on that of Xue and Mellor (1993), to describe the Kuroshio basic state velocity cross section, $V_c(x,z)$:

$$V_c(x,z) = V_o \exp(z/Z_e) \exp\left(\frac{x - X_{co} - z/Z_m}{L}\right)^2. \qquad (11)$$

They empirically determined the constants (V_o, Z_e, X_{co}, Z_m, L) by fitting to a velocity cross section determined from hydrography referenced with surface ADCP data. Using this formula, an instantaneous Kuroshio velocity cross section, V(x,z,t), can be approximated by shifting this basic state shape horizontally a distance $x_o(t)$ and multiplying it by a strength factor, S(t).

The position and strength of the Kuroshio were determined as follows. At each time, t, $x_o(t)$, and S(t), were chosen such that $[V_{LP}(x,z,t) - S(t)\cdot V_c(x-x_o(t), z)]^2$ was minimized where V_{LP} is the 20-day lowpass-filtered observed velocity (shorter period fluctuations were not well reproduced). This was carried out for the region between x = 35 km (location of CPIES 1) and x = 100 km near the edge

of the recirculation and between the surface and 400 dbar. Once the location and strength were determined for a given time in this manner, they were used with the shape formula and constants from James et al. (1999) to estimate velocities over the upper slope and shelf: $V_e(x,z,t) = S(t) \cdot V_c(x - x_o(t), z)$, $-15 \text{ m} \leq x \leq 35 \text{ km}$. The velocities were integrated to determine the net transport over the upper slope and shelf.

9. List of References

Andres M., K.-I. Chang, C.-S. Hong, H. Ichikawa, D.-K. Lee, J.-H. Lee, B.-H. Lim, D.A. Mitchell, J.-H. Park, W. Teague K. Tracey, D.R. Watts, and M. Wimbush (2005), East China Sea Kuroshio 2002-2004 data report, *GSO Technical Report No. 2005-02*, Graduate School of Oceanography, University of Rhode Island.

Bingham F.M., and L.D. Talley (1991), Estimates of Kuroshio transport using an inverse technique, *Deep-Sea Res., 38*(S1), S21-S43.

Book, J.W., M. Wimbush, S. Imawaki, H. Ichikawa, H. Uchida, and H. Kinoshita (2002), Kuroshio temporal and spatial variations South of Japan determined from inverted echo sounder measurements, *J. Geophys. Res., 107*, doi: 10.1029/2001JC000795.

Bretherton, F.P., R.E. Davis, and C.B. Fandry (1976), A technique for objective analysis and design of oceanographic experiments applied to MODE-73, *Deep-Sea Res., 23,* 559–582.

Choi, B.H., K.O. Kim, and H.M. Eum (2002), Digital bathymetric and topographic data for neighboring seas of Korea, *J. Korean Soc. Coastal and Ocean Engrs., 14*(1), 41-50 (in Korean).

Fujiwara, I., Y. Hanzawa, I. Eguchi, and K. Hirano (1987), Seasonal oceanic conditions on a fixed line in the East China Sea, *Oceanogr. Mag., 37*, 37-46.

Guan, B. (1980), Some results from the study of the variation of the Kuroshio in the East China Sea, In *The Kuroshio IV*, Saikon Publishing Co. Tokyo, 897-911.

Guo, X., H. Hukuda, Y. Miyazawa, and T. Yamagata (2003), A triply nested ocean model for simulating the Kuroshio – Roles of horizontal resolution on JEBAR. *J. Phys. Oceanogr., 33*, 146-169.

Guo, X., Y. Miyazawa, and T. Yamagata (2006), The Kuroshio onshore intrusion along the shelf break of the East China Sea: The origin of the Tsushima Warm Current, *J. Phys. Oceanogr., 36*, 2205-2231.

He, Y.R., D.R. Watts, and K.L. Tracey (1998), Determining geostrophic velocity shear profiles with IESs, *J. Geophys. Res., 103*(C3), 5607-5622.

Hinata, T. (1996), Seasonal variation and long-term trends of the oceanographic conditions along a fixed hydrographic line crossing the Kuroshio in the East China Sea, *Oceanogr. Mag., 45*, 9-32.

Ichikawa, H., and R.C. Beardsley (1993), Temporal and spatial variability of volume transport of the Kuroshio in the East China Sea, *Deep-Sea Res. I, 40*(3), 583-605.

Ichikawa, H., H. Nakamura, A. Nishina, and M. Higashi (2004), Variability of north-eastward current southeast of northern Ryukyu Islands. *J. Oceanogr., 60*, 351-363.

Ito T., A. Kaneko, H. Furukawa, N. Gohda, and W. Koterayama (1995), A structure of the Kuroshio and its related upwelling on the East China Sea shelf slope. *J. Oceanogr., 51*, 267-278.

James, C., M. Wimbush, and H. Ichikawa (1999), Kuroshio meanders in the East China Sea, *J. Phys. Oceanogr., 29*, 259-272.

Johns, W.E., T.N. Lee, D. Zhang, and R. Zantopp (2001), The Kuroshio east of Taiwan: moored transport observations from the WOCE PCM-1 array, *J. Phys. Oceanogr., 31*, 1031-1053.

Kawabe, M. (1988), Variability of Kuroshio velocity assessed from the sea-level difference between Naze and Nishinoomote, *J. Oceanogr. Soc. Jpn., 44*, 293-304.

Kawabe, M. (1995), Variations of current path, velocity, and volume transport of the Kuroshio in relation with the large meander, *J. Phys. Oceanogr., 25*(12), 3103-3117.

Lim, B.H. (2008), Near 60-day variation in the Kuroshio observed in the East China Sea, M.Sc. thesis, 44 pp., Seoul Natl. Univ., Seoul, Korea.

Macdonald, A.M., T. Suga, and R.G. Curry (2001), An isopycnally averaged North Pacific climatology, *J. Atmos. Oceanic Technol., 18,* 394-420.

Meinen, C.S. (2001), Structure of the North Atlantic current in stream-coordinates and the circulation in the Newfoundland basin, *Deep-Sea Res. I, 48*(7), 1553-1580.

Nakamura, H. (2005), Numerical study on the Kuroshio path states in the northern Okinawa Trough of the East China Sea, *J. Geophys. Res.*, 110, C04003, doi:10.1029/2004JC002656.

Nitani, H. (1972), Beginning of the Kuroshio. In: *Kuroshio, Physical Aspects of the Japan Current*, H. Stommel and K. Yoshida, editors, University of Washington Press, Seattle, pp. 129-164.

Park, J.-H., D.R. Watts, K.L. Tracey, and D.A. Mitchell (2005), A multi-index GEM technique and its application to the southwestern Japan/East Sea, *J. Atmos. Ocean. Tec., 22*, 1282-1293.

Park, J.-H., M. Andres, P. Martin, M. Wimbush, and D.R. Watts (2006), Second-mode internal tides in the East China Sea deduced from historical hydrocasts and a model, *Geophys. Res. Lett., 33*(5), L05602, doi:10.1029/2005GL024732.

Oka, E., and M. Kawabe (2003), Dynamic structure of the Kuroshio south of Kyushu in relation to the Kuroshio path variations, *J. Oceanogr., 59*, 595-608.

Qiu, B., and S. Chen (2005), Variability of the Kuroshio Extension jet, recirculation gyre, and mesoscale eddies on decadal time scales, *J. Phys. Oceanogr., 35*, 2090–2103 doi: 10.1175/JPO2807.1.

Qiu, B., T. Toda, and N. Imasato (1990), On Kuroshio front fluctuation in the East China Sea using satellite and in situ observation data, *J. Geophys. Res., 95*(C10), 18191-18204.

Rodrigues, R. (2004), An observational and numerical study of the South Atlantic circulation. University of Rhode Island, Graduate School of Oceanography, Ph.D. dissertation.

Sibuet, S.-K. Hsu, C.-T. Shyu, and C.-S. Liu (1995), Structural and kinematic evolutions of the Okinawa Trough backarc basin, In: *Backarc Basins Tectonics and Magmatism*, B. Taylor, editor, Plenum Press, New York, 343-377.

Su, J.L., B.X. Guan, and J.Z. Jiang (1990), The Kuroshio.Part I. Physical Features, *Oceanogr. Mar. Biol. Ann. Rev., 28*, 11-71.

Sun, C., and D.R. Watts (2001), A circumpolar gravest empirical mode for the Southern Ocean hydrography, *J. Geophys. Res., 106*(2), 2833-2855.

Teague, W.J., G.A. Jacobs, D.S. Ko, T.Y. Tang, K.-I. Chang, and M.-S.Suk (2003), Connectivity of the Taiwan, Cheju and Korea Straits, *Continental Shelf Res., 23*, 63-77.

Watts, D.R., K.L. Tracey, and A.I. Friedlander (1989), Producing accurate maps of the Gulf Stream thermal front using objective analysis, *J. Geophys. Res. 94*(C6), 8040-8052.

Willeford, B.D. (2001), Using stream function coordinates to study the circulation and water masses of the North Pacific, University of Rhode Island, Graduate School of Oceanography, M.S. thesis.

Wong, G.T.F., S.-Y. Chao, Y.-H. Li, and F.-K. Shiah (2000), The Kuroshio edge exchange processes (KEEP) study - an introduction to hypotheses and highlights, *Continental Shelf Res., 20*, 335-347.

Xue, H., and G.L. Mellor (1993), Instability of the Gulf Stream front in the South Atlantic Bight, *J. Phys. Oceanogr., 23*, 2326-2350.

Yamashiro, T., and M. Kawabe (2002), Variations of the Kuroshio axis south of Kyushu in relation to the large meander of the Kuroshio, *J. Oceanogr. 58*, 487-503.

Yuan, Y., A. Kaneko, J. Su, X. Zhu, Y. Liu, N. Gohda, and H. Chen (1998), The Kuroshio east of Taiwan and in the East China Sea and the currents east of Ryukyu Islands during early summer of 1996, *J. Oceanogr., 54*, 217-226.

Zhang, D., T.N. Lee, W.E. Johns, C.-T. Liu, and R. Zantopp, 2001. The Kuroshio east of Taiwan: Modes of variability and relationship to interior ocean mesoscale eddies, *J. Phys. Oceanogr., 31*, 1054-1074.

Zhu, X.-H., I.-S. Han, J.-H. Park, H. Ichikawa, K. Murakami, A. Kaneko, and A. Ostrovskii (2003), The northeastward current southeast of Okinawa Island observed during November 2000 to August 2001, *Geophys. Res. Lett., 30*(2), 1071, doi:1029/2002GL015867.

Chapter 2

Study of the Kuroshio/ Ryukyu Current system based on satellite altimeter and *in situ* measurements

10. Abstract

Data from satellite altimeters and from a 13-month deployment of *in situ* instruments are used to determine an empirical relationship between sea-level anomaly difference (ΔSLA) across the Kuroshio in the East China Sea (ECS-Kuroshio) and net transport near 28°N. Applying this relationship to the altimeter data, we obtain a 12-year time series of ECS-Kuroshio transport crossing the C-line (KT). The resulting mean transport is 18.7 ± 0.2 Sv with 1.8 Sv standard deviation. This KT is compared with a similarly-determined time series of net Ryukyu Current transport crossing the O-line near 26°N southeast of Okinawa (RT). Their mean sum (24 Sv) is less than the mean predicted Sverdrup transport. These KT and RT mean-flow estimates form a consistent pattern with historical estimates of other mean flows in the East China Sea/Philippine Basin region. While mean KT is larger than mean RT by a factor of almost 4, the amplitude of the KT annual cycle is only half as large. At the 95% confidence level the transports are coherent at periods of about 2 years and 100-200 days, with RT leading KT by about 60 days in each case. At the annual period, the transports are coherent at the 90% confidence level with KT leading RT by 5 months. While the bulk of the Kuroshio enters the ECS through the channel between Taiwan and Yonaguni-jima, analysis of satellite altimetry maps, together with the transport time series, indicates that the effect of mesoscale eddies is transmitted to the ECS

via the Kerama Gap southwest of Okinawa. Once the effect of these eddies is felt by the ECS-Kuroshio at 28°N, it is advected rapidly to the Tokara Strait.

11. Introduction

According to Sverdrup theory, the North Pacific subtropical gyre transports water southward in response to the integrated wind stress curl. Convergence in this southward flow feeds the broad North Equatorial Current (NEC) which, in the mean, carries about 60 Sv westward across 137°E, roughly in accord with the transport expected from the basin-wide North Pacific wind stress curl (Qiu and Joyce, 1992). This current bifurcates east of the Philippines. The Kuroshio is the branch of the bifurcation that returns water northward as a swift western boundary current (Nitani, 1972). On reaching Taiwan, most of the Kuroshio enters the East China Sea (ECS) over a ~775 m deep sill (Choi et al., 2002), called the Ilan Ridge, between Taiwan and Yonaguni-jima, the southernmost island of Japan's Ryukyu Island chain. This current, the ECS-Kuroshio, exits the ECS through the Tokara Strait. A branch, the Ryukyu Current, sometimes flows on the seaward side of the Ryukyu Islands (Yuan et al., 1998; Kawabe, 2001). The Ryukyu Current is ephemeral near the southern-most Ryukyu Islands (e.g., Yuan et al., 1991; Yuan et al., 1994; Yuan et al., 1996) and it is unknown how much of it comes from the Kuroshio east of Taiwan and how much from the ocean interior. There is evidence that the Ryukyu Current intensifies as it flows northeastward along the Ryukyu Islands (e.g., You and Yoon, 2004; Ichikawa et al., 2004; Nagano et al., 2007, Zhu et al., 2008b; Nagano et al., 2008). South of Kyushu, the Ryukyu Current joins the

ECS-Kuroshio as it leaves the Tokara Strait. Finally, the Kuroshio leaves the Japan coast as an eastward flowing free jet, the Kuroshio Extension, closing the North Pacific subtropical gyre.

The ocean regions east of Taiwan and the Ryukyu Islands are characterized by the frequent arrival of mesoscale eddies from the ocean interior at intervals of about 100 days (Yang et al., 1999; Zhang et al., 2001; Konda et al., 2005). These eddies originate in a zonal band of high eddy kinetic energy between 19°N and 25°N and may be generated by baroclinic instability associated with the vertical shear between the shallow, eastward flowing Subtropical Countercurrent (STCC) and the underlying portion of the NEC (Qiu, 1999). There is also evidence that some eddies may be generated by the passage of typhoons (e.g., Lee et al., 2003). Typical eddies, which can be cyclonic or anticyclonic, are about 500 km in diameter (Roemmich and Gilson, 2001) with westward propagation speeds of 7-8 cm/s (e.g., Konda et al., 2005), temperature anomalies of ±3°C, flow velocities around 20-40 cm s^{-1} and surface height anomalies around 20-30 cm (e.g., Zhu et al., 2008a). Eddies hamper the evaluation of ECS-Kuroshio and Ryukyu Current mean transports from isolated hydrographic sections. Moreover, when these eddies arrive off Taiwan, they may change the proportions of transport flowing in the ECS-Kuroshio and the Ryukyu Current (Yang et al., 1999; Zhang et al., 2001; Liu et al., 2004).

Previous studies of Kuroshio transport suggest that the annual range of variability on entering the ECS is less than 10 Sv (Lee et al., 2001, and references therein), which is small compared to that expected from non-topographic, time-

dependent Sverdrup theory. The seasonally varying wind stress curl integrated over the Philippine Basin predicts a 20 Sv peak-to-peak annual range in Sverdrup transport (from Lee et al., 2001 based on COADS data integrated from 125°E to 142°E) and that integrated over the entire North Pacific predicts about 50 Sv annual variation in transport (Sakamoto and Yamagata, 1996; their Fig. 1 based on climatological winds of Hellerman and Rosenstein, 1983). An additional enigma is that North Pacific winds are strongest in winter (e.g., Hellerman and Rosenstein, 1983) but the highest ECS-Kuroshio transport is typically observed in summer (e.g., Ichikawa and Beardsley, 1993).

A significant portion of the Sverdrup return flow may be carried as a western boundary current on the eastern side of the Ryukyu Islands (Hautala et al., 1994; Lee et al., 2001). Lee et al. (2001) suggest such a scenario based on a 20-month time series of flow entering the ECS and the Sverdrup transport calculated from integrated wind stress curl over the Philippine Basin. With their observed 4 Sv annual variation of transport entering the ECS, they suggest that the Ryukyu Current should carry about 12 Sv in the mean, with a 16 Sv (peak-to-peak) annual range. Others suggest that, while Sverdrup flow does prevail in the interior (Kagimoto and Yamagata, 1997), the reduced seasonal signal in the ECS arises from "JEBAR rectification" (Sakamoto and Yamagata, 1996; Sakamoto, 2005).

Time series of velocity structure and transport of the ECS-Kuroshio north of Okinawa were calculated from November 2003 - November 2004 using data from 11 inverted echo sounders (IESs) and 2 ADCPs (Andres et al., 2008). Here we employ a technique similar to that of Zhu et al. (2004) and Imawaki et al.

(2001a) to determine an empirical relationship between this ECS-Kuroshio transport and satellite altimeter data, in order to extend the transport time series using the altimeter data. We analyze the long period (> 60 days) variability in this extrapolated time series and compare ECS-Kuroshio transport with the time series of Ryukyu Current transport and other regional signals.

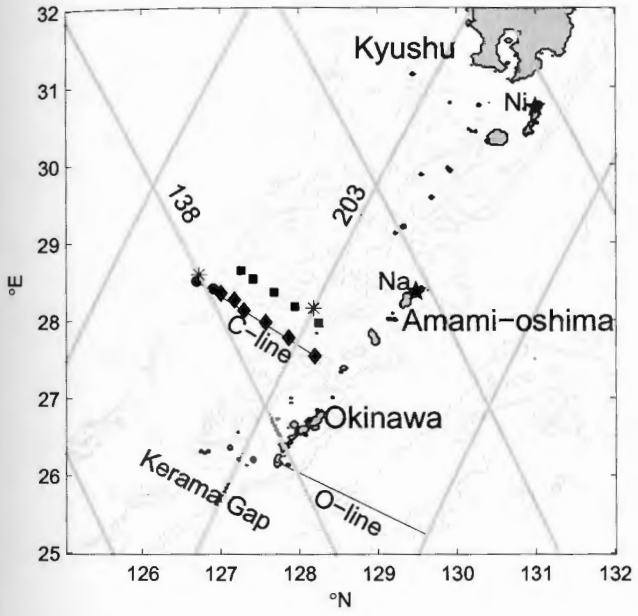

Figure 25. Instrument map.
Symbols show locations of CPIESs (diamonds), PIESs (squares) and ADCPs (circles). Jason-1 satellite tracks are shown. Depth contours are shown for 500, 1000 and 5000 m. Asterisks show locations (126.727°E, 28.586°N and 128.184°E, 28.151°N) of satellite altimeter measurements used in determining the empirical relationship between ΔSLA and net transport (see Methods). Stars show locations of Naze (Na) and Nishinoomote (Ni).

To date, ECS transport studies have relied mainly on snapshots taken over many years (e.g., Ichikawa and Beardsley 1993; Yuan et al., 1998; Isobe 2008), or data collected quarterly (Ichikawa and Chaen, 2000). Thus, the month-by-month seasonal signal of the ECS-Kuroshio has not been well resolved. In addition, a long-term comparison between concurrent ECS-Kuroshio and Ryukyu Current

transports has not been possible since the combined flow in these two Kuroshio branches has been reported only for isolated snapshots (e.g., Yuan et al., 1991; Yuan et al., 1994; Yuan et al., 1996; Zhu et al., 2006). The role of eddies in steering the Kuroshio has not been thoroughly examined. The following questions are addressed in this paper.

- How are the ECS-Kuroshio and Ryukyu Current transports related at intra-annual to interannual periods?
- What is the annual range in ECS-Kuroshio and Ryukyu Current transports and how do these compare with theoretical predictions?
- How does the Ryukyu Current/ECS-Kuroshio system respond to the arrival of mesoscale eddies from the east?
- Is the combined mean transport of the ECS-Kuroshio and Ryukyu Current equal to the expected mean Sverdrup transport?

12. Data

12.1 Transport and velocity structure time series

Time series of the ECS-Kuroshio's net absolute transport and velocity structure in the ECS north of Okinawa are available for 13 months, from November 2003 to November 2004 (Andres et al., 2008). This flow was measured for a 210 km span, referred to as the C-line (close to the so-called PN-line), from a point 15 km shoreward of the continental shelf-break (taken as the 170 m isobath) to a site near the Ryukyu Island chain (see Figure 25). These time series were determined using data from inverted echo sounders equipped with pressure sensors

(PIESs) and from ADCPs. The eleven PIESs measured hourly round-trip, bottom-to-surface acoustic-travel-time, τ, and bottom pressure. The six PIESs deployed along the C-line were further equipped with current sensors moored 51 m above the seafloor (CPIES). Hourly τ data were two-day low-pass filtered and then used to determine time series of specific volume anomaly profiles, $\delta(z)$, by the GEM method (e.g., Watts et al., 2001; Book et al., 2002). Using the thermal wind equation, velocity shear was then calculated from $\partial\delta/\partial x$. Finally, this shear was referenced with deep pressure and current data to obtain absolute velocity and transport according to the method described by Andres et al. (2008). The two bottom-mounted ADCPs measured the portion of ECS-Kuroshio flow shoreward of the 550 m isobath on the western edge of the Okinawa Trough which was not captured by the IESs.

12.2 Satellite altimetry

During the PIES/ADCP deployment, the Jason-1 satellite (J1) occupied an orbit with tracks 138 and 203 passing 5.3 km and 26.2 km from the western and eastern ends of the C-line, respectively (Figure 25). The repeat cycle for satellite passes was 9.9156 days. On each cycle, track 138, a descending track, was followed 2.5375 days later by the ascending track 203. From October 1992 until August 2002, these same tracks were occupied by the TOPEX/Poseidon satellite (T/P).

Along-track sea-level anomaly (SLA) data, produced by Ssalto/Duacs and distributed by Aviso, with support from Cnes, are used in this study. Aviso's Reference Product is used to assure continuity in the time series. Aviso reports

SLA data corrected for the following: dry and wet troposphere, ionosphere, sea state bias, ocean and pole tides, and a combined atmospheric (including inverse barometer) correction; the data are not corrected for the Large Wavelength Error (for details, see the Aviso website: www.aviso.oceanobs.com).

In addition to the along-track SLA data, merged SLA maps at 7-day intervals from Aviso are used to track eddies in order to study their effects on the ECS-Kuroshio and the Ryukyu Current.

12.3 Ryukyu Current

We analyzed ECS-Kuroshio transport crossing the C-line (KT) in conjunction with Ryukyu Current transport crossing the O-line (RT) calculated by Zhu et al. (2004). During November 2000 – August 2001, 9 PIESs and an upward looking ADCP were deployed southeast of Okinawa (Zhu et al., 2003) to obtain a transport time series. Zhu et al. (2004) obtained an empirical relationship between the net northeastward volume transport (their NVT) between Okinawa and 129.5°E (O-line, see Figure 25) and the sea-level anomaly difference (ΔSLA) across the current, where ΔSLA was determined with a combination of tide-gauge data and satellite-altimeter data. This technique provided a temporal extrapolation, resulting in a time series of NVT beginning in 1992 (Zhu et al., 2004). Here we refer to this NVT as RT to distinguish it from the northeastward Kuroshio flow inside the ECS. Note that this RT had a strong eddy component. Its associated error was 5.9 Sv (2.1 Sv for the 10-month low-pass filtered values).

12.4 Other regional signals

Absolute transport entering the ECS through the East Taiwan Channel (ETC) between Taiwan and the Ryukyu Islands was measured by Johns et al. (2001) from September 1994 until May 1996 with a line of moored current meters and ADCPs located across the channel (the PCM-1 array of the World Ocean Circulation Experiment). Transport, relative to 700 dbar, exiting the ECS through the Tokara Strait determined four times per year from 12 CTD stations across the strait was reported in Nakamura et al. (2006).

13. Methods

In this section, we first use C-line velocity cross-sections, determined from 2-day lowpass filtered *in situ* measurements taken hourly over 13 months (Andres et al., 2008), to demonstrate that sea surface height difference (ΔSSH) across the Kuroshio can be used as a proxy for full-water-column transport. Next we determine the empirical relationship between full-water-column transport from the *in situ* measurements and ΔSLA from satellite altimetry. Finally, the resulting empirical relationship between these two is used with satellite altimeter data to generate a 12-year time series, beginning in 1992, of ECS-Kuroshio transport crossing the C-line.

In a layered ocean, assuming geostrophy, the net transport in the uppermost layer, VT_{surf}, is proportional to ΔSSH across the current,

$$VT_{surf} = \frac{gD}{f}\Delta SSH\,, \qquad (12)$$

where g is gravity, D is the thickness of the uppermost layer, and f is the Coriolis parameter. Furthermore, if upper-layer transport is well correlated with full-water-column (total) transport, ΔSSH can be used to infer the total transport.

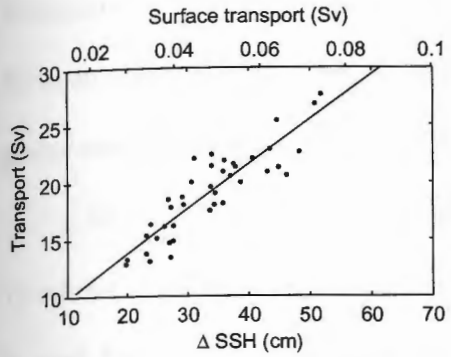

Figure 26. Surface versus total transport.
Correlation between observed surface and total transport in top 10 m and total transport along the C-line between November 2003 and November 2004 at 10-day intervals. ΔSSH shown is computed from surface transport assuming geostrophy using equation (12).

Andres et al. (2008) calculated a time-series of absolute geostrophic velocity cross-sections, determined in 10 m thick layers from the surface to the sea floor, along the C-line. Analysis of this velocity structure time series shows that ΔSSH calculated from net transport in the uppermost layer (Equation 12) is in fact well correlated with net transport in the entire water column (Figure 26). The correlation coefficient, r, for values sub-sampled every 10 days (approximately the transport time-series integral time scale) is 0.88 with an rms error in total transport of 1.7 Sv. This demonstrates that ΔSSH can be used as a proxy for transport in this region. For comparison, the correlation coefficient between surface and total transport for the area-integrated eastward flow in the Kuroshio south of Japan along the ASUKA line is 0.90 with an rms error in transport of 5.6 Sv (Imawaki et al., 2001a).

During the entire T/P deployment, there are no SLA data from the sites on track 203 falling closest to the offshore end of the C-line. Data at these sites become available only when this orbit is occupied by J1. Nevertheless, as demonstrated below, it is still possible to determine a robust empirical relationship between satellite-derived ΔSLA and C-line transport. The locations of the satellite points used are shown in Figure 25 (asterisks).

In order to determine an empirical relationship between low-frequency variations in satellite-derived ΔSLA and C-line transport, the following procedure is used for the November 2003 – November 2004 time period. Time series of satellite-measured SLA at the two satellite points are passed through a 5 point boxcar filter resulting in SLA time series which are essentially 40-day lowpass filtered since the satellite repeat cycle is almost 10 days (Figure 27a and b). Next the filtered SLA time series are interpolated to a common time base with an exact 10-day interval and differenced to calculate ΔSLA across the C-line (Figure 27c). The seasonal signal due to surface warming and cooling, which is apparent in each of the two SLA time series, is assumed to be spatially uniform in this small region and thus cancels out in the ΔSLA calculation. The net absolute ECS-Kuroshio transport across the C-line, determined from the *in situ* instruments (CPIES/PIESs and ADCPs), is also 40-day boxcar filtered (Figure 27d, heavy line). An empirical linear relationship between the resulting ΔSLA and the transport is determined by least-squares fitting, and this relationship is used to calculate satellite-derived transport (Figure 27d, thin line). Net absolute transport, from the *in situ* instruments, and ΔSLA (or satellite-derived transport) are well correlated with $r =$

0.83. Using this empirical relationship, rms difference between satellite-derived transport and transport determined from *in situ* instruments is 1.2 Sv. For the Ryukyu Current crossing the O-line, the correlation coefficient between satellite-derived transport (from ΔSLA) and that from *in situ* instruments was 0.91 with 2.8 Sv rms difference (Zhu et al., 2004), although we note that the calibration procedure of Zhu et al. (2004) was slightly different from that used here (e.g., they smoothed the satellite data spatially, whereas we smoothed them temporally).

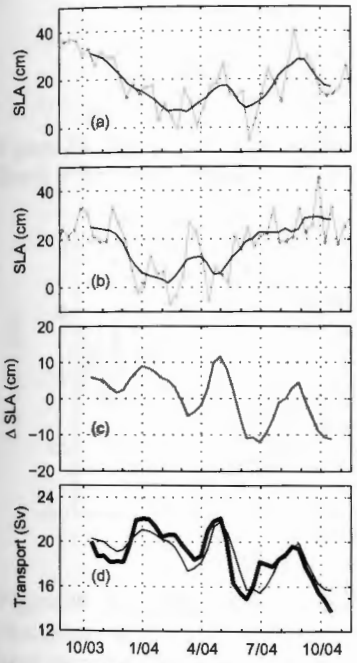

Figure 27. Satellite SLA timeseries.
Panels show (a) J1 SLA near the offshore end of the C-line (raw data = gray line, 5 point boxcar-filtered data = black line), (b) as in panel a, but for a point near the onshore end of the C-line, (c) ΔSLA (a-b), and (d) 40-day boxcar-filtered transport measured along the C-line by CPIES/PIESs and ADCPs (heavy line) and satellite-derived transport (thin line) determined from ΔSLA of panel c using the empirical relationship: *Transport (Sv) = 0.27 ΔSLA(cm) + 18.69*. Vertical dotted lines mark beginnings of indicated months.

Using the empirical relationship between ΔSLA and net absolute transport, satellite altimeter data extending back to October 1992 are used to produce a 12-

year time series of ECS-Kuroshio transport crossing the C-line (Figure 28, black line). We refer to this transport as KT.

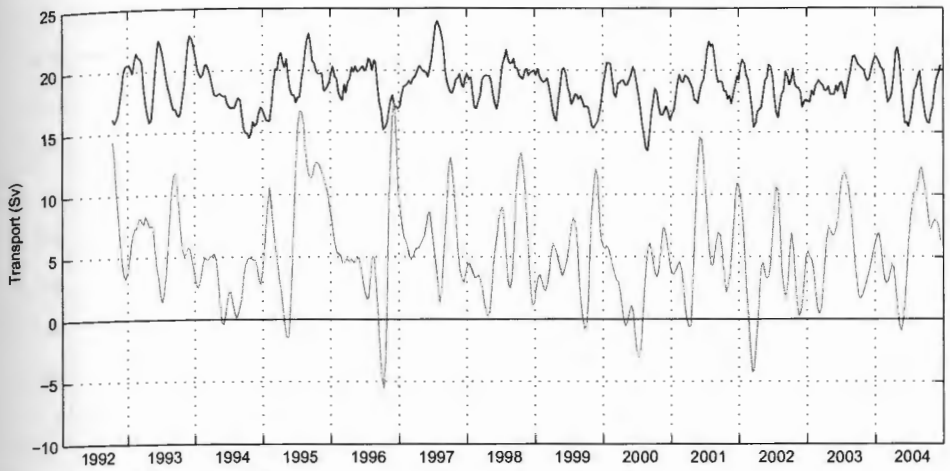

Figure 28. Satellite-derived transports.
Black = KT, gray = RT.

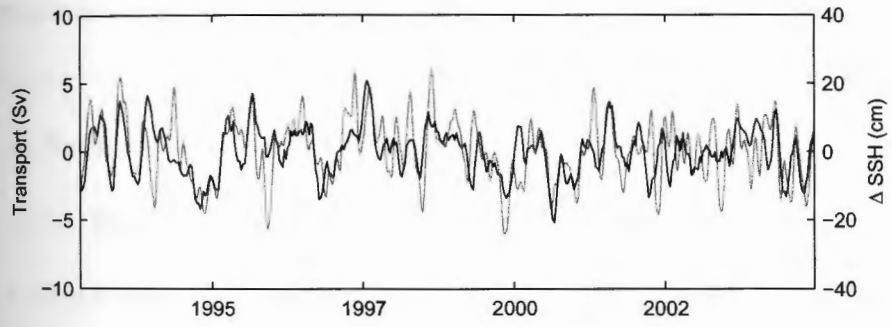

Figure 29. Tokara Strait ΔSSH and KT time series.
Plot shows 40-day lowpass filtered Tokara Strait ΔSSH in gray and with KT in black. Means have been removed from both time series. X-axis marks indicate beginnings of indicated years.

To support the extrapolation method, the 12-year KT time series is compared to ΔSSH across the Tokara Strait calculated using detided sea levels from Naze and Nishinoomote (locations are shown in Figure 25). Tokara Strait ΔSSH is a proxy for transport exiting the ECS through the Tokara Strait (Ichikawa, 2001; Kawabe 1995). In order to make the comparison, the Tokara Strait ΔSSH is

40-day low-pass filtered. The two time series (Figure 29) show moderately good agreement with $r = 0.55$.

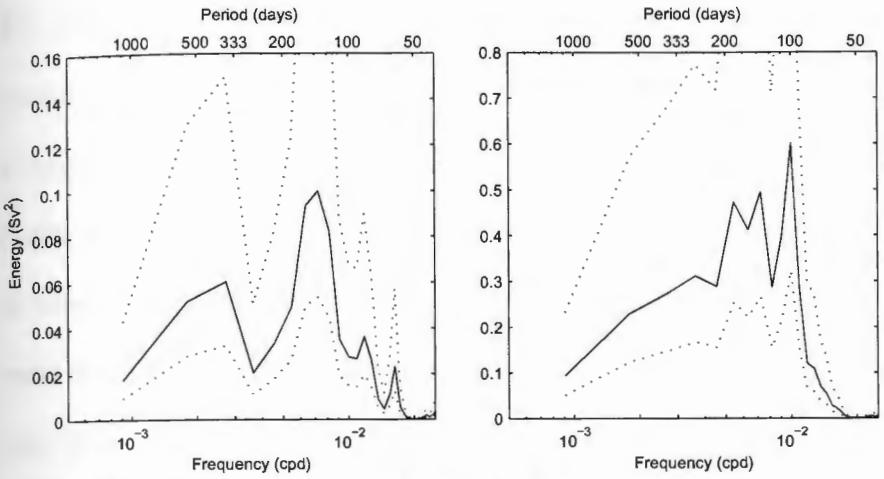

Figure 30. Variance-preserving spectra for KT and RT.
KT is shown on the left and RT on the right. Dashed lines are 95% confidence intervals. Spectra are calculated with Hanning windows, 1100 days wide with 50% overlap (7 overlapping segments). Note the *y*-scales differ by a factor of 5.

14. Results and discussion

The 12-year mean KT is 18.7 Sv with ± 0.2 Sv standard error, compared to 5.4 ± 0.4 Sv for the RT in the same period. Standard errors were calculated using the "blocking" method for correlated data described by Flyvbjerg and Petersen (1989). Transport of the ECS-Kuroshio is less variable than that of the Ryukyu Current with KT standard deviation about half that of RT (1.8 Sv vs. 3.9 Sv). Variance-preserving power spectra of the two transports are shown in Figure 30. KT shows two significant energy peaks, one at periods of 300-600 days and the other at 100-170 days. Also, a small, though significant, peak appears near 60 days. RT is broadly energetic at periods of about 100-500 days, with a couple of peaks between 100 and 200 days.

14.1 Annual cycle

Power spectra contain energy at the annual period in both the KT and the RT, although only the KT has a well-defined peak (Figure 30). In order to investigate the annual cycle further, transport data for the two currents are averaged by month over the 12 year time series for the two currents. These annual cycles and their sum are plotted in Figure 31 together with the standard deviation of transport for each month (dots). Even though KT is stronger than RT in the mean by a factor of 3.5, the annual range in RT is about 3.5 Sv, while that of KT is only about 1.6 Sv. Both currents show significant variability in the monthly transport, particularly from July to October (Figure 31, dots). This probably reflects not only interannual variations in the annual cycle, but also the effect of mesoscale eddies.

The KT monthly-averaged signal has a maximum in August, followed by a sharp minimum in October. From December through August there is only 0.5 Sv variation in the KT monthly averages. The RT annual cycle has a maximum in November and a minimum in March. When the two currents are added together, the resulting combined western boundary current transport has an annual range of almost 4 Sv (peak-to-peak) with a minimum in March and a secondary minimum in October. Maxima occur in July and December. These results are similar to reported seasonal transports 1000 km upstream and downstream from our region: east of southern Taiwan, Gilson and Roemmich (2002) report 8 ± 6 Sv annual range with minimum in April and maximum in July; at the ASUKA line, Imawaki et al. (2001b) report ~5 Sv annual range with minima in March and September and

maxima in July and December. Kakinoki et al. (2008) report 8.3 Sv annual range along the ASUKA line.

An October minimum in ECS-Kuroshio transport has been noted previously in other work (e.g., Kawabe, 1988; Ichikawa and Beardsley, 1993). Moreover, 21 months of transport measurements just upstream of the ECS (Johns et al., 2001) averaged by month also exhibit an October minimum. Nevertheless, this minimum is absent in RT, which supports the possibility that the KT minimum results from local wind forcing (Ichikawa and Beardsley, 1993) or the baroclinicity (Kagimoto and Yamagata, 1997) rather than integrated wind stress over the Pacific or Philippine Basin. Ichikawa and Beardsley (1993) found that transport in the ECS is positively correlated with the downstream component of wind stress.

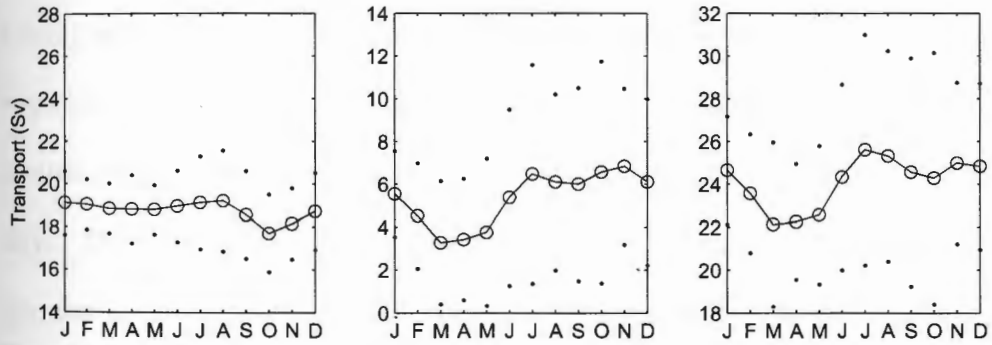

Figure 31. Monthly mean transports.
Transports shown for KT (left), RT (middle) and total (right). Circles represent monthly means for the 12-year ΔSLA-derived transports. Dots represent ± standard deviation of transport each month.

14.2 Co-variation of ECS-Kuroshio and Ryukyu Current

KT and RT shown in Figure 28 are uncorrelated: r is not significantly different from zero. But this changes when one introduces a lag between the two currents (Figure 32): with KT lagging RT by 60 days, the two currents become positively correlated at the 99% confidence level ($r = 0.40$).

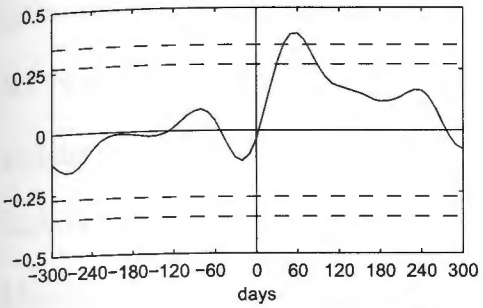

Figure 32. Cross correlation function of KT and RT with time lag.
Positive lag indicates KT lagging RT. The RT time series has 54 degrees of freedom (DOF) while the KT time series has 73 DOF. Dashed lines show the 95% and 99% confidence levels (± 0.273 and ± 0.354, respectively) for a correlation with 50 DOF (Emery and Thomson, 2001).

The coherence spectrum between KT and RT is plotted in Figure 33 (upper panel). Transports are coherent (at the 95% confidence level) at periods of 110 days, 160 days and 2-years. A 2-year spectral peak was also found by Zhu et al. (2004) who report a quasi-biennial oscillation in RT. In addition, Kawabe's (1988) analysis of 18 years of sea-level difference across the Tokara Strait has a spectral peak at 2.1 years. Phases at frequencies of significant coherence are plotted in Figure 33 (lower panel) and show KT generally lagging RT by 33-62 days. This suggests that the previously-noted strong correlation between the two currents occurring at 60 day lag arises from processes occurring over a range of periods from about 100 days to 2 years. Further, the 60-day phase lag at 2-year period is relatively short, suggesting that the 2-year-period component in the ECS-Kuroshio and the Ryukyu Current is caused by the same driving force, possibly wind stress over the North Pacific (Zhu et al., 2004).

There is an annual peak in coherence (Figure 33), but it falls below the 95% confidence level. It is significant only at the 90% confidence level (0.68). Nevertheless it is worth noting that the phase of the annual peak differs by

approximately 180° from that of the other coherence peaks, indicating that annual KT variation *leads* that of the RT by 137° ±13°, which corresponds to a lead of 4.6 months (or a lag of 7.4 months). This is consistent with the 5 month time difference in the monthly-average minima shown in Figure 31 (October for KT vs. March for RT).

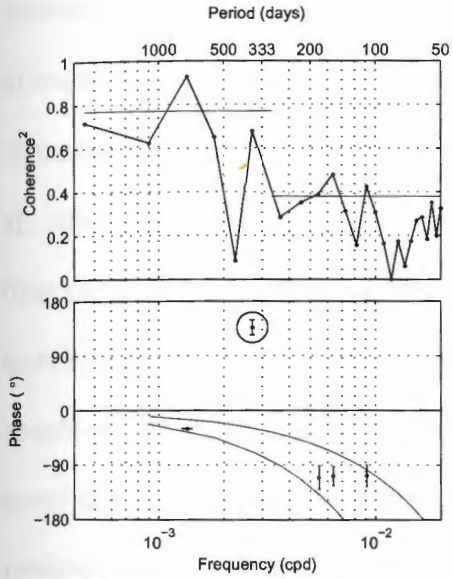

Figure 33. Squared-coherence and phase lag spectra between KT and RT.
For periods longer than 300 days, a 2220-day window was used. For shorter periods a 1100-day window was used. Gray lines on the coherence plot show the 95% confidence level. Phase (with standard error) is shown for frequencies which are coherent at the 95% confidence level. Additionally, the circled dot is the phase for 1-year period coherence (see text). Positive phase indicates RT lagging KT. Gray curves on the phase plot denote phase boundaries for transport lags between 30 and 70 days.

14.3 Eddy effects

The Kuroshio enters the ECS over the Ilan ridge between Taiwan and the Ryukyu Islands. Zhang et al. (2001) suggest eddies arriving east of Taiwan can steer some of the transport either into the ECS or to the east of the Ryukyu Islands. This should result in Ryukyu Current and ECS-Kuroshio transport variations

which are *negatively* correlated at periods typical of mesoscale eddies. However, Figure 33 shows that KT and RT are coherent with 30-70 lag at these eddy-periods and the observed maximum-magnitude correlation is *positive* with a 60 day lag (Figure 32). While eddy-steering east of Taiwan may occur in some instances, it does not seem to play a significant role in our observed 60-day lagged correlation between KT and RT. Rather, these transport co-variations appear to be the effect of many eddies communicated through the Kerama Gap, which lies southwest of Okinawa near 26°N, 127°E (Figure 25) and has a sill depth of ~1050 m (Choi et al., 2002). The associated lag likely arises from the time it takes an eddy to travel from the O-line to the Kerama Gap. Since the O-line lies about 200 km east of the Kerama Gap, this 60-day lag suggests eddies slow down from typical propagation speeds of 7-8 cm/s (Konda et al., 2005) to ~4cm/s. This reduction in propagation speed as eddies approach the Kerama Gap is consistent with a numerical model for inviscid barotropic flow of the interaction of a vortex with a gap in a wall (Johnson and McDonald, 2004, their Figure 8); it may also be a result of advection by the Ryukyu Current.

Current-meter data suggest there is a net mean flow through the Kerama Gap into the ECS (Morinaga et al., 1998). Generally, eddies themselves are not observed to pass through the gap into the ECS, but they appear to induce changes in the flow through the gap. The interaction of eddies with gaps has been treated numerically and analytically (e.g., Simmons and Nof, 2002; Johnson and McDonald, 2004, 2005) and with laboratory tank experiments (e.g., Cenedese et al., 2005; Tanabe and Cenedese, 2008). Results depend on numerous parameters,

such as the ratio of gap diameter to eddy diameter, G/d, relative position of eddy and gap, values of f and β ($=\partial f/\partial y$), orientation of the boundary, whether or not there is background flow, and whether the problem is inviscid (numerical and analytical models) or includes friction (tank experiments). There is great "richness in dynamics," but, in tank experiments with $G/d < 0.4$, eddies are often observed to "funnel" water through gaps between cylinders without themselves passing between the cylinders (Cenedese et al., 2005, their Figure 9). Unfortunately, the parameters used in these studies are not good representations of eddies near the Kerama Gap, so we could not use them to anticipate what we observed. In the context of the present observations, the eddy-effect on ECS-Kuroshio transport is demonstrated below by comparing the transports (Figure 34) with satellite altimetry maps (Figure 35) for 1995, when a series of strong cyclonic and anticyclonic eddies passed through the region.

Figure 34a shows KT and RT from October 1994 through January 1996. During this time there is a series of transport maxima and minima. Three events (I, II, and III) are highlighted and in each case show an extremum first in RT and then in KT.

Figure 35 shows merged SLA maps from February through September 1995. In February 1995, coincident with a RT maximum (Event I), an anticyclonic eddy on the offshore side of the O-line (southeast of Okinawa, crossing the Ryukyu Current) is coupled with an onshore cyclonic eddy. This eddy pair transports water northeastward across the O-line. The anticyclonic eddy moves westward and by March 1995 it reaches the Kerama Gap, where it stalls

until May. While it is stalled, a maximum is observed in KT, suggesting that the eddy by the Kerama Gap is adding to flow through the gap into the ECS. This water flows northward in the ECS and crosses the C-line, increasing the net transport. The maximum in transport across the C-line (KT) lags the O-line transport maximum (RT) by roughly 2 months (Figure 34).

In mid-May a cyclonic eddy on the offshore end of the O-line manifests itself as a minimum in RT (Figure 35, Event II). This eddy moves west and arrives at the Kerama Gap around mid-June where it stays until mid-July. Its effect is felt along the C-line as a minimum in KT at the end of June, suggesting that the cyclonic eddy is reducing (or even reversing) flow through the Kerama Gap into the ECS. In this case, the lag between RT and KT minima is about 1.5 months (Figure 34).

Meanwhile, an anticyclonic eddy arrives at the O-line coincident with a RT maximum at the end of June (Figure 35, Event III). It remains there, but elongates towards the Kerama Gap and into the ECS during August/September coincident with a maximum in KT such that the maximum in KT lags that in RT by about 2 months (Figure 34).

During this time period, Kuroshio transport entering the ECS through the ETC was measured by Johns et al. (2001) with an array of current meters and ADCPs. A portion of their 21 month (Sept. 1994 – May 1996) time series (40-day lowpass filtered for compatibility) is shown in Figure 34b. The correlation coefficient between this ETC transport and the corresponding 21 months of KT has its maximum at zero lag with value 0.43, but this correlation is not significant,

even at the 90% confidence level. In contrast, the correlation coefficient for the same 21 months between KT and RT, has its maximum at 40 days lag with value 0.63, and this correlation is significant at the 95% confidence level. Thus while the main Kuroshio transport passes into the ECS through the ETC, transport variations at the C-line occurring over time scales on the order of 1.5 years or less are related mainly to variations of flow through the Kerama Gap rather than those through the ETC.

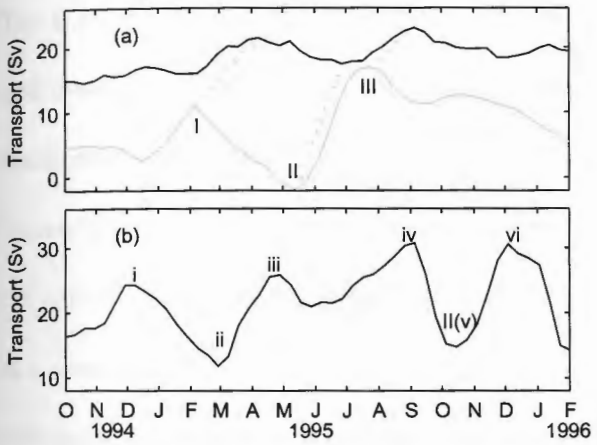

Figure 34. Subset of satellite-derived transports.
Plots show (a) KT (black line) and RT (gray line) as in Figure 28 but for period from October 1994 to January 1996. Influences of three eddies are apparent: Events I (anticyclonic), II (cyclonic), and III (anticyclonic) – see text. (b) the concurrent Kuroshio transport through the ETC from Johns et al. (2001) and 40-day lowpass filtered. Eddies i through vi are discussed in the text. Marks indicate beginning of designated month.

To discern the effect of eddies on ETC transport, KT, and RT, we tracked eddies using merged SLA maps available at 7-day intervals (Figure 36). While ETC-transport shows many extrema during the period from October 1994 through January 1996 (e.g. Events i through vi in Figure 34b), only one of these (Event v, the minimum in October 1995) can be clearly related to an event affecting

transport across the O- and C- lines (Event II, track shown in Figure 36b). Event I appears to decay near the Kerama Gap around June 1995 (Figure 36a) and thus never reaches the region east of Taiwan. While Event III does eventually make it to the region east of Taiwan (Figure 36c), it does not arrive until May 1996, which is after Johns et al.'s (2001) ETC-transport measurements.

Five of the six pronounced extrema in ETC-transport appear to be related to eddies which never encounter the O-line or the Kerama Gap (Figure 36d and e). The ETC-transport maximum in December 1994 (i), minimum in March 1995 (ii), and maximum in May 1995 (iii) appear to be related to eddies coming from the southeast (Figure 36d). ETC-transport maxima in September 1995 (iv) and December 1995 (vi) appear to be caused by anticyclonic eddies approaching from the east (Figure 36e). For all six of these eddy-associated events at the ETC, there is a consistent pattern: transport maxima are associated with anticyclonic eddies and minima with cyclonic eddies, regardless of the direction of eddy arrival. This pattern is in agreement with the findings of Yang et al. (1999) who based their conclusion on analysis of tide gauge-derived sea-level difference across the ETC, satellite altimetry and surface drifting buoys. There is one exception to this overall pattern: a weak ETC transport minimum in June 1995 (Liu et al., 2004) appears to be due to the same anticyclonic eddy which eventually causes a transport maximum in September 1995 (Event iv). This unusual eddy has a large diameter and stalls for about 1 month in June 1995 near 124.5°N, 22.5°E (Figure 36e). During that month the eddy appears to cause an offshore deflection of the Kuroshio away from the ETC resulting in the weak minimum in ETC transport.

This scenario is consistent with coincident drifter tracks (Yang et al., 1999, their Figure 9).

All three transport records shown in Figure 34 have strong oscillations with 3-5 month periods. In each case the oscillations appear to be caused by eddies arriving in the region from the east. Moreover a single eddy, like Event II, can be responsible for transport changes, at different times, in all three places, the O-line, the C-line, and the ETC line. However, many eddies arrive at the ETC from the east or southeast rather than from the northeast. These affect ETC-transport without first influencing transports across the C- and O- lines.

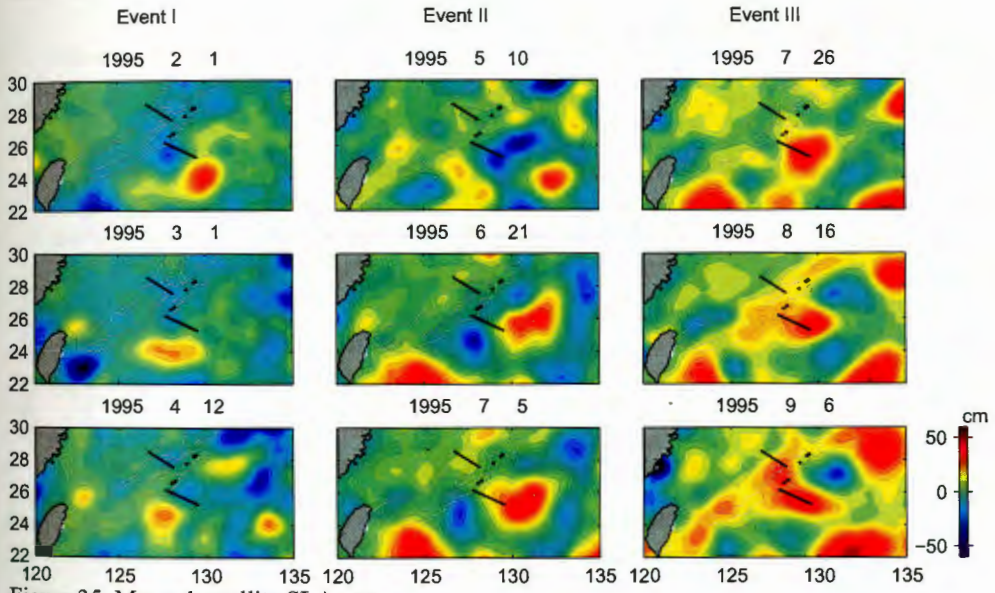

Figure 35. Merged satellite SLA maps.
Each column tracks a different event (I, II, III) identified in Figure 34a. Heavy black lines show C-line (north of Okinawa) and O-line (southeast of Okinawa). Gray contours show the 900 m isobath. In each panel the area-mean SLA was first removed to eliminate the effect of seasonal heating and cooling.

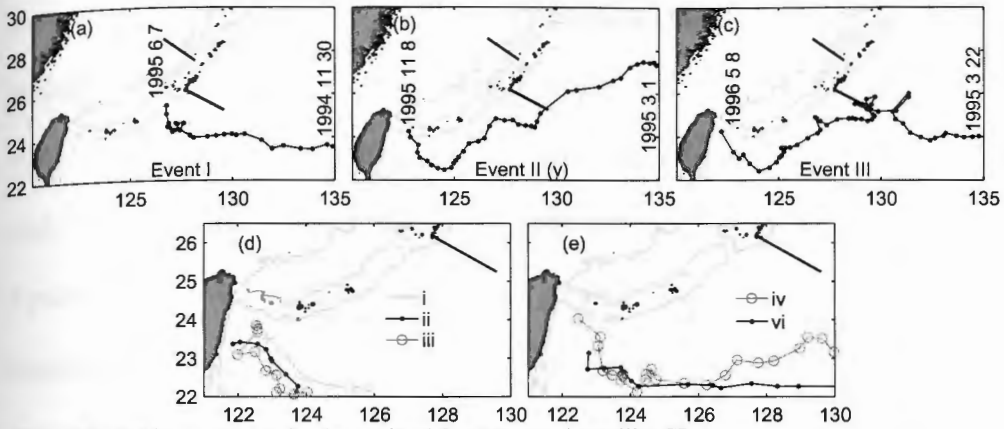

Figure 36. Eddy-center tracks determined from merged satellite SLA maps.
Positions are marked at 7-day intervals. Panels (a), (b), and (c) show Events I, II and III, respectively, with dates of first and last position indicated. Panels (d) and (e) show tracks of eddies which do not cross the O-line or approach the Kerama Gap. Last plotted positions of i, ii, and iii are on 1994 12 7, 1995 3 29, and 1995 5 10, respectively. Last plotted positions of iv and vi are on 1995 9 20 and 1995 12 17, respectively. Events II(v) and ii are both cyclonic, the rest are anticyclonic.

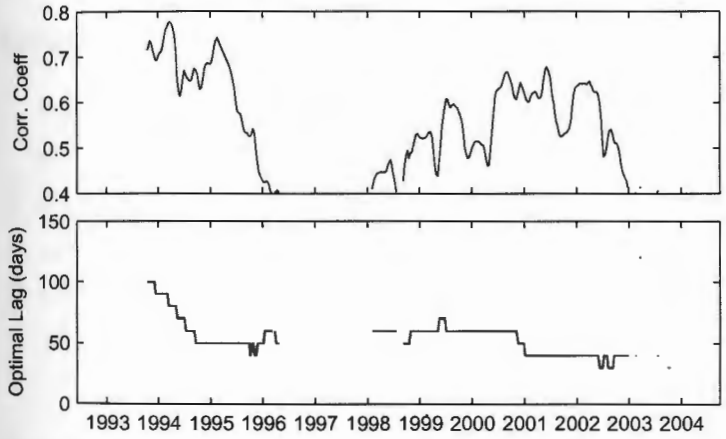

Figure 37. Time dependent correlation coefficient.
Correlation coefficient, r, at optimal lag (top) between RT and KT. Optimal lag (bottom). Values are shown only for $r > 0.4$. Tick marks indicate beginnings of designated years.

The influence of eddies on the flow in the ECS may be communicated through the Kerama Gap with a typical time lag (relative to the Ryukyu Current crossing the O-line) of 60 days. The peak correlation ($r = 0.4$) between RT and KT at 60-day lag represents a mean condition over the 12-year period. When correlation is calculated over a moving 2-year window, the lag resulting in the highest correlation coefficient (optimal lag) varies with time. This 2-year

correlation coefficient and optimal lag are plotted in Figure 37. In each case, p (the probability that there is no correlation) is less than 0.05. From mid-1993 to mid=1994 the optimal lag gradually drops from 100 to 50 days. From mid-1996 to mid-1997 the highest correlation coefficient is less than 0.4, implying that the Ryukyu Current transport crossing the O-line and ECS-Kuroshio transport crossing the C-line are behaving somewhat independently. This may be related to anomalous ECS-Kuroshio transport during 1997-1998 when an El-Niño event occurred (Yuan et al., 2001). From 1998 to 2001 the optimal lag is 60 days; thereafter it drops to 40 days. We do not know what causes these changes in optimal lag, but they suggest that the propagation speed of eddies between the O-line and the Kerama Gap is variable.

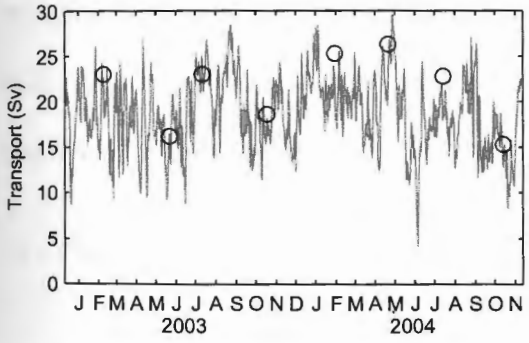

Figure 38. Comparison of C-line and Tokara Strait transport time series.
Gray line is 2-day lowpass filtered transport across the C-line as determined from *in situ* instruments deployed from December 2002 to November 2004 (Andres et al., 2008). Open circles are the volume transport relative to 700 dbar through the Tokara Strait determined from hydrographic casts (see text). Tick marks indicate beginnings of designated years.

From the preceding analysis of satellite SLA maps, it seems that rather than entering the ECS as coherent eddies, eddies sit at the Kerama Gap and add to or subtract from the mean flow through the gap into the ECS. The ~ 5 Sv variations in KT induced by these eddies would require flow variations through the Kerama

Gap on the order of 20 cm/s (assuming uniform flow through the top 500 m of a 50 km-wide gap). How this eddy-induced change in transport is propagated within the ECS (i.e., from the C-line to the Tokara Strait) can be investigated by comparing transport crossing the C-line (determined from the *in situ* instruments) with transport passing through the Tokara Strait. Figure 38 shows C-line net transport (2-day low-pass filtered, determined with CPIESs and ADCPs). Also shown is net geostrophic transport relative to 700 dbar through the Tokara Strait which is determined four times per year from 12 CTD stations (Nakamura et al., 2006). The eight Tokara Strait transports measured during the CPIES/ADCP deployment are well correlated with the contemporaneous C-line transport (r = 0.87), and this correlation drops rapidly with lags (or leads) greater than one week implying that eddy-induced transport variations are advected rapidly inside the ECS. This is in contrast to the slow advection (~60 days) of eddies from the O-line to the Kerama Gap.

14.4 Comparison with regional mean flows and Sverdrup transport

The 12-year mean net transports crossing the C- and O- lines (KT and RT, respectively) sum to 24 Sv. This total transport is low compared to the throughflow across the ASUKA line south of Japan (42 Sv, Imawaki et al., 2001a). Figure 39 is a diagram of the region. The 12-year mean transports across the C-, O-, and ASUKA lines are shown, as is the 4-year (1998-2002) mean of the current east of Amami-oshima determined by Ichikawa et al. (2004) with moored current meters. We note that the respective 4-year means of KT, RT and throughflow across the ASUKA line calculated for 1998-2002 are each within 1 Sv of their full

12-year-means. Thus we can use C-, O-, and ASUKA line means in conjunction with the 4-year mean east of Amami-oshima to deduce a consistent mean-transport picture.

A mass balance using the mean transports on Figure 39 suggests the following. An 18 Sv increase in transport between the sum of the mean RT and KT (~24 Sv) and the ASUKA line throughflow transport (~42 Sv) arises from a strengthening of the Ryukyu Current as it flows east of the Ryukyu Islands. This western boundary current intensification is independent of the recirculation south of Japan (~15 Sv, Imawaki et al., 2001a) and must be fed by North Pacific interior flow. The mean flow east of Amami-oshima (18 Sv) suggests about 13 Sv of this interior flow joins the Ryukyu Current between Okinawa and Amami-oshima and ~ 5 Sv joins between Amami-oshima and the ASUKA line. This ~5 Sv estimate represents a lower bound, if leakage from the ECS-Kuroshio between the C-line and the Tokara Strait feeds some of the flow through the Korea/Tsushima Strait. But the location of leakage from the ECS-Kuroshio is not well constrained (Isobe, 2008, and references therein), so it is not known what proportion occurs downstream of the C-line. Additionally, the preceding mass balance assumes that flow through the Ryukyu Islands between Okinawa and Amami-oshima is negligible; modeling by You and Yoon (2004) suggests the exchange there is < 1 Sv.

Additional information about the mean flows in this region can be inferred using the results of Hautala et al. (1994) who found that the southward flow across 24°N between the eastern boundary and 137°E is 34 Sv (consistent with Sverdrup

flow induced by climatological winds over the North Pacific). By mass balance arguments, about 10 Sv of the 13 Sv-intensification between the O-line and Amami-oshima probably originates south of 24°N. The result is C-line flow (19 Sv), O-line flow (5 Sv) and interior flow (10 Sv) balancing the 34 Sv southward flow. The remaining 3 Sv of the 13 Sv-intensification between the O-line and Amami-oshima and the 5 Sv-intensification occurring between Amami-oshima and the ASUKA line presumably both come from the ocean interior north of 24°N. The inferred transports are shown as dashed gray lines in Figure 39.

This is consistent with a snapshot of the region based on 9 hydrographic sections throughout the region and an inverse technique (Zhu et al., 2006). Their Figure 5 shows strengthening of the current between Okinawa and Amami-oshima which could be fed by interior flow, rather than recirculation. This intensification is qualitatively consistent with the 1/6° model of You and Yoon (2004) and the 1/12° model of You (2005). The 1/12° model has ~8 Sv of flow from the interior joining the current between Okinawa and Amami-oshima.

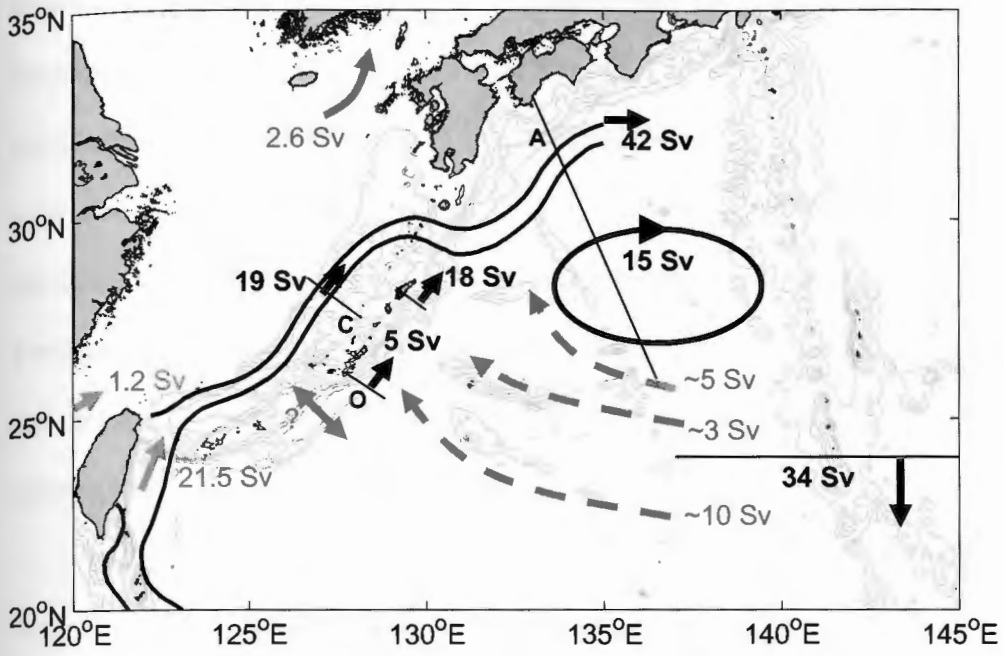

Figure 39. Diagram of mean transports in the ECS and Philippine Basin.
Gray dashed arrows show transports (joining the western boundary current system) which are inferred in this study: flow joining between (1) Okinawa and Amami-oshima (~10 Sv + ~3 Sv) and (2) Amami-oshima and the ASUKA line (~5 Sv). The mean transports used to infer these flows are shown as black solid arrows: mean transport across the C-line (19 Sv, this study), O-line (5 Sv, Zhu et al., 2004), ASUKA line (42 Sv, Imawaki et al., 2001a), in the recirculation south of Japan (15 Sv, Imawaki, 2001a), across 24°N from the eastern boundary to 137°E (34 Sv, Hautala et al., 1994), and east of Amami-oshima (18 Sv, Ichikawa et al., 2004). Other regional flows not used directly in these calculations are shown for reference as gray solid lines: Taiwan Strait (1.2 Sv, Isobe, 2008), Korea/Tsushima Strait (2.6 Sv, Isobe, 2008), and between Taiwan and Yonaguni-jima (21.5 Sv, Johns et al., 2001). Flow through the Ryukyu Islands south of Okinawa is not well constrained. Flow through the Ryukyu Islands north of Okinawa is assumed negligible here (<1 Sv, You and Yoon , 2004).

15. Summary

Using satellite data calibrated with *in situ* transport measurements we have obtained a 12-year time series of net transport crossing the C-line (KT) and compared it to simultaneous transport crossing the O-line (RT). Our study confirms what previous studies have suggested, that the annual variation in KT is smaller than that predicted by the non-topographic, time-dependent Sverdrup

balance and the wind stress curl over the entire North Pacific. In addition, while the annual variation in RT is stronger than that of KT by a factor of 2, RT does not provide the 16 Sv annual variation predicted by Lee et al. (2001) for transport calculated using the Sverdrup balance over just the Philippine Basin. Our study provides more observational evidence to support the model of Sakamoto and Yamagata (1996) in which the annual range in transport is suppressed (relative to that predicted by Sverdrup theory) by the interaction of stratified flow with topography.

Despite the presence of the Ryukyu Island chain which shields the ECS from the Philippine Basin, arrival of eddies appears to cause much of the variability in the ECS-Kuroshio. The Kerama Gap, which is the deepest passage into the ECS, may be the conduit for communication of much of this eddy-influence to the ECS even though the bulk of the Kuroshio transport enters the ECS near Taiwan. Maps of satellite SLA, together with positive correlation between RT and KT with ~60-day lag suggest the following portrayal. Eddies approach the Ryukyu Islands from the east with typical speeds of 7-8 cm/s (e.g., Konda et al., 2005). Their speeds are reduced to about 3-4 cm/s when they encounter the Ryukyu Island chain and the Gap. Once eddies encounter the Kerama Gap they induce flow changes through the gap into the ECS resulting in KT variations along the C-line which are about half as strong as those felt in RT along the O-line. These observations (slowing of eddies near a gap and eddies inducing flow through a gap) are consistent with numerical and laboratory studies (Johnson and McDonald, 2004; Cenedese et al., 2005). Some of these eddies then

move to the southwest reaching the region east of Taiwan after many months, but their effect on the C-line transport is more clearly communicated through the Kerama Gap than through the ETC as demonstrated by comparison of correlation coefficients between the various transport time series. Once transport variations are felt along the C-line, they are advected quickly to the Tokara Strait by the fast-moving ECS-Kuroshio. This conclusion is consistent with the findings of other authors who have noted a 60-day lag between the Ryukyu Current transport and sea surface height anomalies in the Tokara Strait (Zhu et al., 2004) and between sea surface height outside the Ryukyu Islands and volume transport through the Tokara Strait (Ichikawa, 2001). Hence the additional lag from the line where KT is determined to the Tokara Strait must be small. Furthermore, modeling in the region (You and Yoon, 2004) demonstrates the likelihood of communication through the Ryukyu Islands, particularly through the Kerama Gap, and Yuan et al. (1994) provide observational evidence with a salinity section through the Gap suggesting intrusion of water from east to west (their Figure 6b).

Finally, the combined KT and RT mean transports are less than the throughflow across the ASUKA line and less than the southward Sverdrup transport across 24°N from the eastern boundary to 137°E. These mismatches in mean flow each independently suggest that intensification of the Ryukyu Current downstream of Okinawa must be fed from the ocean interior rather than simply the recirculation south of Japan.

16. List of References

Andres M., M. Wimbush, J.-H. Park, K.-I. Chang, B.-H. Lim, D.R. Watts, H. Ichikawa, and W.J. Teague (2008): Observations of Kuroshio flow variations in the East China Sea, *J. Geophys. Res.*, **113**, C05013, doi:10.1029/2007JC004200.

Book, J.W., M. Wimbush, S. Imawaki, H. Ichikawa, H. Uchida, and H. Kinoshita (2002): Kuroshio temporal and spatial variations South of Japan determined from inverted echo sounder measurements, *J. Geophys. Res.*, **107**, doi:10.1029/2001JC000795.

Cenedese, C., C. Adduce, and D.M. Fratantoni (2005): Laboratory experiments on mesoscale vortices interacting with two islands, *J. Geophys. Res.*, **110**, C09023, doi:10.1029/2004JC002734.

Choi, B.H., K.O. Kim, and H.M. Eum (2002): Digital bathymetric and topographic data for neighboring seas of Korea, *J. Korean Soc. Coastal and Ocean Engrs.*, **14**(1), 41-50 (in Korean).

Emery, W.J., and R.E. Thomson (2001): Data Analysis Methods in Physical Oceanography, New York, Elsevier, 636pp.

Flyvbjerg, H, and H.G. Petersen (1989): Error estimates on averages of correlated data, *J. Chem. Phys.*, **91**(1), 461-466.

Gilson, J., and D. Roemmich (2002): Mean and temporal variability in Kuroshio geostrophic transport south of Taiwan (1993-2001). *J. Oceanogr.*, **58**, 183-195.

Hautala, S.L., D.H. Roemmich, and W.J. Schmitz, Jr. (1994): Is the North Pacific in Sverdrup balance along 24°N?, *J. Geophys. Res.*, **99**(C8), 16,041-16,052.

Hellerman, S., and M. Rosenstein (1983): Normal monthly wind stress over the world ocean with error estimates, *J. Phys. Oceanogr.*, **13**, 1093-1104.

Ichikawa, K. (2001): Variation of the Kuroshio in the Tokara Strait induced by meso-scale eddies, *J. Oceanogr.*, **57**, 55-68.

Ichikawa, H., and R.C. Beardsley (1993): Temporal and spatial variability of volume transport of the Kuroshio in the East China Sea, *Deep-Sea Res. I*, **40**(3), 583-605.

Ichikawa, H., H. Nakamura, A. Nishina, and M. Higashi (2004): Variability of north-eastward current southeast of northern Ryukyu Islands. *J. Oceanogr.*, **60**, 351-363.

Ichikawa, H., M. Chaen (2000): Seasonal variation of heat and freshwater transports by the Kuroshio in the East China Sea, *J. Mar. Sys.*, **24**, 119-129.

Imawaki, S., H. Uchida, H. Ichikawa, M. Fukasawa, S. Umatani, and the ASUKA group (2001a): Satellite altimeter monitoring the Kuroshio transport south of Japan, *Geophys. Res Lett.*, **28**(1), 17-20.

Imawaki, S., S. Aoki, Y. Fukuda, K. Ichikawa, S. Ito, H. Kawamura, M. Kubota, T. Kuragano, K. Matsumoto, T. Nagai, A. Sengoku, and H. Yoritaka (2001b): Mass, heat, and salt transports in the western North Pacific, *Aviso News Lett.*, **8**, 62-64.

Isobe, A. (2008): Recent advances in ocean-circulation research for the Yellow Sea and East China Sea shelves, *J. Oceanogr.*, **64**(4), 569-584.

Johns, W.E., T.N. Lee, D. Zhang, and R. Zantopp (2001): The Kuroshio east of Taiwan: moored transport observations from the WOCE PCM-1 array, *J. Phys. Oceanogr.*, **31**, 1031-1053.

Johnson, E.R., and N.R. McDonald (2004): The motion of a vortex near a gap in a wall, *Physics of Fluids*, **16**(2), 462-469.

Johnson, E.R., and N.R. McDonald (2005): Vortices near barriers with multiple gaps, *J. Fluid Mech.*, **531**, 335-358.

Kagimoto, T., and T. Yamagata (1997): Seasonal transport variations of the Kuroshio: an OGCM simulation, *J. Phys. Oceanogr.*, **27**, 402-418.

Kakinoki, K., S. Imawaki, H. Uchida, H. Nakamura, K. Ichikawa, S. Umatani, A. Nishina, H. Ichikawa, and M. Wimbush (2008): Variations of Kuroshio geostrophic transport south of Japan estimated from long-term IES observations, *J. Oceanogr.*, **64**, 373-384.

Kawabe, M. (1988): Variability of Kuroshio velocity assessed from the sea-level difference between Naze and Nishinoomote, *J. Oceanogr.*, **44**, 293-304.

Kawabe, M. (1995): Variations of current path, velocity, and volume transport of the Kuroshio in relation with the large meander, *J. Phys. Oceanogr.*, **25**, 3103-3117.

Kawabe, M. (2001): Interannual variations of sea level at Nansei Islands and volume transport of the Kuroshio due to wind changes, *J. Oceanogr.*, **57**, 189-205.

Konda, M., H. Ichikawa, I.-S. Han, X.-H. Zhu (2005): Variability of current structure due to meso-scale eddies on the bottom slope southeast of Okinawa Island, *J. Oceanogr.*, **61**, 1089-1099.

Lee, I.-H., W.-S. Chuang, and D.-P. Wang (2003): Structure and propagation of a large cyclonic eddy in the western North Pacific from analysis of XBT and altimetry data and numerical simulation, *TAO: Terrestrial, Atmoshperic and Oceanic Sciences*, **14**(2), 183-200.

Lee, T.N., W.E. Johns, C.-T. Liu, D. Zhang, R. Zantopp, and Y. Yang (2001): Mean transport and seasonal cycle of the Kurhoshio east Taiwan with comparison to the Florida Current, *J. Geophys. Res.*, **106**(C10), 22,143-22,158.

Liu, W., Q. Liu, and Y. Jia (2004): The Kuroshio transport east of Taiwan and the sea surface height anomaly from the interior ocean, *J. Ocean Univ. China*, **3**, 135-140.

Morinaga, K., N. Nakagawa, K. Osamu, and B. Guo (1998): Flow pattern of the Kuroshio west of the main Okinawa Island, *Proceedings of Japan-China Joint Symposium on Cooperative Study of Subtropical Circulation System, 1-4 December 1997, Nagasaki, Japan,* Seikai National Fisheries Research Institute, Nagasaki, pp. 203-210.

Nagano, A., H. Ichikawa, T. Miura, K. Ichikawa, M. Konda, Y. Yoshikawa, K. Obama, K. Murakami (2007): Current system east of the Ryukyu Islands, *J. Geophys. Res.*, **112**, C06009, doi:10/1029.2006JC003917.

Nagano, A., H. Ichikawa, T. Miura, K. Ichikawa, M. Konda, Y. Yoshikawa, K. Obama, and K. Murakami (2008): Reply to comment by Xiao-Hua Zhu et al. on "Current system east of the Ryukyu Islands", *J. Geophys. Res.*, **113**, C03021, doi: 10.1029/2007JC004561.

Nakamura, H., T. Yamashiro, A. Nishina, and H. Ichikawa (2006): Time-frequency variability of Kuroshio meanders in Tokara Strait, *Geophys. Res. Lett.*, **33**, L21605, doi:10.1029/2006GL027516.

Nitani, H. (1972): Beginning of the Kuroshio. In: *Kuroshio, Physical Aspects of the Japan Current*, H. Stommel and K. Yoshida, editors, University of Washington Press, Seattle, pp. 129-164.

Qiu, B. (1999): Seasonal eddy field modulation of the North Pacific Subtropical Countercurrent: TOPEX/Poseidon observations and theory, *J. Phys. Oceanogr.*, **29**, 2471-2486.

Qiu, B., and T.M. Joyce (1992): Interannual variability in the mid- and low-latitude western north Pacific, *J. Phys. Oceanogr.*, **22**, 1062-1079.

Roemmich, D., and J. Gilson (2001): Eddy transport of heat and thermocline waters in the North Pacific: a key to interannual/decadal climate variability?, *J. Phys. Oceanogr.*, **31**,675-687.

Sakamoto, T. (2005): Effect of air-sea heat exchange on seasonal transport variation of the Kuroshio, *J. Marine Res.*, **63**, 579-600.

Sakamoto, T., and T. Yamagata (1996): Seasonal transport variations of the wind-driven ocean circulation in a two-layer planetary geostrophic model with a continental slope, *J. Marine Res.*, **54**, 261-284.

Simmons, H.L. and D. Nof (2002): The squeezing of eddies through gaps, *J. Phys. Oceanogr.*, **32**, 314-335.

Tanabe, A., and C. Cenedese (2008): Laboratory experiments on mesoscale vortices colliding with an island chain, *J. Geophys. Res.*, **113**, C04022, doi:1029/2007JC004322.

Watts, D.R., C. Sun, and S. Rintoul (2001): Two-dimensional gravest empirical modes determined form hydrographic observations in the Subantarctic Front, *J. Phys. Oceanogr.*, **31**, 2186-2209.

Yang, Y., C.-T. Liu, J.-H. Hu, and M. Koga (1999): Taiwan Current (Kuroshio) and impinging eddies, *J. Oceanogr.*, **55**, 609-617.

You, S.-H., and J.-H. Yoon (2004): Modeling of the Ryukyu Current along the Pacific side of the Ryukyu Islands, *Pacific Oceanogr.*, **2**, 44-51.

You, S.-H. (2005), A Numerical Study of the Kuroshio System Southewest of Japan, Ph.D. Thesis, Kyushyu University.

Yuan, Y., M. Endoh, and H. Ishizaki (1991): The study of the Kuroshio in the East China Sea and the current east of the Ryukyu Islands. *Acta Oceanol. Sin*, **10**(3), 371-391.

Yuan, Y., K. Takano, Z. Pan, J. Su, K. Kawatate, S. Imawaki, H. Yu, H. Chen, H. Ichikawa, and S. Umatani (1994): The Kuroshio in the East China Sea and the currents east of the Ryukyu Islands during autumn 1991, *La Mer*, **32**, 235-244.

Yuan, Y., C. Liu, Z. Pan, and S. Zheng (1996): Circulation east of Taiwan and in the East China Sea and east of the Ryukyu Islands during early summer 1985. Acta Oceanol. Sin,, **15**(4), 423-435.

Yuan, Y., A. Kaneko, J. Su, X. Zhu, Y. Liu, N. Gohda, and H. Chen (1998): The Kuroshio east of Taiwan and in the East China Sea and the currents east of Ryukyu Islands during early summer of 1996, *J. Oceanogr.*, **54**, 217-226.

Yuan, Y.-C., Y.-G. Lui, and J.-L. Su (2001): Variability of the Kuroshio in the East China Sea During El-Niño to La Niña phenomenon of 1997 and 1998, *Chinese J. Geophys.*, **44**, 199-210 (in Chinese with English abstract).

Zhang, D., T.N. Lee, and W.E. Johns (2001): The Kuroshio east of Taiwan: modes of variability and relationship to interior ocean mesoscale eddies, *J. Phys. Oceanogr.*, **31**, 1054-1074.

Zhu, X.-H., I.-S. Han, J.-H. Park, H. Ichikawa, K. Murakami, A. Kaneko, and A. Ostrovskii (2003): The northeastward current southeast of Okinawa Island observed during November 2000 to August 2001, *Geophys. Res. Lett.*, **30**(2), 1071, doi:10.1029/2002GL015867.

Zhu, X.-H., H. Ichikawa, K. Ichikawa, and K. Takeuchi (2004): Volume transport variability southeast of Okinawa Island estimated from satellite altimeter data, *J. Oceanogr.*, **60**, 953-962.

Zhu, X.-H., J.-H. Park, and I. Kaneko (2006): Velocity structures and transports of the Kuroshio and the Ryukyu Current during fall of 2000 estimated by an inverse technique, *J. Oceanogr.*, **62**, 587-596.

Zhu, X.-H., J.-H. Park, and D. Huang (2008a): Observation of baroclinic eddies southeast of Okinawa Island, *Science in China Series D: Earth Sciences*, **51**, 1802-1812.

Zhu, X.-H., J.-H. Park, M. Wimbush, and C. Yang (2008b): Comment on "Current system east of the Ryukyu Islands" by A. Nagano et al., *J. Geophys. Res.*, **113**, C03020 doi: 10.1029/2007JC004458.

Chapter 3

Manifestation of the Pacific Decadal Oscillation in the North Pacific Western Boundary Current System

17. Abstract

PDO index correlates positively with North Pacific western boundary current transports determined from satellite altimetery calibrated with *in situ* data. The correlations, which are highest at zero lag, are 0.76 for the ECS-Kuroshio and 0.49 for the Ryukyu Current. The combined transport variation correlated with PDO index variations is about 4 Sv. PDO index is strongly negatively correlated with NCEP wind stress curl over the central North Pacific. The magnitude of the observed western boundary current variations suggests that they arise from a barotropic response to wind stress curl over a region stretching from the western North Pacific to the central North Pacific. PDO index is also negatively correlated with Kuroshio Position Index (in the Tokara Strait) and Tsushima Current transport; this can be explained by a model in which ECS-Kuroshio path is steered by topography when transport is low and is inertially controlled when transport is high. Estimated ASUKA-line throughflow is not correlated with PDO index, yet the recirculation strength is negatively correlated at the 85% confidence level. This may arise from a misallocation of eastward transport south of Japan into throughflow and recirculation components.

18. Introduction

Changes in Pacific climate occur on various time scales (Mantua and Hare, 2002 and references therein). *Interannual* changes in sea surface temperature (SST) and sea-level pressure (SLP) are associated with El Niño/Southern Oscillation (ENSO; e.g., Deser and Wallace, 1987). *Interdecadal* Pacific climate variability is reflected in the Pacific Decadal Oscillation (PDO; Mantua et al., 1997). Here we investigate how the PDO manifests itself in the mid-latitude North Pacific western boundary current (WBC) system.

Previous researchers have developed proxies for Pacific interdecadal variability from empirical orthogonal function (EOF) analyses of North Pacific monthly mean SST anomalies (Zhang et al., 1997; their NP index) and SLP anomalies (Hare, 1996). PDO index (Mantua et al., 1997) is the time series of the first mode from EOF analysis of SST poleward of 20°N from 1900 to 1993. When PDO index is positive ("warm phase"), SST is warmer than average near the west coast of America and cooler in the central North Pacific and the eastern North Pacific near the Kuroshio/Oyashio region. Associated with this warm phase SST distribution are (1) lower than average SLP from 20°N to 60°N causing an enhanced Aleutian low (Hare, 1996; Mantua et al., 1997; Zhang et al., 1997), (2) positive wind stress curl anomalies centered on ~40°N, 155°W, and (3) negative wind stress curl anomalies centered on ~25°N, 170°W (Qiu, 2003). During periods with negative PDO index ("cool phase"), this SST spatial pattern is reversed and the associated SLP distribution leads to wind stress curl anomalies which are negative at ~40°N and positive at ~25°N.

Ecological responses to interdecadal Pacific climate change have been well-documented. For example, Alaska salmon catch rates were low in the 1960s to the mid-1970s during a cool PDO phase, and high from the mid 1970s to the mid 1990s during a warm phase (Mantua et al., 1997; their Figure 6). Also, biomass of large copepods south of Japan has been linked to decadal-scale climate variations, with high levels of biomass before the mid 1970s, low levels through the 1990s and high levels returning in the early 2000s (Nakata and Hidaka, 2003; their Figure 3a).

Despite research documenting wide-ranging effects of PDO on North Pacific biology, the physical mechanisms underlying PDO remain uncertain. It is not clear how observed SST changes in different ocean regions are interconnected. Nor is it known how SST variability is related to changes in the ocean interior. Miller et al. (1998) and Deser et al. (1999) investigated decadal-scale changes in North Pacific thermal structure. Using historical hydrographic data, Deser et al. inferred decadal-scale variability in the strength of the Kuroshio Extension jet. Their inferred transport variations lagged wind stress curl variations by about 4-5 years, leading Deser et al. to suggest that Kuroshio Extension transport variations are a result of wind driven changes in interior Sverdrup flow with the response first carried to the western boundary by baroclinic Rossby waves and then advected to the Kuroshio Extension region by the WBC.

Qiu (2003) also found evidence of low frequency modulation of Kurohsio Extension strength lagging PDO index by about 4 to 5 years. His analysis of satellite altimetry data indicated that the inferred transport variability is a response

to changes in wind stress curl over the eastern Pacific carried westward as sea surface height anomalies by baroclinic Rossby waves. However, this model short-circuits the role of the Sverdrup transport and WBC advection suggested by Deser et al., (1999) since oppositely signed anomalies are generated and propagate north and south of the Kuroshio Extension directly from the east.

Seager et al. (2001), using an ocean general circulation model coupled with an atmospheric mixed layer model, suggested that SST variations in the central North Pacific result from an immediate response to wind, while SST variations in the Kuroshio/Oyashio region arise due to a north-south shift of this confluence region which lags the wind variability by about 3 years.

Here we present a remarkable positive correlation, at zero lag, between PDO index and low frequency variations in North Pacific WBC transport. We examine the role of winds in driving this system. Currents in the mid-latitude western North Pacific are summarized in Section 19. The data sets used in our analysis are discussed in Section 20. Section 21 demonstrates the correlations between PDO and transports of the Kuroshio in the East China Sea (ECS-Kuroshio) and the Ryukyu Current. Next, in Section 22, we present an analysis of North Pacific wind stress curl and compare Sverdrup transport calculations with the observations. We confirm an inverse relationship between ECS-Kuroshio and Korea/Tsushima Strait transports and discuss how this may be related with the PDO in Section 23. Finally, in Section 24, we discuss the connection of the PDO with throughflow south of Japan crossing the ASUKA-line and the Philippine Basin recirculation. Results are summarized in Section 25.

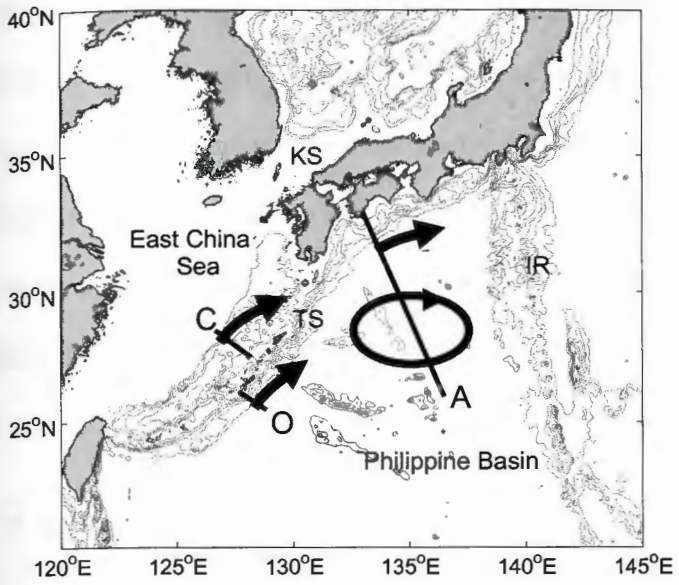

Figure 40. Schematic of the circulation in the western North Pacific.
ASUKA-line, C-line (across which the ECS-Kuroshio flows), and O-line (across which the Ryukyu Current flows) are labeled A, C, and O, respectively. Labels denoting the Tokara Strait (TS), Korea/Tsushima Strait (KS), and Izu Ridge (IR) are shown. Isobaths at 500 m intervals to 3000 m depth are gray.

19. Study Area

Negative wind stress curl over the mid-latitude North Pacific sets up the subtropical wind-driven circulation: water flows southward, undergoes horizontal convergence giving rise to westward transport, and finally returns north as a WBC system. Figure 40 shows a schematic of currents in the western North Pacific. Part of the WBC return flow enters the East China Sea (ECS) as the ECS-Kuroshio where it is largely shielded from the ocean interior by the Ryukyu Islands. Inside the ECS, some of the ECS-Kuroshio feeds the Tsushima Current (Isobe, 2008) which flows through the Korea/Tsushima Strait into the Japan/East Sea. The remaining ECS-Kuroshio exits the ECS through the Tokara Strait. Another part of the WBC system, the Ryukyu Current, flows outside the ECS along the eastern

edge of the Ryukyu Islands, intensifying as it flows northeastward (e.g., Ichikawa et al., 2004; Zhu et al., 2006). The Ryukyu Current and ECS-Kuroshio rejoin south of Kyushu and continue eastward. Some water recirculates in the Philippine Basin south of Japan as an anticyclonic gyre (e.g., Qiu and Joyce, 1992) and some passes over the Izu Ridge where it enters the North Pacific as a free jet, the Kuroshio Extension, south of which there is another recirculation cell.

20. Data

Transports at 10-day interval have been determined by calibration of satellite altimetry data with *in situ* measurements. Transports of the ECS-Kuroshio (Andres et al., 2008a), Ryukyu Current (Zhu et al., 2004), ASUKA-line throughflow (Imawaki et al., 2001a and b; Kakinoki et al., 2008), and Philippine Basin recirculation (Imawaki et al., 2001a and b) are available since the TOPEX-Poseidon (and later Jason-1) satellite began altimeter measurements in late 1992.

Daily sea-level data from tide gages at Nishinoomote, Nakanoshima, and Naze, corrected for the inverse barometer effect, are used to calculate both the sea-level difference (SLD) across the Tokara Strait (TS_{SLD}), which is a proxy for Kuroshio transport exiting the ECS (Ichikawa, 2001; Kawabe, 1995), and the Kuroshio Position Index (KPI), which is a proxy for the location of the Kuroshio as it exits the strait (Kawabe, 1995).

Tsushima Current transport through the Korea/Tsushima Strait has been determined from SLD between Moji, Japan and Pusan, Korea, and bimonthly hydrographic data (Lyu and Kim, 2003; H. Na, personal communication, 2008).

The data were calibrated using transport determined from moored ADCP measurements taken during May 1999 – March 2000 (Teague et al., 2002).

Wind data at ~2° horizontal resolution and 6 hour interval is available from the National Center for Environmental Prediction (NCEP; Kalnay et al., 1996). We use the data for 1993 through 2006 to calculate the wind stress curl field over the North Pacific.

The primary climate index used in this study is the PDO index (Zhang et al., 1997; Mantua et al., 1997). This is available through the Joint Institute for the Study of the Atmosphere and Ocean (JISAO) at the University of Washington. We also make use of several other indexes. The Southern Oscillation Index (SOI), which is calculated from the SLP difference between Darwin and Tahiti, is provided by the NCEP Climate Prediction Center. Another ENSO indicator is the Cold Tongue Index (CTI), which is the average SST anomaly over 6°N – 6°S and 180°W – 90°W (Deser and Wallace, 1990). This is available through JISAO. The North Pacific Index (NPI), which is the area weighted SLP in the region 30°N – 65°N, 160°E – 140°W (Trenberth and Hurrell, 1994), is provided by the Climate Analysis Section, NCAR, Boulder, USA.

21. The connection between PDO and WBC transport

Pacific climate changed markedly around 1976/1977 (Nitta and Yamada, 1989; Trenberth, 1990) causing a well-documented "regime shift" from a cool PDO phase to a warm phase (e.g., Miller et al., 1994). This shift is evident in the time series of PDO index (Figure 41a) which switched from negative to positive

values. Another possible regime shift in 1998/1999 was reported by Minobe (2002) although subsequent years of PDO index data suggest that this shift was relatively short lived (Figure 41b).

The mid-1970s change in PDO phase may have been accompanied by a change in ECS-Kuroshio strength. Kawabe (1995, 2001) derived estimates of ECS-Kuroshio transport from the early 1960s through 1995 from SLD across the Tokara Strait calibrated with geostrophic transports calculated from quarterly hydrographic data taken in the ECS along the PN-line (very close to the C-line; Figure 40). ECS-Kuroshio transport was relatively low from the early 1960s until the mid-1970s and large through about 1990 with a ~2 Sv difference in mean transports during these periods (Kawabe; 2001; his Figure 8).

Although not explicitly stated by Kawabe (2001), the observation of low transport coincident with the pre-1976 cool PDO phase and high transport during the subsequent warm phase suggests a dynamical connection between PDO and ECS-Kuroshio transport. This possibility is investigated here by comparing PDO index with recently obtained ECS-Kuroshio and Ryukyu Current transport estimates, paying particular attention to the 1998/99 change in PDO phase.

Figure 41c shows 14 years of ECS-Kuroshio transport determined from satellite altimetry calibrated with 13 months of *in situ* measurements (Andres et al., 2008a). Similarly determined Ryukyu Current transport (Zhu et al, 2004) is also plotted (Figure 41d). Superimposed on these 10-day interval transports are their 1-year running means. A positive correlation between the smoothed PDO index and ECS-Kuroshio transport time series is clearly visible. Ryukyu Current

transport also appears positively correlated with PDO index, although the agreement is not as strong, particularly around 1995.

Table 3 lists the correlation coefficients between annual mean transports and annual means of various Pacific climate indexes from 1993 through 2007. The largest magnitude correlation, 0.76, is between ECS-Kuroshio and PDO index. This is statistically significant at better than the 99% level. Correlation magnitudes of ECS-Kuroshio transport with the indexes associated with ENSO (SOI and CTI) and with NPI are lower but still significant at the 85%, 95%, and 90% levels, respectively.

The correlation of Ryukyu Current transport (Figure 41d) with PDO index is 0.49 which is statistically significant at the 90% confidence level. While the magnitude of the Ryukyu Current-PDO correlation is lower than that of ECS-Kuroshio with PDO, their 95% confidence intervals do overlap (-0.12 to 0.83 for the Ryukyu Current and 0.41 to 0.92 for the ECS-Kuroshio). When the Ryukyu Current and ECS-Kuroshio transports are combined, their sum correlates with PDO index with a correlation coefficient of 0.61 which is statistically significant at the 97% confidence level. The 95% confidence interval on this correlation coefficient is 0.06 to 0.88.

Figure 42 shows linear regressions of transport with the PDO index. The ranges of the regression lines show transport variations associated with the PDO are roughly 2 Sv each for the ECS-Kuroshio and Ryukyu Current, and 4 Sv for their sum.

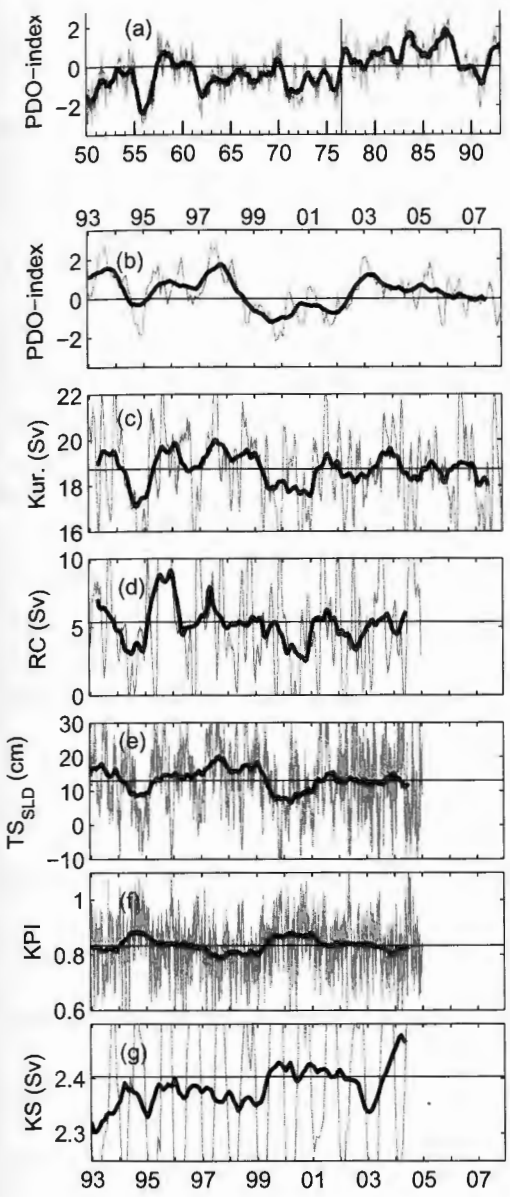

Figure 41. Time series comparisons with PDO index.
Panels show (a) monthly-mean PDO index, 1950-1993, with vertical line indicating the 1976/1977 "regime shift", (b) monthly-mean PDO index, 1993 – 2007, (c) 10-day interval ECS-Kuroshio transport, (d) 10-day interval Ryukyu Current transport, (e) daily SLD across the Tokara Strait, (f) daily KPI, and (g) transport through the Korea/Tsushima Strait. All transports in Sv (10^6 m^3 s^{-1}). One-year moving averages are superimposed on each plot. Tick marks denote the beginnings of the years. Years shown (inclusive) are (a) 1950-1992, (b-c) 1993-2007, (d-g) 1993-2004.

Table 3. Correlation coefficients (r).

	PDO Index[a]	p-value[b]	NPI[c]	SOI[d]	CTI[e]
ECS-Kuroshio	0.76	0.0009	-0.43	-0.39	0.53
Ryukyu Current	0.49	0.11	-0.62	-0.17	0.16
ECS-Kuros. + RC	0.61	0.03	-0.68	-0.25	0.29
ASUKA Throughflow	0.02	0.93	-0.14	-0.07	-0.03
ASUKA Recirculation	-0.39	0.15	-0.25	0.29	-0.35
Tsushima Current	-0.50	0.10	0.14	0.35	-0.42
TS_{SLD}	0.70	0.01	-0.40	-0.37	0.57
KPI	-0.66	0.02	0.46	0.30	-0.48

[a] Available from http://jisao.washington.edu/pdo/PDO.latest.

[b] Probability of PDO index correlation coefficient having this magnitude if the two time series are in fact uncorrelated.

[c] Available from http://www.cgd.ucar.edu/cas/jhurrell/npindex.html.

[d] Available from http://www.cpc.ncep.noaa.gov/data/indices/.

[e] Data through April 2007 available from http://jisao.washington.edu/data/cti/.

(Note: Ryukyu Current, TS_{SLD}, KPI, and Tsushima Current data are available through 2004, so their correlations are calculated over 12, rather than 15, years.)

The mid-1970s increase in ECS-Kuroshio transport documented by Kawabe (1995, 2001) is similar in magnitude to that observed here, and corresponded to the increase in PDO index in the "regime shift". Likewise, the 1993-2007 ECS-Kuroshio and Ryukyu Current transport changes presented here are in phase with the PDO index. This is evident in lagged correlations of the transports with PDO index, which peak at zero lag (Figure 43). In contrast, previous research (e.g., Deser et al., 1999; Qiu, 2003) has found a 4-5 year lag between inferred Kuroshio Extension strength and PDO index. This suggests that the mechanism causing changes in ECS-Kuroshio transport may be different from those affecting the Kuroshio Extension

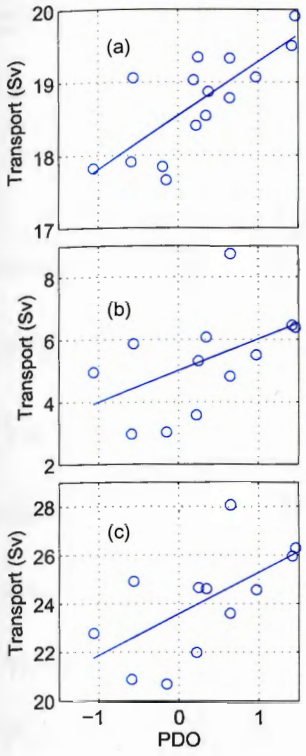

Figure 42. Correlation plots.
Plots of annual mean transports with annual mean PDO index for (a) ECS-Kuroshio, (b) Ryukyu Current, and (c) sum of ECS-Kuroshio and Ryukyu Current. In each panel, the least-squares-fitted straight line is shown.

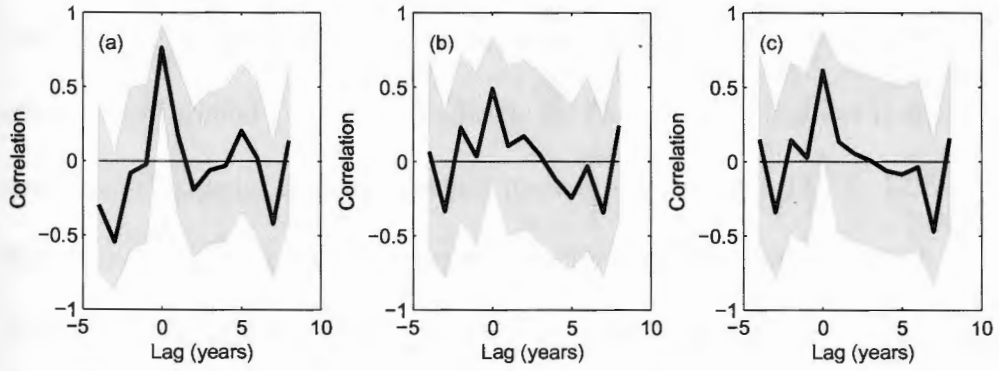

Figure 43. Lagged correlations of transports with PDO index.
Panel (a) ECS-Kuroshio, (b) Ryukyu Current, and (c) sum of Ryukyu Current and ECS-Kuroshio. 95% confidence intervals are shaded in gray. Positive lag values indicate transports lagging PDO index.

22. Role of the wind

22.1 Correlations with wind-stress-curl

To investigate the role wind plays in the observed covariance of WBC transport and PDO index, we analyzed the vertical component of the North Pacific wind stress curl field, $\nabla_H \times \boldsymbol{\tau}_w$, calculated from NCEP wind stress data. Here $\nabla_H \times \boldsymbol{\tau}_w$ is $\left(\partial \tau^y / \partial x - \partial \tau^x / \partial y\right)$. For reference, the overall 1993-2006 mean $\nabla_H \times \boldsymbol{\tau}_w$ is shown in Figure 44a. To evaluate correlations with wind stress curl, we first averaged $\nabla_H \times \boldsymbol{\tau}_w$ over year-long chunks for each grid point in the North Pacific. Then we compared this field of annual means with time series of annual means of PDO index, ECS-Kuroshio transport, and Ryukyu Current transport to identify regions of strong correlation.

The resulting correlation maps are shown in Figure 44b-d. $\nabla_H \times \boldsymbol{\tau}_w$ is negatively correlated with PDO index in the central North Pacific, from about 160°E to 170°W and 20°N to 30°N (Figure 44b). The correlation coefficient reaches -0.80 around 176°W, 24°N. Inside the Philippine Basin, there is another small area of negative correlation which reaches -0.60 at 26°N, 137°E. ECS-Kuroshio and Ryukyu Current transports are also negatively correlated with $\nabla_H \times \boldsymbol{\tau}_w$ in the central North Pacific (Figure 44c and d). However, the regions of significant correlation are smaller and the maximum negative correlations (-0.78 and -0.69, respectively) are not quite as strong. We also calculated maps of correlation with $\nabla_H \times \boldsymbol{\tau}_w$ allowing for lags (maps not shown), but in each map, the

strongest correlations occur with zero lag. Additionally, maps of lagged correlation do not show regions of significant correlation extending over more than a few grid points. This is in agreement with the findings of the previous section that PDO index and WBC transport changes are in phase.

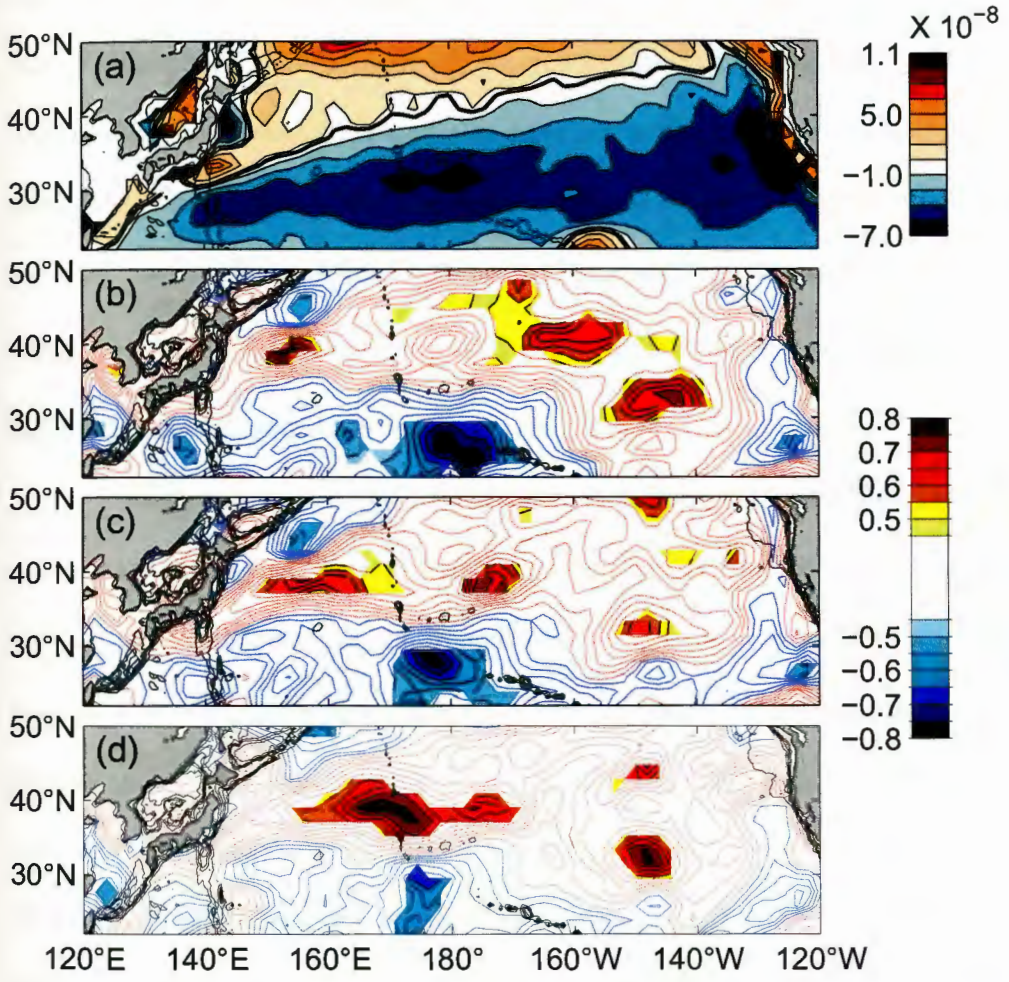

Figure 44. NCEP wind stress curl mean and correlation maps.
Panel (a) shows overall 1993 to 2006 mean $\nabla_H \times \tau_w$. Contour interval is 1.5×10^{-8} N/m^3. Thick line shows zero contour. Values over water shallower than 100 m are masked. Correlations (r) of annual mean $\nabla_H \times \tau_w$ with (b) PDO index, (c) ECS-Kuroshio transport, and (d) Ryukyu Current transport. Filled areas in b-d show regions of correlation significant at the 90% level with 0.05 contour intervals (see color bar on left). Cool (warm) colors are regions of negative (positive) correlation. In regions with confidence levels lower than 90%, contour lines at 0.10 intervals denote regions of negative (positive) correlation in blue (red). Isobaths are shown at 500 and 3000 m depth.

The correlations noted above suggest the following scenario, consistent with Sverdrup theory. Enhanced westerly winds result in cooling of central North Pacific SST, either by increased atmospheric heat transfer or by southward displacement of the isotherms by Ekman drift (e.g., Seager et al., 2001). This central Pacific cooling is a signature of the PDO "warm phase" (positive PDO index, with warming in the region off the coastal region of the northeast Pacific). Enhanced negative wind stress curl also drives enhanced southward flow in the subtropical North Pacific gyre. This is compensated by a stronger return flow in the WBC system (higher ECS-Kuroshio and Ryukyu Current transports). Since correlations of WBC transport with PDO index and $\nabla_H \times \boldsymbol{\tau}_w$ are strongest at zero lag, this appears to be a barotropic response to wind forcing.

This scenario leaves open the question of whether or not feedback from the ocean to the atmosphere plays a significant role in modulating the PDO. Based on results from a coupled ocean-atmosphere model, Latif and Barnett (1994) suggested that the following feedback mechanism was important in setting the decadal timescale in Pacific SST variability. Anomalously strong negative wind stress curl drives increased southward Sverdrup transport resulting in stronger WBC transport. This in turn transports more subtropical waters to the Kuroshio Extension region, decreasing the SST gradient there. The reduced SST gradient feeds back to the atmosphere and leads to reduced westerlies, which results in reduced Sverdrup transport and a reversal of the entire process.

In contrast to this model, in which heat transport by the WBC plays a central role, Qiu (2003) concluded that the changes in Sverdrup flow and

consequent changes in the WBC transport are not important in feedback associated with the PDO. This conclusion is based on Qiu's finding that changes in Kuroshio Extension strength are caused by westward propagating SSH anomalies forced by winds over the eastern Pacific (the speed of propagation is latitude dependent). However, the WBC transport changes found in this study (4 Sv) are about half as strong as those Qiu found associated with westward propagating SSH anomalies (10 Sv), suggesting that advection of heat by the WBC may in fact be an important part of the PDO related atmosphere-ocean feedback loop.

22.2 Magnitude of the total wind-driven response

While the maps in Figure 44b-d confirm significant correlations of PDO index, ECS-Kuroshio and Ryukyu Current transports with $\nabla_H \times \boldsymbol{\tau}_w$, they do not establish whether the magnitudes of the observed transport variations match the expected response to variations in the wind field. We address this question next by using the Sverdrup relation which is the steady state vorticity balance between meridional transport and wind stress curl,

$$Q_y = \frac{1}{\rho\beta} \nabla_H \times \vec{\tau} \,. \tag{13}$$

where Q_y is the meridional volume transport anomaly per unit width (zonal), ρ is the density of seawater taken as 1030 kg/m^3, β is the variation of Coriolis parameter, f, with latitude, df/dy, and $\nabla_H \times \boldsymbol{\tau}$ is the wind stress curl anomaly. For a given latitude, the total Sverdrup transport anomaly crossing a zonal section, T_{Sv}, is Q_y integrated over the length of that section. At each latitude, due to mass balance, WBC transport anomalies are expected to balance Q_y integrated across the entire

basin. Additionally, if the WBC response to the winds is rapid relative to changes in the wind field (e.g., if the ocean's response to the wind is transmitted via barotropic Rossby waves) Equation (13) can be used to determine a quasi-steady solution. Table 4 summarizes statistics comparing the observed transport anomalies with T_{Sv} calculated as described in the following sections.

Table 4. Statistics comparing observed and calculated transport anomalies.

	$\nabla_H \times \boldsymbol{\tau}$ (whole basin)	$\nabla_H \times \boldsymbol{\tau}_{PDO}$ (whole basin)	$\nabla_H \times \boldsymbol{\tau}_{PDO}$ (from Hawaii)
Ryukyu Current			
$\sigma_o = 1.63$ Sv			
σ_{Sv}	2.31 Sv	1.40 Sv	1.47 Sv
Rms	2.25 Sv		1.65 Sv
ECS-Kuroshio			
$\sigma_o = 0.67$ Sv			
σ_{Sv}	1.86 Sv	1.11 Sv	1.05 Sv
Rms	1.44 Sv		0.80 Sv

Using the time series of annual mean $\nabla_H \times \boldsymbol{\tau}_w$ anomalies in Equation (13) and integrating over the entire basin, we calculate T_{Sv} and compare this with the observed annual mean WBC transport anomalies. Since the Ryukyu Islands largely shield the ECS from the ocean interior, ECS-Kuroshio transport north of Okinawa (crossing the C-line) is comparable to that entering the ECS east of Taiwan and thus the calculations are performed along 24°N. For the case of the Ryukyu Current, we perform the calculations at 26°N which falls along the southern edge of Okinawa by the O-line measurements.

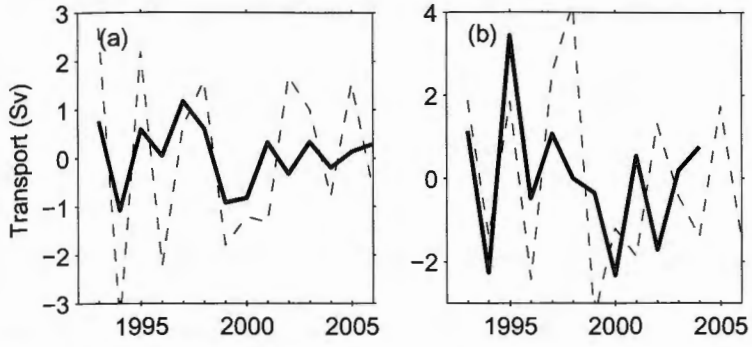

Figure 45. WBC transport anomalies.
Plots show observations (heavy solid lines) and T_{Sv} calculated using $\nabla_H \times \tau_w$ anomalies and integrating over the whole basin (dashed lines). (a) ECS-Kuroshio, calculated along 24°N integrated from 121.8°E to 120°W and (b) Ryukyu Current, calculated along 26°N integrated from 129.4°E to 120°W.

Figure 45 shows that the Sverdrup calculations integrated over the whole basin (dashed lines) do not reproduce the observed WBC transport anomalies (heavy solid lines) well, either in the magnitude of the response, nor in the shape of the response. The rms difference between calculations and observations is 1.44 Sv for the ECS-Kuroshio and 2.25 Sv for the Ryukyu Current.

In both the ECS-Kuroshio and the Ryukyu Current, the observed transport variability from one year to the next is generally smaller than that predicted from the winds. This is demonstrated by comparing standard deviations of observed and calculated transports (denoted with σ_o, and σ_{Sv}). For the ECS-Kuroshio, σ_o is 0.67 Sv, while σ_{Sv},is 1.86 Sv. For the Ryukyu Current σ_o is 1.63 Sv while σ_{Sv} is 2.31 Sv.

These calculations indicate that there are components of the wind field, $\nabla_H \times \boldsymbol{\tau}_w$, which (at zero time lag) are 1) not correlated with PDO index and 2) not reflected in the WBC transport observations.

22.3 Magnitude of the PDO-related wind-driven response

Next we isolate $\nabla_H \times \boldsymbol{\tau}_{PDO}$, that part of $\nabla_H \times \boldsymbol{\tau}_w$ which is correlated with the PDO index. We then use the Sverdrup relation (13) with this part of the wind field to assess whether variations in yearly mean $\nabla_H \times \boldsymbol{\tau}_{PDO}$ can drive the observed variations in WBC transport.

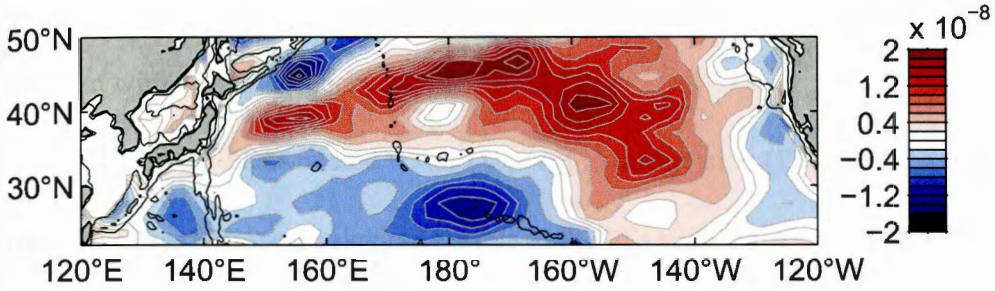

Figure 46. Annual mean $\nabla_H \times \tau_w$ regressed onto annual mean PDO index anomalies. Contour interval is 0.2 $\times 10^{-8}$ N/m^3. Isobaths are shown at 500 and 3000 m depth.

In order to determine which part of North Pacific $\nabla_H \times \boldsymbol{\tau}_w$ is associated with PDO, annual mean wind stress curl, is regressed onto PDO index anomalies as follows. At each grid point in the North Pacific, $\nabla_H \times \boldsymbol{\tau}_w$ is averaged over year-long chunks, giving a 14-year record of annual means. Annual mean PDO index anomalies are calculated by subtracting the 14-year overall mean PDO index (0.296) from each annual mean PDO index. Then for each location, annual mean $\nabla_H \times \boldsymbol{\tau}_w$ is regressed onto the annual mean PDO index anomalies, resulting in a map of regression coefficients. The resulting pattern in Figure 45 represents that part of the wind stress curl field associated with a PDO index anomaly of 1. Its spatial distribution is very similar to the 1st EOF of wind stress curl anomalies calculated by Qiu (2003). Multiplying the pattern in

Figure 46 by the PDO index anomaly time series gives a $\nabla_H \times \boldsymbol{\tau}_{PDO}$ time series; this extracts the part of the North Pacific wind stress curl field which varies in concert with PDO index. As PDO index increases (decreases), $\nabla_H \times \boldsymbol{\tau}_{PDO}$ becomes more (less) strongly negative in a band between 20°N and 35°N and stretching from the western boundary to 160°W. This is consistent with the positive relation noted previously between PDO index and WBC transport (Figure 44), and with Sverdrup theory.

Using the PDO-related winds ($\nabla_H \times \boldsymbol{\tau}_{PDO}$) in Equation (13) and integrating over the entire basin, we calculate T_{Sv} due to the PDO-related winds. The variability in the calculated and observed transport anomalies match fairly well for the Ryukyu Current (σ_o = 1.63 Sv, σ_{Sv} = 1.40 Sv). However, for the ECS-Kuroshio, as was the case for the calculations using $\nabla_H \times \boldsymbol{\tau}_W$, discussed in Section 22.2, the variability predicted by Sverdrup calculations (σ_{Sv} = 1.11 Sv) is larger than the observed variability (σ_o = 0.67 Sv).

Figure 47 shows zonal cross-sections of the mean depth in 1° wide swaths across the Pacific centered on 26°N and 24°N. The Hawaiian Ridge is a prominent feature which falls just east of the regions of high correlation noted in Figure 44. This ridge may play a role in blocking the ocean's response to wind stress curl anomalies from further east. But it is not clear why the Hawaiian Ridge would block responses which are not blocked by the Izu Ridge. Nevertheless we investigate the possibility that the WBC transport variations are not responding to

winds blowing over the entire width of the North Pacific, but only the portion west of the Hawaiian Ridge.

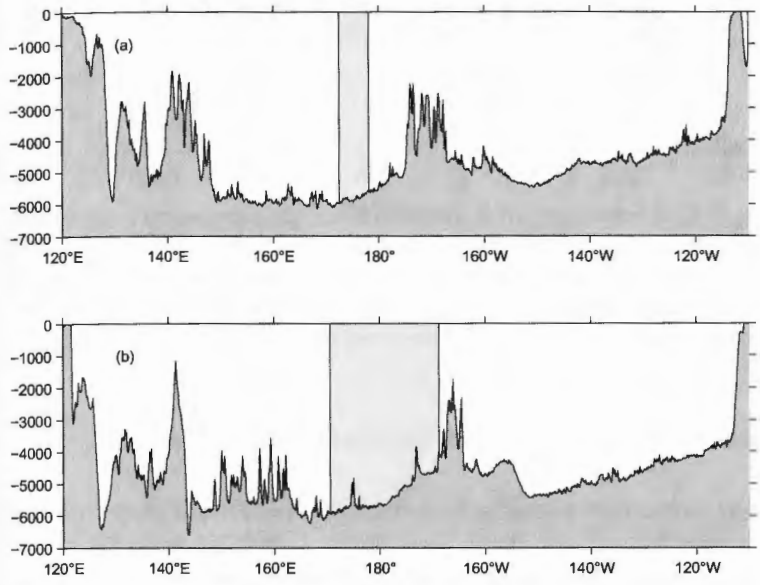

Figure 47. Zonal cross-sections of North Pacific bathymetry.
Panel (a) is a swath along 26°N. Shaded area shows region where the correlation between $\nabla_H \times \tau_{PDO}$ and Ryukyu Current transport observations is significant (see Figure 44d). Panel (b) as in (a) for a swath along 24°N with shaded area showing region of significant correlation between $\nabla_H \times \tau_{PDO}$ and ECS-Kuroshio transport observations (see Figure 44c).

We calculate Q_y using $\nabla_H \times \boldsymbol{\tau}_{PDO}$ in Equation (13) and integrating, not from Baja California, but from the Hawaiian Ridge to the western boundary. The results are shown in Figure 48. For the ECS-Kuroshio (panel a), observations (heavy line) and calculations (light line) match moderately well: the rms difference between observations and T_{Sv} is 0.80 Sv and the variability agrees within a factor of 2 (σ_{Sv} is 1.05 Sv compared with σ_o is 0.67 Sv). For the Ryukyu Current (panel b) the variability in the observed and calculated transports are similar (σ_{Sv} is 1.47 Sv compared with σ_o = 1.63 Sv for the observations), but the rms difference is somewhat large, 1.65 Sv).

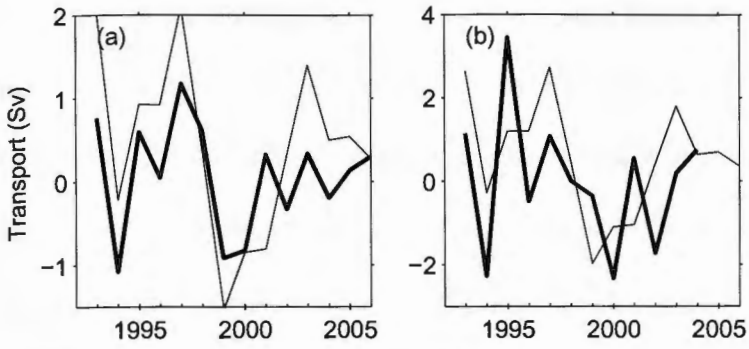

Figure 48. Comparisons of T_{Sv} and observed WBC transports.
Panel (a) shows T_{Sv} calculated for the region between Taiwan and the Hawaiian Ridge (168.75°E) along 24°N with de-meaned ECS-Kuroshio transport shown for comparison (heavy solid line). Panel (b) as in (a) but calculated for the region between Okinawa and the Hawaiian Ridge (176.25°E) along 26°N with the heavy solid line showing the de-meaned Ryukyu Current transport.

The calculations described above suggest that the observed WBC transport variability in the ECS-Kuroshio results from a barotropic response to the effect of wind stress curl integrated from the western boundary to the central North Pacific rather than the full width of the North Pacific. This eastern part of this area of integration is also the region where the correlation maps peak (see 5c and d).

22.4 Comparisons with previous research

Kawabe (2001) successfully reproduced observed ECS-Kuroshio transport variations, including the marked mid-1970s increase, using a model of wind-driven Rossby waves (using winds from the Ocean Research Institute and NCEP). His model, which includes a dissipation term, shows that variations in sea surface height along the Ryukyu Islands recorded by tide gages are largely due to the arrival of barotropic Rossby waves, and secondarily to first-baroclinic-mode Rossby waves. By comparing the model results and tide gage measurements, Kawabe concluded that to a large extent, the Izu-Ogasawara Ridge does not block the barotropic Rossby wave energy and that volume transport variations of the

ECS-Kuroshio are mainly a response to barotropic Rossby waves. It is possible that the poorer fit between observations and calculations for the Ryukyu Current compared with the ECS-Kuroshio is related to northward shoaling of the Izu Ridge which therefore obstructs the barotropic response to the wind more at 26°N (affecting the Ryukyu Current) than at 24°N (affecting the ECS-Kuroshio).

Gilson and Roemmich (2002) investigated Kuroshio variability upstream of the ECS, at 21°N -22°N, east of Taiwan. In contrast to the results presented here, their transport estimates, based on quarterly sampling with XBTs and XCTDs between 1993 and 2001, do not correlate with PDO index. In fact, they report a transport maximum in 1999 - 2000 when we find low PDO index, ECS-Kuroshio transport, and Ryukyu Current transport. They report a transport minimum in 1997 when we find relatively high PDO index and transports. Their high-transport years tend to coincide with high SOI (their Figure 8b) which is the opposite of our findings for the ECS-Kuroshio and Ryukyu Current (see Table 3). PDO-like responses similar to ours may in fact be present off Taiwan, but being mainly barotropic, as suggested here and by the modeling of Kawabe (2001), would be missed by the Gilson and Roemmich measurements which give only the baroclinic transport.

23. Response to the PDO in the ECS

Inside the ECS, the ECS-Kuroshio flows along the shelf break towards the northern Okinawa Trough. Near 28°N the current turns eastward, separates from the shelf break, and exits the ECS through the Tokara Strait (Nakamura et al.,

2006; his Figure 1 using data from Yamashiro and Kawabe, 2002). The position of the Kuroshio in the Tokara Strait varies over about 100 km and may lead transitions in Kuroshio path south of Japan by several months. Southerly positions in the strait have been correlated with the No Large Meander path and northerly positions with the Large Meander path (Kawabe, 1995) although this is a complicated relationship (see for example Akitomo, 2007).

KPI, a proxy for Kuroshio position in the Tokara Strait (Kawabe, 1995), is the ratio of the SLD anomaly across the southern part of the strait between Naze and Nakanoshima to the SLD anomaly across the whole strait between Naze and Nishinoomote (Figure 49). The mean position in the strait is 29.9°N with standard deviation of 0.17° (Nakamura et al., 2006). Additionally, SLD across the Tokara Strait between Naze and Nishioomote (TS_{SLD}) has been used as a proxy for Kuroshio transport (Ichikawa, 2001; Kawabe, 1995).

Before exiting the ECS, 1-3 Sv of ECS-Kuroshio water intrudes onto the shelf, contributing to the northward flow transporting 1-4 Sv as the Tsushima Current through the shallow Korea/Tsushima Strait and into the Japan/East Sea (Isobe, 2008; Teague et at., 2003). The transport of this intrusion varies seasonally and is highest in autumn (Isobe, 1999; 2000). Based on geostrophic transport estimates and mass balance arguments, it is thought that the Tsushima Current and the ECS-Kuroshio annual mean transports may be anti-correlated (Nitani, 1972, his Figure 29 panels b and f). The seasonally varying ECS-Kuroshio is weakest in October (Andres et al., 2008b; Ichikawa and Beardsley, 1993; Kawabe, 1988)

which is when the Tsushima Current transport has been found to be highest (Teague et al., 2002).

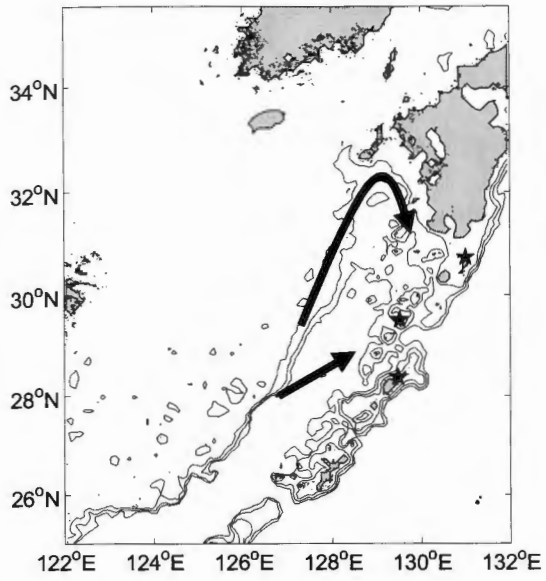

Figure 49. Map of the northern Okinawa Trough and Tokara Strait.
Contour lines at 200 m, 500 m, and 800 m depths. Stars show from north to south: Nishinoomote, Nakanoshima, and Naze. Arrows show alternative paths of the Kuroshio. The straight arrow is the "gap leaping" path, which results in the Kuroshio passing through the Tokara Strait in a southerly position (low KPI). The curved arrow shows the "topography-following" path in which the Kuroshio is constrained to flow through the Tokara Strait in a northerly position (high KPI).

A theory proposed by Gordon and Giulivi (2004) to explain the observed anti-correlation between ECS-Kuroshio and Tsushima Current transports relies on the assumption of constant water volume above the subtropical thermocline, as proposed by Shaw and Wyrtki (1972). In this case, a relaxed thermocline tilt results in a weaker, but broader, WBC. This would result in less transport in the ECS-Kuroshio core but more flow on the shelf feeding the Tsushima Current. This model is consistent with Gordon and Giulivi's (2004) observations of sea surface height determined from satellite altimetry (1992-2002) and historical hydrocasts (1927-1999) in the Japan/East Sea. They found that sea surface height

is negatively correlated with PDO such that during negative PDO phases, the surface water in the Japan/East Sea is warmer and saltier presumably due to the import of more subtropical waters.

The correlations listed in Table 3 show that the PDO index is positively correlated with ECS-Kuroshio transport and TS_{SLD} and negatively correlated with KPI and Korea/Tsushima Strait transport. These correlations suggest an alternative mechanism which does not rely on the assumption of constant water volume above the subtropical thermocline, but is still consistent with the correlation between sea surface height and PDO index noted by Gordon and Giulivi (2004). The observed covariations may result from competition between topographic and inertial steering of the Kuroshio jet. Sheremet (2001) investigated the behavior of a WBC flowing past a boundary gap and found that potential vorticity conservation tends to make the current follow isobaths and hence loop into in the gap, while inertia tends to make the current leap the gap. As can be seen in Figure 49, in the ECS, along the shelf break, there is a kink in the isobaths at about 28°N. When inertially controlled, the jet continues in a straight path from this kink, it "jumps the gap" across the northern Okinawa Trough (Figure 49, straight arrow) and enters the Tokara Strait near its southern end (low KPI). On the other hand, when transport is relatively low, the jet is constrained to follow the topography, so it follows the shelf break and "loops" anticyclonically towards the Tokara Strait (Figure 49, curved arrow), which it encounters at its northern end (high KPI). When PDO index and ECS-Kuroshio transport both increase in response to wind stress curl (as described in the previous section) the ECS-Kuroshio may become

inertially controlled. This leads to (1) less transport intruding from the ECS-Kuroshio onto the shelf and lower Tsushima Current transport, (2) a more southerly position in the Tokara Strait (i.e., lower KPI), and (3) increased transport exiting the ECS (higher TS_{SLD}).

Based on modeling and data, Nakamura (2005) and Nakamura et al. (2006) correlate changes in KPI with changes in the current's background state and transport. They report that a highly stable southern path state in the Tokara Strait (low KPI) is associated with an upstream cyclonic Kuroshio meander and thick inflow condition (large transport), while a weakly stable northern path state (high KPI) is associated with an upstream anticyclonic Kuroshio meander and a thin inflow condition (low transport). However, Nakamura (2005) suggests that the cause for the change in Kuroshio path state is a growing ECS-Kuroshio frontal meander such that a cyclonic eddy pushes the path from the northern to the southern state once it reaches the scale of the Okinawa Trough (Nakamura et al., 2003). This contrasts with our suggestion above that the jet position is controlled by the interplay of inertia and topography, however, the frequency range investigated by Nakamura (2005) and Nakamura et al. (2003, 2006) is much higher (30-90 days) than the interannual variability investigated here.

24. PDO and downstream variations

After exiting the Tokara Strait, the Kuroshio is rejoined by the Ryukyu Current, crosses the ASUKA-line south of Japan, and finally passes over the Izu Ridge. The ASUKA-line has been studied intensively and calibration of satellite

altimetry with *in situ* data (Imawaki et al., 2001a, b) has resulted in transport time series of both the Kuroshio throughflow and the anticyclonic recirculation gyre (Figure 40) in the Philippine Basin south of this throughflow (Hasunuma and Yoshida, 1978). The westward flowing part of this recirculation is referred to as the Kuroshio Countercurrent by Qiu and Joyce (1992) and Su et al. (1990).

Since the ASUKA-line falls along a satellite altimeter track, the along-track data have been used to determine the location along the ASUKA-line at which flow direction reverses from eastward to westward. The eastward flow between the coast and this point consists of both throughflow and recirculation components. The recirculation component is determined by assuming that its magnitude is equivalent to the westward flow across the ASUKA-line between this point and a fixed point to the south, 26°N (Imawaki et al., 2001b). The difference between eastward and westward flow is taken as the throughflow. The mean throughflow is 42 Sv and mean recirculation is 15 Sv (Imawaki et al., 2001a).

Despite the correlations between the ECS-Kuroshio and the Ryukyu Current with PDO index, we find that ASUKA-line throughflow is not significantly correlated with PDO index (Table 3). This is surprising, since the ECS-Kuroshio and Ryukyu Current presumably feed the ASUKA-line throughflow. ASUKA-line recirculation, on the other hand is negatively correlated with PDO index, though only at the 85% confidence level ($r = 0.39$), which suggests that as PDO index increases, recirculation strength decreases.

However, it may be that the procedure of Imawaki et al. (2001a and b) described above for splitting the eastward flow across the ASUKA-line into

throughflow and recirculation components is flawed because of the use of a fixed point (26°N) to locate the offshore edge of the recirculation gyre. There is a shallow current, the Subtropical Countercurrent, which flows eastward south of the recirculation gyre (Qiu and Joyce, 1992; Uda and Hasunuma, 1969). In the mean, this flow lies between 24°N and 27°N (Qiu and Joyce, 1992 their Figure 4). If the westward flow across the southern part of the ASUKA-line includes not only recirculation, but also interior flow feeding the western boundary current (i.e., the Ryukyu Current) and/or the Subtropical Countercurrent, then the ASUKA recirculation strength will be overestimated and ASUKA throughflow will be underestimated.

Additional evidence that the ASUKA-line calculations result in a misallocation of transport into recirculation and throuoghflow components comes from Nagano (2008). He reports on a series of PIES and current-meter measurements along the ASUKA-line and along ~30°N from the ASUKA-line to the Izu Ridge in 2004 and 2005. The part of this array along 30°N was used to determine the recirculation strength. Using these data, Nagano then recalibrated satellite altimetry data, resulting in a time series of Kuroshio net transport which is quantitatively and qualitatively very different from that which relies on the fixed southern extent of the recirculation gyre.

Finally, there is some historical data surrounding the 1976/77 "regime shift" which support our expectation that increases in PDO index ought to be accompanied by increased Kuroshio throughflow south of Japan. Qiu and Joyce (1992) calculated the net transport south of Japan in this region in order to

investigate its relationship with the large meander south of Japan. Their net Kuroshio transport calculations (i.e., the throughflow), referenced to 1250 m, are based on twice yearly hydrographic surveys along 137°E from the Japan coast to 2°S taken by the Japan Meteorological Agency from the late 1960s through the late 1980s. They do not report the pre- and post- regime shift mean transports separately, but their Figure 7 shows that net transport from 1969-1974 is lower than that between 1977-1988. This is the sense of variation one would expect from increased PDO index correlated with increased ECS-Kuroshio and Ryukyu Current transport feeding increased throughflow south of Japan.

25. Conclusions

The use of *in situ* data to calibrate 15 years of satellite altimeter measurements has allowed us to establish that there is a positive correlation, at zero lag, between PDO index and WBC transport. This has been foreshadowed in the literature, but not established explicitly. Nitani (1972) shows a figure (29d) with semi-annual transport relative to 1200 dbar, calculated by the Nagasaki Marine Observatory. From 1958 to 1961 this transport dropped, followed by a transport increase from 1962 through the late 1960s. This 1961 minimum is also apparent in the PDO index time series (Figure 41a).

PDO-related responses have also been reported in the Kuroshio Extension. The magnitude of the WBC response to the PDO documented here is smaller than that of the Kuroshio Extension reported by Deser et al. (1999) (about 4 Sv compared to11.6 Sv) and we find no evidence of a time lag between PDO index

and WBC transport. Thus the ECS response to PDO is different from that in the Kuroshio Extension. The data presented here suggest that interannual changes in the North Pacific WBC system arise from the integrated effect of the wind stress between the western boundary and the central North Pacific. Since correlations are highest at zero lag, the response is presumably barotropic.

The findings reported here do not preclude the suggestion by Qiu (2003) that the PDO effect reaches the Kuroshio Extension region by baroclinic Rossby waves; both phenomena could occur. However, since the baroclinic effect of Qiu (2003) is much larger in magnitude (~10 Sv) than the barotropic effect discussed here (a few Sv), the latter could be difficult to detect in measurements taken in the Kuroshio Extension region.

Finally, we note that in the Philippine Basin there are alternating bands of eastward and westward flow (e.g., Qiu and Joyce, 1992). Some westward flow constitutes the anticyclonic recirculation south of the Kuroshio, while some is interior flow feeding the Ryukyu Current which, in the mean, triples in strength between Okinawa and Amami oshima (e.g. Andres et al., 2008a; Zhu et al., 2006). Due to the complicated flow pattern, in the Philippine Basin as well as the presence of many eddies which pass through the region (e.g, Yang et al. 1999; Zhang et al. 2001), it is difficult to ascertain unambiguously from a single line of measurements which portion of the eastward flow is Kuroshio throughflow. The poor correlation between PDO index and ASUKA-line throughflow (particularly since the ECS-Kuroshio and Ryukyu Current are each well correlated with PDO

index) suggests that more study is needed in the area to establish a reliable throughflow time series.

26. List of References

Akitomo, K. (2007): Effects of stratification and mesoscale eddies on Kuroshio path variation south of Japan, *Deep Sea Research (I Oceanogr. Res. Pap.)*. **55**(8), 997-1008.

Andres, M., J.-H. Park, M. Wimbush, X.-H. Zhu, K.-I. Chang, and H. Ichikawa (2008a): Study of the Ryukyu Current - Kuroshio system based on the integrated use of satellite altimetry and *in situ* data, *J. Oceanogr.*, **64**, 937-950.

Andres M., M. Wimbush, J.-H. Park, K.-I. Chang, B.-H. Lim, D.R. Watts, H. Ichikawa, and W.J. Teague (2008b): Observations of Kuroshio flow variations in the East China Sea, *J. Geophys. Res.*, **113**, C05013, doi:10.1029/2007JC004200.

Choi, B.H., K.O. Kim, and H.M. Eum (2002): Digital bathymetric and topographic data for neighboring seas of Korea, *J. Korean Soc. Coastal and Ocean Engrs.*, **14**(1), 41-50 (in Korean).

Deser, C., and J.M. Wallace (1987): El Nino events and their relation to the Southern Oscillation: 1925-1986, *J. Geophys. Res.*, **92**, C13, 14189-14196.

Deser, C., and J.M. Wallace (1990): Large-scale atmospheric circulation features of warm and cold episodes in the tropical Pacific, *J. Climate,* **3**, 1254–1281.

Deser, C., M.A. Alexander, and M.S. Timlin (1999): Evidence for a wind-driven intensification of the Kuroshio Current Extension from the 1970s to the 1980s, *J. Climate*, **12**, 1697-1706.

Gilson, J., and D. Roemmich (2002): Mean and temporal variability in Kuroshio geostrophic transport south of Taiwan (1993-2001). *J. Oceanogr.*, **58**, 183-195.

Gordon, A.L., and C.F. Giulivi (2004): Pacific decadal oscillation and sea level in the Japan/East sea, *Deep Sea Res. I*, **51**, 653-663.

Hare, S.R. (1996): Low-frequency climate variability and salmon production. Ph.D. thesis, University of Washington, Seattle, 306 pp.

Hasunuma, K., and K. Yoshida (1978): Splitting of the subtropical gyre in the western North Pacific, *J. Oceanogr. Soc. Japan*, **34**, 160-172.

Ichikawa, H., and R.C. Beardsley (1993): Temporal and spatial variability of volume transport of the Kuroshio in the East China Sea, *Deep-Sea Res. I*, **40**(3), 583-605.

Ichikawa, H., H. Nakamura, A. Nishina, and M. Higashi (2004): Variability of north-eastward current southeast of northern Ryukyu Islands. *J. Oceanogr.*, **60**, 351-363.

Ichikawa, K. (2001): Variation of the Kuroshio in the Tokara Strait induced by meso-scale eddies, *J. Oceanogr.*, **57**, 55-68.

Imawaki, S., H. Uchida, H. Ichikawa, M. Fukasawa, S. Umatani, and the ASUKA group (2001a): Satellite altimeter monitoring the Kuroshio transport south of Japan, *Geophys. Res Lett.*, **28**(1), 17-20.

Imawaki, S., S. Aoki, Y. Fukuda, K. Ichikawa, S. Ito, H. Kawamura, M. Kubota, T. Kuragano, K. Matsumoto, T. Nagai, A. Sengoku, and H. Yoritaka (2001b): Mass, heat, and salt transports in the western North Pacific, *Aviso News Lett.*, **8**, 62-64.

Isobe, A., (1999): On the origin of the Tsushima Warm Current and its seasonality, *Cont. Shelf Res.*, **19**, 117-133.

Isobe, A., (2000): Two-layer model on the branchin og the Kuroshio southwest of Kyushu, Japan, *J. Phys. Oceanogr.*, **30**, 2461-2476.

Isobe, A. (2008): Recent advances in ocean-circulation research for the Yellow Sea and East China Sea shelves, *J. Oceanogr.*, **64(4)**, 569-584.

Kakinoki, K., S. Imawaki, H. Uchida, H. Nakamura, K. Ichikawa, S.-I. Umatani, A. Nishina, H. Ichikawa, and M. Wimbush, 2008: Variations of Kuroshio geostrophic transport south of Japan estimated from long-term IES observations, *J. Oceanogr.*, **64**, 373-384.

Kalnay, E. M. Kanamitsu, R. Kistler, W. Collins, D. Deaven, L. Gandin, M. Iredell, S. Saha, G. White, J. Woollen, Y. Zhu, A. Leetmaa, R. Reynolds, M. Chelliah, W. Ebisuzaki, W. Higgins, J. Janowiak, K.C. Mo, C. Ropelewski, J. Wang, R. Jenne, and D. Joseph (1996): The NCEP/NCAR Reanalysis 40-year Project, *Bull. Amer. Meteor. Soc.*, **77**, 437-471.

Kawabe, M. (1988): Variability of Kuroshio velocity assessed from the sea-level difference between Naze and Nishinoomote, *J. Oceanogr.*, **44**, 293-304.

Kawabe, M. (1995): Variations of current path, velocity, and volume transport of the Kuroshio in relation with the large meander, *J. Phys. Oceanogr.*, **25**, 3103-3117.

Kawabe, M. (2001): Interannual variations of sea level at Nansei Islands and volume transport of the Kuroshio due to wind changes, *J. Oceanogr.*, **57**, 189-205.

Latif, M. and T.P. Barnett (1994): Causes of decadal climate variability over the North Pacific and North America, *Science*, **266**, 634-637.

Lyu, S.J., and K. Kim (2003): Absolute transport from the sea level difference across the Korea Strait, Geophys. Res. Lett., **30**(6), 1285, doi:1029/2002GL016233.

Mantua, N.J., S.R. Hare, Y. Zhang, J.M. Wallace, and R.C. Francis (1997): A Pacific interdecadal climate oscillation with impacts on salmon production, *Bull. Amer. Meteor. Soc.*, **78**(6), 1069-1079

Mantua, N.J., and S.R. Hare (2002): The Pacific Decadal Oscillation, *J. Oceanogr.*, **58**, 35-44.

Miller A.J., D.R. Cayan, T.P. Barnett, N.E. Graham, and J.M. Oberhuber (1994): The 1976-77 climate shift of the Pacific Ocean, *Oceanography,* **7**(1), 21-26.

Miller, A.J., D.R. Cayan., and W.B. White (1998): A westward-intensified decadal change in the North Pacific thermocline and gyre-scale circulation, *J. Climate*, **11**, 3112-3127.

Minobe, S. (2002) Interannual to interdecadal changes in the Bering Sea and concurrent 1998/99 changes of the North Pacific, *Progr. Oceanogr.*, **55**, 45-64.

Nagano, A. (2008): Observation of Kuroshio volume and heat transport time series south of Japan (II), *Proc. Oceanogr. Soc. Japan, fall 2008 meeting*, abstract (in Japanese).

Nakamura, H. (2005): Numerical study on the Kurohsio path states in the northern Okinawa Trough of the East China Sea, *J. Geophys. Res.*, **110,** C04003, doi:1029/2004JC002656.

Nakamura, H., H. Ichikawa, A. Nishina, and H.-J. Lie (2003): Kuroshio path meander between the continental slope and the Tokara Strait in the East China Sea, *J. Geophys. Res.*, **108**(C11), 3360, doi:1029/2002JC001450.

Nakamura, H., T. Yamashiro, A. Nishina, and H. Ichikawa (2006): Time-frequency variability of Kuroshio meanders in the Tokara Strait, *Geophys. Res. Lett.*, **33**, L21605, doi:10.1029/2006GL027516.

Nakata K., and K. Hidaka (2003): Decadal-scale variability in the Kuroshio marine ecosystem in winter, *Fish. Oceanogr.*, **12**:4/5, 234-244.

Nitta T., and S. Yamada (1989): Recent warming of tropical sea surface temperature and its relationship to the Northern Hemisphere circulation. *J. Meteor. Soc. Japan*, **67**, 375–383.

Nitani, H. (1972): Beginning of the Kuroshio. In: *Kuroshio, Physical Aspects of the Japan Current*, H. Stommel and K. Yoshida, editors, University of Washington Press, Seattle, pp. 129-164.

Qiu, B. (2003): Kuroshio Extension variability and forcing of the Pacific Decadal Oscillations: responses and potential feedback, *J. Phys. Oceanogr.*, **33**, 2465-2482.

Qiu, B., and T.M. Joyce (1992): Interannual variability in the mid- and low-latitude western north Pacific, *J. Phys. Oceanogr.*, **22**, 1062-1079.

Seager R., Y. Kushnir, N.H. Naik, M.A. Cane, and J. Miller (2001): Wind-driven shifts in the latitude of the Kuroshio-Oyashio Extension and generation of SST anomalies on decadal timescales, *J. Climate*, **14**, 4249-4265.

Shaw, R., and K. Wyrtki (1972): The shape of the warm surface layer in a subtropical gyre. In: Gordon, A.L. (Ed.), Studies in Physical Oceanography-A tribute to George Wust on His 80th Birthday, Vol. 2, Gordon and Breach, New York, Science Publ., N.Y., pp. 179-194.

Sheremet, V.A. (2001): Hysteresis of a western boundary current leaping across a gap, *J. Phys. Oceanogr.*, **31**, 1247-1259).

Su, J.L., B.X. Guan, and J.Z. Jiang (1990): The Kuroshio. Part I. Physical Features, *Oceanogr. Mar. Biol. Ann. Rev.*, **28**, 11-71.

Teague, W.J., G.A. Jacobs, H.T. Perkins, J.W. Book, K.I. Chang, and M.-S. Suk (2002): Low frequency current observations in the Korea/Tsushima Strait, *J. Phys. Oceanogr.*, **32**, 1621-1641.

Teague, W.J., G.A. Jacobs, D.S. Ko, T.Y. Tang, K.-I. Chang, M.S. Suk (2003): Connectivity of the Taiwan, Cheju, and Korea straits, *Cont. Shelf Res.*, **23**(1), pp. 63-77.

Trenberth, K.E. (1990): Recent observed interdecadal climate changes in the northern hemisphere, *Bull. Amer. Meteor. Soc.*, **71**(7), 988-993.

Trenberth. K.E., and J.W. Hurrell (1994): Decadal Atmosphere-Ocean Variations in the Pacifc. *Climate Dynamics,* **9**, 303-319.

Uda, M., and K. Hasunuma (1969): The eastward subtropical countercurrent in the western North Pacific Ocean, *J. Oceanogr. Soc. Japan,* **25**, 201-210.

Yamashiro, T., and M. Kawabe (2002): Variations of the Kuroshio axis south of Kyushu in relation to the Large Meander of the Kuroshio, *J. Oceanogr.*, **58**, 487-503.

Yang, Y., C.-T. Liu, J.-H. Hu, and M. Koga (1999): Taiwan Current (Kuroshio) and impinging eddies, *J. Oceanogr.*, **55**, 609-617.

Zhang, Y., J.M. Wallace, and D.S. Battisti (1997): ENSO-like interdecadal variability: 1900-93, *J. Climate*, **10**, 1004-1020.

Zhang, D., T.N. Lee, and W.E. Johns (2001): The Kuroshio east of Taiwan: modes of variability and relationship to interior ocean mesoscale eddies, *J. Phys. Oceanogr.*, **31**, 1054-1074.

Zhu, X.-H., H. Ichikawa, K. Ichikawa, and K. Takeuchi (2004): Volume transport variability southeast of Okinawa Island estimated from satellite altimeter data, *J. Oceanogr.*, **60**, 953-962.

Zhu, X.-H., J.-H. Park, and I. Kaneko (2006): Velocity structures and transports of the Kuroshio and the Ryukyu Current during fall of 2000 estimated by an inverse technique, *J. Oceanogr.*, **62**, 587-596.

Bibliography

Akitomo, K. (2007). Effects of stratification and mesoscale eddies on Kuroshio path variation south of Japan, *Deep-Sea Research I*, 55(8), 997-1008.

Andres M., K.-I. Chang, C.-S. Hong, H. Ichikawa, D.-K. Lee, J.-H. Lee, B.-H. Lim, D.A. Mitchell, J.-H. Park, W. Teague' K. Tracey, D.R. Watts, and M. Wimbush (2005). East China Sea Kuroshio 2002-2004 data report, *GSO Technical Report No. 2005-02*, Graduate School of Oceanography, University of Rhode Island.

Andres, M., J.-H. Park, M. Wimbush, X.-H. Zhu, K.-I. Chang, and H. Ichikawa (2008a). Study of the Ryukyu Current - Kuroshio system based on the integrated use of satellite altimetry and *in situ* data, *Journal of Oceanography*, 64, 937-950.

Andres M., M. Wimbush, J.-H. Park, K.-I. Chang, B.-H. Lim, D.R. Watts, H. Ichikawa, and W.J. Teague (2008b). Observations of Kuroshio flow variations in the East China Sea, *Journal of Geophysical Research*, 113, C05013, doi:10.1029/2007JC004200.

Bingham F.M., and L.D. Talley (1991). Estimates of Kuroshio transport using an inverse technique, *Deep Sea Research, 38*(S1), S21-S43.

Book, J.W., M. Wimbush, S. Imawaki, H. Ichikawa, H. Uchida, and H. Kinoshita (2002). Kuroshio temporal and spatial variations South of Japan determined from inverted echo sounder measurements, *Journal Geophysical Research, 107*, doi:10.1029/2001JC000795.

Bretherton, F.P., R.E. Davis, and C.B. Fandry (1976). A technique for objective analysis and design of oceanographic experiments applied to MODE-73, *Deep Sea Research, 23,* 559–582.

Cenedese, C., C. Adduce, and D.M. Fratantoni (2005). Laboratory experiments on mesoscale vortices interacting with two islands, *Journal of Geophysical Research*, 110, C09023, doi:10.1029/2004JC002734.

Choi, B.H., K.O. Kim, and H.M. Eum (2002). Digital bathymetric and topographic data for neighboring seas of Korea, *Journal Korean Soc. Coastal and Ocean Engrs., 14*(1), 41-50 (in Korean).

Deser, C., M.A. Alexander, and M.S. Timlin (1999). Evidence for a wind-driven intensification of the Kuroshio Current Extension from the 1970s to the 1980s, *Journal of Climate*, 12, 1697-1706.

Deser, C., and J.M. Wallace (1987). El Nino events and their relation to the Southern Oscillation: 1925-1986, *Journal of Geophysical Research,* 92, C13, 14189-14196.

Deser, C., and J.M. Wallace (1990). Large-scale atmospheric circulation features of warm and cold episodes in the tropical Pacific, *Journal of Climate,* 3, 1254–1281.

Emery, W.J., and R.E. Thomson (2001). Data Analysis Methods in Physical Oceanography, New York, Elsevier, 636pp.

Flyvbjerg, H, and H.G. Petersen (1989). Error estimates on averages of correlated data, *Journal of Chemical Physics*, 91(1), 461-466.

Fujiwara, I., Y. Hanzawa, I. Eguchi, and K. Hirano (1987). Seasonal oceanic conditions on a fixed line in the East China Sea, *Oceanographical Magazine, 37*, 37-46.

Gilson, J., and D. Roemmich (2002). Mean and temporal variability in Kuroshio geostrophic transport south of Taiwan (1993-2001). *Journal of Oceanography*, 58, 183-195.

Gordon, A.L., and C.F. Giulivi (2004). Pacific decadal oscillation and sea level in the Japan/East sea, *Deep Sea Research I*, 51, 653-663.

Guan, B. (1980). Some results from the study of the variation of the Kuroshio in the East China Sea, In *The Kuroshio IV*, Saikon Publishing Co. Tokyo, 897-911.

Guo, X., H. Hukuda, Y. Miyazawa, and T. Yamagata (2003). A triply nested ocean model for simulating the Kuroshio – Roles of horizontal resolution on JEBAR. *Journal of Physical Oceanography, 33*, 146-169.

Guo, X., Y. Miyazawa, and T. Yamagata (2006). The Kuroshio onshore intrusion along the shelf break of the East China Sea: The origin of the Tsushima Warm Current, *Journal of Physical Oceanography, 36*, 2205-2231.

Hare, S.R. (1996). Low-frequency climate variability and salmon production. Ph.D. thesis, University of Washington, Seattle, 306 pp.

Hasunuma, K., and K. Yoshida (1978). Splitting of the subtropical gyre in the western North Pacific, *Journal of the Oceanographic Society of Japan*, 34, 160-172.

Hautala, S.L., D.H. Roemmich, and W.J. Schmitz, Jr. (1994). Is the North Pacific in Sverdrup balance along 24°N?, *Journal of Geophysical Research*, 99(C8), 16,041-16,052.

He, Y.R., D.R. Watts, and K.L. Tracey (1998). Determining geostrophic velocity shear profiles with IESs, *Journal of Geophysical Research, 103*(C3), 5607-5622.

Hellerman, S., and M. Rosenstein (1983). Normal monthly wind stress over the world ocean with error estimates, *Journal of Physical Oceanography,* 13, 1093-1104.

Hinata, T. (1996). Seasonal variation and long-term trends of the oceanographic conditions along a fixed hydrographic line crossing the Kuroshio in the East China Sea, *Oceanographical Magazine, 45*, 9-32.

Ichikawa, K. (2001). Variation of the Kuroshio in the Tokara Strait induced by meso-scale eddies, *Journal of Oceanography*, 57, 55-68.

Ichikawa, H., and R.C. Beardsley (1993). Temporal and spatial variability of volume transport of the Kuroshio in the East China Sea, *Deep-Sea Research I, 40*(3), 583-605.

Ichikawa, H., M. Chaen (2000). Seasonal variation of heat and freshwater transports by the Kuroshio in the East China Sea, *Journal of Marine Systems*, 24, 119-129.

Ichikawa, H., H. Nakamura, A. Nishina, and M. Higashi (2004). Variability of north-eastward current southeast of northern Ryukyu Islands. *Journal of Oceanography, 60*, 351-363.

Imawaki, S., S. Aoki, Y. Fukuda, K. Ichikawa, S. Ito, H. Kawamura, M. Kubota, T. Kuragano, K. Matsumoto, T. Nagai, A. Sengoku, and H. Yoritaka (2001a). Mass, heat, and salt transports in the western North Pacific, *Aviso News Letter*, 8, 62-64.

Imawaki, S., H. Uchida, H. Ichikawa, M. Fukasawa, S. Umatani, and the ASUKA group (2001b). Satellite altimeter monitoring the Kuroshio transport south of Japan, *Geophysical Research Letters*, 28(1), 17-20.

Isobe, A., (1999). On the origin of the Tsushima Warm Current and its seasonality, *Continental Shelf Research*, 19, 117-133.

Isobe, A., (2000). Two-layer model on the branchin og the Kuroshio southwest of Kyushu, Japan, *Journal of Physical Oceanography*, 30, 2461-2476.

Isobe, A. (2008). Recent advances in ocean-circulation research for the Yellow Sea and East China Sea shelves, *Journal of Oceanography*, 64(4), 569-584.

Ito T., A. Kaneko, H. Furukawa, N. Gohda, and W. Koterayama (1995). A structure of the Kuroshio and its related upwelling on the East China Sea shelf slope. *Journal of Oceanography, 51*, 267-278.

James, C., M. Wimbush, and H. Ichikawa (1999). Kuroshio meanders in the East China Sea, *Journal of Physical Oceanography, 29*, 259-272.

Johns, W.E., T.N. Lee, D. Zhang, and R. Zantopp (2001). The Kuroshio east of Taiwan: moored transport observations from the WOCE PCM-1 array, *Journal of Physical Oceanography, 31*, 1031-1053.

Johnson, E.R., and N.R. McDonald (2004). The motion of a vortex near a gap in a wall, *Physics of Fluids*, 16(2), 462-469.

Johnson, E.R., and N.R. McDonald (2005). Vortices near barriers with multiple gaps, *Journal of Fluid Mechanics*, 531, 335-358.

Kagimoto, T., and T. Yamagata (1997). Seasonal transport variations of the Kuroshio: an OGCM simulation, *Journal of Physical Oceanography*, 27, 402-418.

Kakinoki, K., S. Imawaki, H. Uchida, H. Nakamura, K. Ichikawa, S. Umatani, A. Nishina, H. Ichikawa, and M. Wimbush (2008). Variations of Kuroshio geostrophic transport south of Japan estimated from long-term IES observations, *Journal of Oceanography,* 64, 373-384.

Kalnay, E. M. Kanamitsu, R. Kistler, W. Collins, D. Deaven, L. Gandin, M. Iredell, S. Saha, G. White, J. Woollen, Y. Zhu, A. Leetmaa, R. Reynolds, M. Chelliah, W. Ebisuzaki, W. Higgins, J. Janowiak, K.C. Mo, C. Ropelewski, J. Wang, R. Jenne, and D. Joseph, (1996). The NCEP/NCAR Reanalysis 40-year Project, *Bulletin of the American Meteorological Society*, 77, 437-471.

Kawabe, M. (1988). Variability of Kuroshio velocity assessed from the sea-level difference between Naze and Nishinoomote, *Journal of Oceanography*, 44, 293-304.

Kawabe, M. (1995). Variations of current path, velocity, and volume transport of the Kuroshio in relation with the large meander, *Journal of Physical Oceanography*, 25, 3103-3117.

Kawabe, M. (2001). Interannual variations of sea level at Nansei Islands and volume transport of the Kuroshio due to wind changes, *Journal of Oceanography*, 57, 189-205.

Konda, M., H. Ichikawa, I.-S. Han, X.-H. Zhu (2005). Variability of current structure due to meso-scale eddies on the bottom slope southeast of Okinawa Island, *Journal of Oceanography*, 61, 1089-1099.

Latif, M. and T.P. Barnett (1994), Causes of decadal climate variability over the North Pacific and North America, *Science*, 266, 634-637.

Lee, I.-H., W.-S. Chuang, and D.-P. Wang (2003). Structure and propagation of a large cyclonic eddy in the western North Pacific from analysis of XBT and altimetry data and numerical simulation, *TAO: Terrestrial, Atmospheric and Oceanic Sciences*, 14(2), 183-200.

Lee, T.N., W.E. Johns, C.-T. Liu, D. Zhang, R. Zantopp, and Y. Yang (2001). Mean transport and seasonal cycle of the Kurhoshio east Taiwan with comparison to the Florida Current, *Journal of Geophysical Research*, 106(C10), 22,143-22,158.

Lim, B.H. (2008). Near 60-day variation in the Kuroshio observed in the East China Sea, M.Sc. thesis, 44 pp., Seoul Natl. Univ., Seoul, Korea.

Liu, W., Q. Liu, and Y. Jia (2004). The Kuroshio transport east of Taiwan and the sea surface height anomaly from the interior ocean, *Journal Ocean Univ. China*, 3, 135-140.

Lyu, S.J., and K. Kim (2003). Absolute transport from the sea level difference across the Korea Strait, *Geophysical Research Letters*, 30(6), 1285, doi:1029/2002GL016233.

Macdonald, A.M., T. Suga, and R.G. Curry (2001). An isopycnally averaged North Pacific climatology, *J. Atmos. Oceanic Technol., 18,* 394-420.

Mantua, N.J., S.R. Hare, Y. Zhang, J.M. Wallace, and R.C. Francis (1997). A Pacific interdecadal climate oscillation with impacts on salmon production, *Bulletin of the American Meteorological Society*, 78(6), 1069-1079

Mantua, N.J., and S.R. Hare (2002). The Pacific Decadal Oscillation, *Journal of Oceanography*, 58, 35-44.

Meinen, C.S. (2001). Structure of the North Atlantic current in stream-coordinates and the circulation in the Newfoundland basin, *Deep Sea Research I, 48*(7), 1553-1580.

Miller A.J., D.R. Cayan, T.P. Barnett, N.E. Graham, and J.M. Oberhuber (1994). The 1976-77 climate shift of the Pacific Ocean, *Oceanography,* 7(1), 21-26.

Miller, A.J., D.R. Cayan., and W.B. White (1998). A westward-intensified decadal change in the North Pacific thermocline and gyre-scale circulation, *Journal of Climate*, 11, 3112-3127.

Minobe, S. (2002) Interannual to interdecadal changes in the Bering Sea and concurrent 1998/99 changes of the North Pacific, *Progress in Oceanography*, 55, 45-64.

Morinaga, K., N. Nakagawa, K. Osamu, and B. Guo (1998). Flow pattern of the Kuroshio west of the main Okinawa Island, *Proceedings of Japan-China Joint Symposium on Cooperative Study of Subtropical Circulation System, 1-4 December 1997, Nagasaki, Japan,* Seikai National Fisheries Research Institute, Nagasaki, pp. 203-210.

Nagano, A. (2008). Observation of Kuroshio volume and heat transport time series south of Japan (II), *Proceedings of the Oceanographic Society of Japan, fall 2008 meeting*, abstract (in Japanese).

Nagano, A., H. Ichikawa, T. Miura, K. Ichikawa, M. Konda, Y. Yoshikawa, K. Obama, K. Murakami (2007). Current system east of the Ryukyu Islands, *Journal of Geophysical Research*, 112, C06009, doi:10/1029.2006JC003917.

Nagano, A., H. Ichikawa, T. Miura, K. Ichikawa, M. Konda, Y. Yoshikawa, K. Obama, and K. Murakami (2008). Reply to comment by Xiao-Hua Zhu et al. on "Current system east of the Ryukyu Islands", *Journal of Geophysical Research*, 113, C03021, doi: 10.1029/2007JC004561.

Nakamura, H. (2005). Numerical study on the Kuroshio path states in the northern Okinawa Trough of the East China Sea, *Journal of Geophysical Research*, 110, C04003, doi:10.1029/2004JC002656.

Nakamura, H., H. Ichikawa, A. Nishina, and H.-J. Lie (2003). Kuroshio path meander between the continental slope and the Tokara Strait in the East China Sea, *Journal of Geophysical Research*, 108(C11), 3360, doi:1029/2002JC001450.

Nakamura, H., T. Yamashiro, A. Nishina, and H. Ichikawa (2006). Time-frequency variability of Kuroshio meanders in Tokara Strait, *Geophysical Research Letters*, 33, L21605, doi:10.1029/2006GL027516.

Nakata K., and K. Hidaka (2003). Decadal-scale variability in the Kuroshio marine ecosystem in winter, *Fisheries Oceanography,* 12, 234-244.

Nitani, H. (1972). Beginning of the Kuroshio. In: *Kuroshio, Physical Aspects of the Japan Current*, H. Stommel and K. Yoshida, editors, University of Washington Press, Seattle, pp. 129-164.

Nitta T., and S. Yamada (1989). Recent warming of tropical sea surface temperature and its relationship to the Northern Hemisphere circulation. *Journal of the Meteorological Society of Japan*, 67, 375–383.

Oka, E., and M. Kawabe (2003). Dynamic structure of the Kuroshio south of Kyushu in relation to the Kuroshio path variations, *Journal of Oceanography, 59*, 595-608.

Park, J.-H., M. Andres, P. Martin, M. Wimbush, and D.R. Watts (2006). Second-mode internal tides in the East China Sea deduced from historical hydrocasts and a model, *Geophysical Research Letters, 33*(5), L05602, doi:10.1029/2005GL024732.

Park, J.-H., D.R. Watts, K.L. Tracey, and D.A. Mitchell (2005). A multi-index GEM technique and its application to the southwestern Japan/East Sea, *Journal of Atmospheric and Oceanographic Technology, 22*, 1282-1293.

Qiu, B. (1999). Seasonal eddy field modulation of the North Pacific Subtropical Countercurrent: TOPEX/Poseidon observations and theory, *Journal of Physical Oceanography*, 29, 2471-2486.

Qiu, B. (2003). Kuroshio Extension variability and forcing of the Pacific Decadal Oscillations: responses and potential feedback, *Journal of Physical Oceanography*, 33, 2465-2482.

Qiu, B., and S. Chen (2005). Variability of the Kuroshio Extension jet, recirculation gyre, and mesoscale eddies on decadal time scales, *Journal of Physical Oceanography, 35*, 2090–2103 doi:10.1175/JPO2807.1.

Qiu, B., and T.M. Joyce (1992). Interannual variability in the mid- and low-latitude western north Pacific, *Journal of Physical Oceanography*, 22, 1062-1079.

Qiu, B., T. Toda, and N. Imasato (1990). On Kuroshio front fluctuation in the East China Sea using satellite and in situ observation data, *Journal of Geophysical Research, 95*(C10), 18191-18204.

Rodrigues, R. (2004). An observational and numerical study of the South Atlantic circulation. University of Rhode Island, Graduate School of Oceanography, Ph.D. dissertation.

Roemmich, D., and J. Gilson (2001). Eddy transport of heat and thermocline waters in the North Pacific: a key to interannual/decadal climate variability?, *Journal of Physical Oceanography*, 31,675-687.

Sakamoto, T. (2005). Effect of air-sea heat exchange on seasonal transport variation of the Kuroshio, *Journal of Marine Research*, 63, 579-600.

Sakamoto, T., and T. Yamagata (1996). Seasonal transport variations of the wind-driven ocean circulation in a two-layer planetary geostrophic model with a continental slope, *Journal of Marine Research*, 54, 261-284.

Seager R., Y. Kushnir, N.H. Naik, M.A. Cane, and J. Miller (2001). Wind-driven shifts in the latitude of the Kuroshio-Oyashio Extension and generation of SST anomalies on decadal timescales, *Journal of Climate*, 14, 4249-4265.

Shaw, R., and K. Wyrtki (1972). The shape of the warm surface layer in a subtropical gyre. In: Gordon, A.L. (Ed.), Studies in Physical Oceanography-A tribute to George Wust on His 80th Birthday, Vol. 2, Gordon and Breach, New York, Science Publ., N.Y., pp. 179-194.

Sheremet, V.A. (2001). Hysteresis of a western boundary current leaping across a gap, *Journal of Physical Oceanography*, 31, 1247-1259).

Sibuet, S.-K. Hsu, C.-T. Shyu, and C.-S. Liu (1995). Structural and kinematic evolutions of the Okinawa Trough backarc basin, In: *Backarc Basins Tectonics and Magmatism*, B. Taylor, editor, Plenum Press, New York, 343-377.

Simmons, H.L. and D. Nof (2002). The squeezing of eddies through gaps, *Journal of Physical Oceanography*, 32, 314-335.

Su, J.L., B.X. Guan, and J.Z. Jiang (1990). The Kuroshio.Part I. Physical Features, *Oceanography and Marine Biology, an Annual Review, 28*, 11-71.

Sun, C., and D.R. Watts (2001). A circumpolar gravest empirical mode for the Southern Ocean hydrography, *Journal of Geophysical Research, 106*(2), 2833-2855.

Tanabe, A., and C. Cenedese (2008). Laboratory experiments on mesoscale vortices colliding with an island chain, *Journal of Geophysical Research*, 113, C04022, doi:1029/2007JC004322.

Teague, W.J., G.A. Jacobs, D.S. Ko, T.Y. Tang, K.-I. Chang, and M.-S.Suk (2003). Connectivity of the Taiwan, Cheju and Korea Straits, *Continental Shelf Research, 23*, 63-77.

Teague, W.J., G.A. Jacobs, H.T. Perkins, J.W. Book, K.I. Chang, and M.-S. Suk (2002). Low frequency current observations in the Korea/Tsushima Strait, *Journal of Physical Oceanography*, 32, 1621-1641.

Trenberth, K.E. (1990). Recent observed interdecadal climate changes in the northern hemisphere, *Bulletin of the American Meteorological Society*, 71(7), 988-993.

Trenberth. K.E., and J.W. Hurrell (1994). Decadal Atmosphere-Ocean Variations in the Pacifc. *Climate Dynamics,* 9, 303-319.

Uda, M., and K. Hasunuma (1969). The eastward subtropical countercurrent in the western North Pacific Ocean, *Journal of the Oceanographic Society of Japan,* 25, 201-210.

Watts, D.R., C. Sun, and S. Rintoul (2001). Two-dimensional gravest empirical modes determined form hydrographic observations in the Subantarctic Front, *Journal of Physical Oceanography*, 31, 2186-2209.

Watts, D.R., K.L. Tracey, and A.I. Friedlander (1989). Producing accurate maps of the Gulf Stream thermal front using objective analysis, *Journal of Geophysical Research, 94*(C6), 8040-8052.

Willeford, B.D. (2001). Using stream function coordinates to study the circulation and water masses of the North Pacific, University of Rhode Island, Graduate School of Oceanography, M.S. thesis.

Wong, G.T.F., S.-Y. Chao, Y.-H. Li, and F.-K. Shiah (2000). The Kuroshio edge exchange processes (KEEP) study - an introduction to hypotheses and highlights, *Continental Shelf Research, 20*, 335-347.

Xue, H., and G.L. Mellor (1993). Instability of the Gulf Stream front in the South Atlantic Bight, *Journal of Physical Oceanography, 23*, 2326-2350.

Yamashiro, T., and M. Kawabe (2002). Variations of the Kuroshio axis south of Kyushu in relation to the large meander of the Kuroshio, *Journal of Oceanography, 58*, 487-503.

Yang, Y., C.-T. Liu, J.-H. Hu, and M. Koga (1999). Taiwan Current (Kuroshio) and impinging eddies, *Journal of Oceanography*, 55, 609-617.

You, S.-H. (2005). A Numerical Study of the Kuroshio System Southewest of Japan, Ph.D. Thesis, Kyushyu University.

You, S.-H., and J.-H. Yoon (2004). Modeling of the Ryukyu Current along the Pacific side of the Ryukyu Islands, *Pacific Oceanography*, 2, 44-51.

Yuan, Y., M. Endoh, and H. Ishizaki (1991). The study of the Kuroshio in the East China Sea and the current east of the Ryukyu Islands. *Acta Oceanologica Sinica* 10(3), 371-391.

Yuan, Y., C. Liu, Z. Pan, and S. Zheng (1996). Circulation east of Taiwan and in the East China Sea and east of the Ryukyu Islands during early summer 1985. *Acta Oceanologica Sinica*, 15(4), 423-435.

Yuan, Y., A. Kaneko, J. Su, X. Zhu, Y. Liu, N. Gohda, and H. Chen (1998). The Kuroshio east of Taiwan and in the East China Sea and the currents east of Ryukyu Islands during early summer of 1996, *Journal of Oceanography, 54*, 217-226.

Yuan, Y., K. Takano, Z. Pan, J. Su, K. Kawatate, S. Imawaki, H. Yu, H. Chen, H. Ichikawa, and S. Umatani (1994). The Kuroshio in the East China Sea and the currents east of the Ryukyu Islands during autumn 1991, *La Mer*, 32, 235-244.

Zhang, Y., J.M. Wallace, and D.S. Battisti (1997). ENSO-like interdecadal variability: 1900-93, *Journal of Climate*, 10, 1004-1020.

Zhang, D., T.N. Lee, W.E. Johns, C.-T. Liu, and R. Zantopp, 2001. The Kuroshio east of Taiwan: Modes of variability and relationship to interior ocean mesoscale eddies, *Journal of Physical Oceanography, 31*, 1054-1074.

Zhu, X.-H., I.-S. Han, J.-H. Park, H. Ichikawa, K. Murakami, A. Kaneko, and A. Ostrovskii (2003). The northeastward current southeast of Okinawa Island observed during November 2000 to August 2001, *Geophysical Research Letters*, 30(2), 1071, doi:10.1029/2002GL015867.

Zhu, X.-H., H. Ichikawa, K. Ichikawa, and K. Takeuchi (2004). Volume transport variability southeast of Okinawa Island estimated from satellite altimeter data, *Journal of Oceanography*, 60, 953-962.

Zhu, X.-H., J.-H. Park, and D. Huang (2008a). Observation of baroclinic eddies southeast of Okinawa Island, *Science in China Series D: Earth Sciences, 51*, 1802-1812.

Zhu, X.-H., J.-H. Park, and I. Kaneko (2006). Velocity structures and transports of the Kuroshio and the Ryukyu Current during fall of 2000 estimated by an inverse technique, *Journal of Oceanography*, 62, 587-596.

Zhu, X.-H., J.-H. Park, M. Wimbush, and C. Yang (2008b). Comment on "Current system east of the Ryukyu Islands" by A. Nagano et al., *Journal of Geophysical Research*, 113, C03020 doi: 10.1029/2007JC004458.